Revelations from Time Series Spectroscopy of Pulsating White Dwarf Stars

by
Susan E. Thompson

A dissertation submitted to the faculty of the University of North Carolina at Chapel Hill in partial fulfillment of the requirements for the degree of Doctor of Philosophy in the Department of Physics & Astronomy.

Chapel Hill
2004

Approved by

Advisor: Dr. J. Christopher Clemens

Reader: Dr. Marten H. van Kerkwijk

Reader: Dr. Bruce W. Carney

Reader: Dr. Charles R. Evans

Reader: Dr. James A. Rose

ABSTRACT

SUSAN E. THOMPSON: Revelations from Time Series Spectroscopy of Pulsating White Dwarf Stars
(Under the Direction of Dr. J. Christopher Clemens)

We use optical spectra from the Keck Observatory to identify the pulsation modes and measure the associated Doppler shifts on the ZZ Ceti class of white dwarf pulsators. We introduce two new variations on the technique of time series spectroscopy that improve the measurements of the variabilities associated with these stars. Pulsating stars provide the only known way to measure the interior of a star without destroying it. However, a difficulty arises in measuring the characteristics of each pulsation mode, namely the eigenvalues associated with its spherical harmonic (ℓ and m) and the number of radial nodes. The ZZ Ceti pulsators have presented a formidable challenge to the identification of its gravity-modes; most do not excite enough pulsations to find revealing patterns in the photometric observations alone. This prompted the introduction of time series spectroscopic observations in order to measure the amplitude variations across the hydrogen Balmer lines and identify the spherical degree (ℓ) of each mode. These spectra also directly measure the gas velocity variations associated with the pulsations, providing a method to test the convective driving theory. With our data on G 29-38, we apply the first *high*-resolution, time series spectra to a DAV and show that this technique produces a significant improvement in the velocity measurements over the low-resolution counterpart. Unexpectedly, our improved velocity curve shows a phenomenon only previously seen in the light curves, a frequency with the exact sum of two other modes. With our series of low-resolution spectra on PY Vul, we apply an innovative analysis technique to successfully obtain identifications of the six largest pulsations. Our results reveal the first ℓ=4 mode discovered on a ZZ Ceti star. We discuss all the observations of PY Vul in light of this discovery, and show how it explains all the mysteries associated with the pulsations of PY Vul.

ACKNOWLEDGMENTS

Many thanks are owed to the abundance of people who helped develop the ideas in these pages and provide the moral support necessary to finish this task. Chris, my adviser, deserves special recognition for being the one person to play an important role on both these accounts. He put this project before me, helped me understand what I was working on, and provided many valuable insights. Also, his inspiration, enthusiasm, and encouragement were indispensable as I muddled through reducing data and writing papers. Chris, thank you for letting me work with you and providing me with every opportunity to succeed.

Many friends helped me through this crazy world of graduate school by either sharing their knowledge of science, stars and graduate school, or just getting me away from the books for a few hours. Most importantly, Maggie was a great office mate, roommate and friend. Thank you for the long conversations about nothing in particular, teaching me about sports, and all the laughs. Another fixture in my days of grad school is Kristi. She has been like a big sister to me, teaching me the ropes, being a wonderful role model and an even better friend. Leah, my source of all knowledge biological, has never doubted me and has always managed to make me laugh. Lindsay and Calin deserve special recognition for getting me out for a night of fun every once and a while. Celeste, I'm so glad you have been working on pulsating stars; it was great learning about these stars together. And, thanks for letting me use your reductions of G 226-29. Jane and Melissa have taken my mind off my own worries while exposing me to *Asterisk* and relieving me of my spare change. Finally, I want to recognize Fergal for all his assistance in these last few months as I stressed over finishing my thesis and getting a job. My remaining sanity is owed mostly to you.

Thank you for listening to me gripe, and for making sure I smile from time to time. For these reasons, I dedicate the newly discovered mode with a spherical degree of four to you. I shall forevermore think of it as "Fergal's Frequency".

My family has been there all along. Dad took me to see my first comet and solar eclipse and taught me to question everything. Mom provided a wonderful role model for how a woman *can* do it all while teaching me to balance both work and play. You both taught me to love learning and encouraged me to try anything. Doug, you are a great older brother. Thanks for keeping me in touch with those areas of physics I don't have time to pursue. Becky, because of you I have a duet partner and a few cute outfits. Thanks for keeping in touch with your geeky older sister. I cannot thank you all enough for pushing me to be my best and loving me no matter what.

I would like to thank Marten van Kerkwijk and Detlev Koester for their valuable assistance in creating the papers on which this thesis is based. The Department of Physics and Astronomy at UNC-Chapel Hill provided the the space, the computers, and the resources to do this work. The observations reported here were taken by Chris and Marten at the W. M. Keck Observatory, which is operated by the California Association for Research in Astronomy, a scientific partnership among the California Institute of Technology, the University of California, and the National Aeronautics and Space Administration. It was made possible by the generous financial support of the W. M. Keck Foundation. I also acknowledge support from the National Science Foundation through grant AST-0094289 as well as the Alfred P. Sloan Foundation. Finally, the North Carolina Space Grant Consortium Fellowship deserves recognition for the financial support.

Susan Elizabeth Thompson

May 2004

CONTENTS

LIST OF FIGURES

LIST OF TABLES

LIST OF ABBREVIATIONS

DAV	Hydrogen atmosphere variable white dwarf star (ZZ Ceti)
FT	Fourier transform
HST	Hubble Space Telescope
HIRES	The High Resolution Echelle Spectrograph at Keck Observatory
LRIS	The Low Resolution Imaging Spectrograph at Keck Observatory
WD	White dwarf
WET	Whole Earth Telescope

Chapter 1

Overture

Sing!
Sing a song.
Make it simple
to last your whole life long.

"Sing"
Lyrics by Joe Raposo

Oscillations are everywhere and they play an important role in our interpretation of the world. The combination of the tones produced by an instrument when plucking a string or blowing across a reed makes the variety of sounds heard in a symphony. A decorator may tap on a wall to find a stud before hanging a heavy picture. Kayakers learn to read the waves on the water's surface to avoid shallow rocks. What child has never shaken a present to figure-out what is wrapped-up in the pretty paper? On a more scientific level, seismologists use the shaking created by earthquakes to measure the properties of the Earth's interior and physicists measure the vibrational energy levels of crystals. Similarly, astronomers can use oscillations to learn about stars by measuring the periodic brightness variations produced by many stars. Just as a bassoon will produce an airier sound than a cello, stars with different physical properties will produce different sets of oscillations. Since all the light observed from stars is emitted from the outer layers, this is one of the only ways to actually measure the stellar interiors.

This dissertation focuses on deciphering the observed pulsations of two members of the ZZ Ceti class of stars with spectroscopic observations of their brightness variations. We investigate new techniques and discover new properties of the DAV white dwarf stars. To give some perspective on our results, this chapter provides some background about white dwarf stars and the ZZ Cetis.

1.1 White Dwarf Stars

The first, and probably most well known, white dwarf star is Sirius B. By measuring the motion of Sirius A in the sky, Friedrich Bessel (1844) predicted the existence of a dim second star. Later, Adams (1915) found the temperature of Sirius B to be comparable to Sirius A and realized that its mass must be contained in a very small radius. While white dwarfs are about the mass of the sun, they have a radius similar to the size of the Earth. No theory concerning this dense white dwarf matter existed until Chandrasekhar (1934) explored what happens as a star collapses under its own weight. He discovered that a star can be supported by electron degeneracy pressure. The degenerate matter gives white dwarf stars some interesting properties. Since the degenerate pressure and not the thermal pressure is supporting the star, temperature changes do not affect the size of the white dwarf. As it cools, it maintains a nearly constant radius. The white dwarf stars also obey an inverse mass-radii relationship; higher mass white dwarfs have denser cores and smaller radii.

White dwarf stars (WDs) are believed to be the end-point of stellar evolution for stars with a mass less than $\sim$8 $M_{\odot}$, about 90% of all stars. As such, white dwarfs contain the history of stellar formation and evolution for the lower mass stars. A white dwarf is the hot core of a star after it has lost most of its mass during its evolution through the giant and asymptotic giant branch. Though a variety of stars and evolutionary tracks result in WDs, they appear to make a fairly homogeneous group. They have a log(g)$\sim$ 8 in cgs units and a very narrow mass distribution centering on 0.6 $M_{\odot}$ (Bergeron, Saffer, & Liebert 1992; Koester, Weidemann, & Schulz 1979). Once a star has reached the white dwarf stage of its life, it no longer produces

its own energy through fusion, and is left to radiate its remaining energy into space, becoming cooler and dimmer.

Surrounding the degenerate carbon/oxygen core is a thin stratified envelope composed of predominantly hydrogen and helium gas. The degenerate core of the star is very efficient at conducting its heat outward. However, its thin, non-degenerate outer layers act as an insulating blanket holding in the heat of the star. Mestel (1952) explored the theory of white dwarf cooling, and through some elegant simplifications discovered a direct relationship between a white dwarf's cooling rate and luminosity. For a better description of cooling one must know the thickness of the outer layers, the presence of heavier elements, the presence of convection, and phase changes of the core. Comparing a more realistic cooling curve to the observed luminosity function will ultimately provide an age for some of the oldest stars in the solar neighborhood (Winget et al. 1987; Iben & Laughlin 1989; Wood 1992).

White dwarf stars are classified by the composition of the outer atmosphere. Because of the large gravity, heavier elements tend to settle and WDs show very pure atmospheres with spectral lines of only a few elements. The majority of WDs show hydrogen lines and are known as type DA; those with mainly helium lines are type DB, and those with strong He II lines are known as type DO. Other classifications exist for white dwarfs that have carbon features (DQ), metal lines (DZ), only continuum (DC), or appear to be mixtures of these basic types.

White dwarf stars do not necessarily appear as only one classification during their life. Evidence suggests that many change their spectral classifications as they cool. The fraction of hydrogen atmosphere WDs is a function of temperature. No DA stars have temperatures above 80,000 K and no DB stars exist between 45,000 and 30,000 K (known as the DB gap; Liebert et al. 1986). Below about 10,000 K the ratio of DA to non-DA stars starts to drop as those with metal lines begin to appear (Kepler & Bradley 1995; Fontaine & Wesemael 1987; Liebert, Dahn, & Monet 1988). This evidence caused Fontaine & Wesemael (1987) to propose that many stars evolve from DBs to DAs and some back to DBs again. Physically, this requires very thin hydrogen layers. Extremely hot WDs begin with helium atmospheres, but as they cool, Hydrogen comes to the surface through the effects of diffusion, causing the DB

gap. Then, those with the thinnest hydrogen atmospheres can reappear as DBs when the helium convection zone appears and brings helium to the surface of the star. Those stars with thicker hydrogen atmospheres remain DAs until they cool to about 10,000 K where the hydrogen convection zone can bring other elements up to the surface (Koester 1976), thereby reducing the ratio of DA to non-DAs. This spectral evolution theory can only apply if WDs have thin hydrogen layers ($<10^{-13}$ $M_\star$).

The cooling rates and evolution of WDs are only a couple of directions of WD research. These in particular point out the importance of an independent measure of the WD structure and composition, especially of the outer envelopes. White dwarf research also reaches out to a variety of topics in astronomy including stellar physics, stellar evolution, the age of the solar neighborhood, distances to globular clusters, and Galactic halo dark matter. The high gravities, temperatures and magnetic fields of WDs cannot be reproduced on earth and thus WDs provide a laboratory for exploring the physics of matter under such extreme conditions (Koester & Chanmugam 1990; Koester 2002; Hansen & Liebert 2003). Knowing the internal properties of WDs is simply one piece of the larger puzzle that will enable WDs to fulfill all their potential. Fortuitously, some white dwarf stars show pulsations, providing a method to measure the internal stellar physics.

1.2 Pulsating White Dwarfs

Currently three types of pulsating white dwarfs have been discovered. These stars are otherwise normal stars (McGraw 1979; Fontaine et al. 1985) that have reached a stage of their evolution where an instability causes brightness variations. Each instability strip is composed of a different type of WD. The hottest pulsators are those with atmospheres of ionized helium, the DOVs. They are frequently grouped together with the pulsators in planetary nebula nuclei (PNNV). Helium white dwarf stars show pulsations near 24,000 K (Koester et al. 1985). These stars were predicted to pulsate by Winget (1982) and Winget et al. (1982b) before the discovery of the first DBV, GD 358 (Winget et al. 1982a). The stars that are of interest here are

Table 1.1. The pulsating white dwarf stars.

Type	Known Pulsators	T (10^3 K)	P (s)
DOV (GW Vir)	5	180-65	400-2000
DBV (V777 Her)	13	28-22	300-1000
DAV (ZZ Ceti)	70	12.5-10.5	100-1200

Note. — Information for this table is taken from Mukadam et al. (2004), Nitta (2004), Bergeron et al. (2004), Fontaine, Brassard, & Charpinet (2003), and O'Brien (2003).

the coolest and hence the oldest class of white dwarf pulsators, the DAVs. Table 1.1 summarizes the properties of the variable DO, DB, and DA stars.

Landolt's (1968) observations of HL Tau 76 produced the first light curve of a variable white dwarf star. Later, after discovering the variability of R 548 (ZZ Ceti) (Lasker & Hesser 1971) and other DA white dwarfs (McGraw & Robinson 1976; McGraw & Robinson 1975), the variable DAs were recognized as a distinct class of variable stars. McGraw (1977, 1979) showed that they form a group of periodic, low amplitude, short period pulsators similar to ZZ Ceti and named the class after this prototype.

The ZZ Ceti variables reside in an instability strip with a temperature range of about 10,500 K to 12,500 K. They are multi-periodic with mode periods ranging from about 100 to 1200 s and amplitudes of a few percent. The DAVs fall into two basic groups that roughly follow their temperature. The hot DAVs show a very simple set of low-amplitude, short-period modes. The cool DAVs have longer periods and larger amplitudes with a very complex set of unstable modes, including an abundance of combination and harmonic modes.[1] See Figure 1.1 for an example light curve of two

[1]Combination modes refer to modes whose frequencies are the sum or difference of other modes and harmonics are integer multiples of a mode.

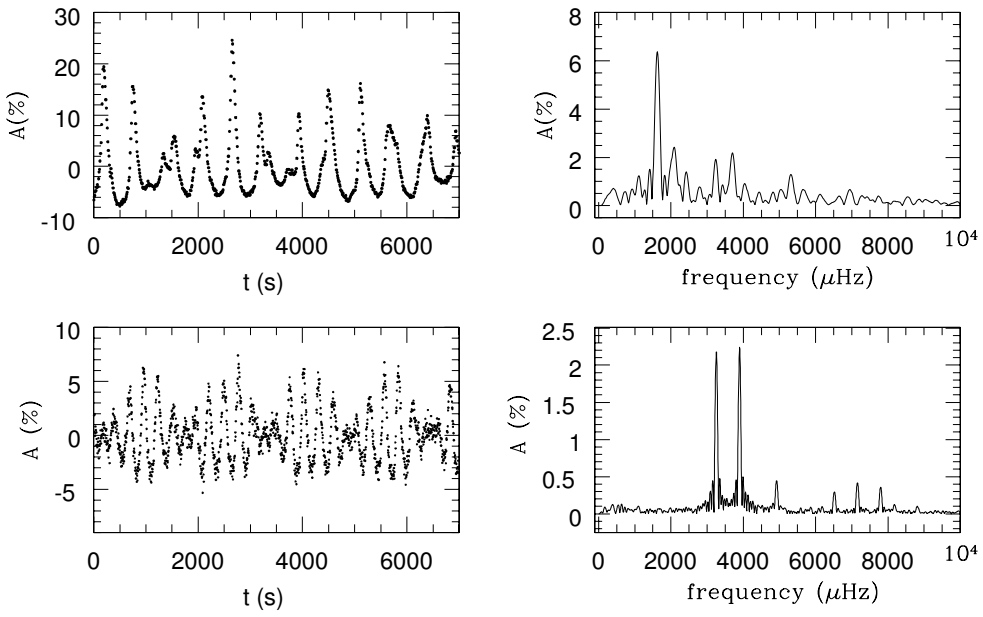

Figure 1.1 The light curve and Fourier transform of GD 244 (bottom) and G 29-38 (top). GD 244 is an example of a hot DAV with simple pulsations. G 29-38 is an example of a cool, complex pulsator. (Both sets of data were taken on the 1.2 m Otto Struve Telescope at McDonald Observatory. GD 244 data was obtained by F. Mullally and S. Thompson with the Argos CCD photometer (Nather & Mukadam 2003). The G 29-38 data was taken by M. Wood with a Nather two-star photometer.)

DAVs. The light curve and Fourier transform (FT) of the bottom star (GD 244) exemplify a simple pulsator with shorter periods and smaller modes than the more complex pulsator (G 29-38) on the top.

1.2.1 About Pulsation

The brightness variations observed on DAVs are created by non-radial, gravity-modes (Robinson, Kepler, & Nather 1982; Dziembowski & Koester 1981). The motion of gas on the stellar surface creates dense and rarefied regions of gas. The dense gas is

perturbed upward slightly and restored to equilibrium by the pull of gravity.[2] Because of the large gravity on these stars, the resultant bulk motion of the gas is primarily parallel to the surface of the star. The pressure changes that accompany the increase and decrease in density cause temperature variations on the stellar surface. Both the changing brightness associated with the temperature changes and the Doppler shifts of spectral lines associated with the motion of the stellar gas are observed on DAVs (van Kerkwijk, Clemens, & Wu 2000).

The gravity-mode pulsation equations are derived by perturbing the hydrodynamic equations of mass and momentum conservation (see Hansen & Kawaler 1994, Unno et al. 1989, or Cox 1980). Along with the equation of state, they reveal that the relationship between the frequency of oscillation (ω) and horizontal wavenumber (k_h) depends on two characteristic frequencies of the star: the Brunt-Väisällä frequency, N, and the Lamb frequency, L.[3] Oscillations with frequencies larger than both N and L are restored by pressure and are known as p-modes, another type of non-radial mode. G-modes occur where the oscillation frequency is smaller than N and L. Since the Lamb and Brunt-Väisällä frequencies vary with depth, g-modes only propagate in certain regions of the star.

The observed brightness variations are described as a combination of sine waves, each with their own period, amplitude, and phase. If we could resolve the surface of a pulsating white dwarf we would see that the entire star does not change brightness at the same time; each pulsation is spatially distributed over the surface and interior of the star. We describe the pulsations as standing waves where the location of the nodes are given by the eigenvalues of a spherical harmonic (ℓ and m) and a radial number (k). These represent the number of nodal lines in the radial direction (radial order, k), the number along the surface (spherical degree, ℓ), and the number on the surface that cross the rotation (or magnetic) axis of the star (azimuthal order, m). Though

[2]The restoring force is actually the buoyant force; the less dense gas will rise upward.

[3]N is also known as the buoyancy frequency. It is the oscillation frequency associated with perturbing a bit of fluid in a medium. $N^2 = -gA(r)$ where $A(r)$ is the Schwarzchild discriminant, $\frac{dln\rho}{dr} - \frac{1}{\Gamma_1}\frac{dlnP}{dr}$. In a convection zone N^2 is negative. L, also known as the sound frequency, depends on the sound speed, v_s. $L^2 = \ell(\frac{\ell+1}{r^2})v_s^2$.

the non-radial pulsations are described in this way, they do not easily advertise their spatial character. Since this information is necessary to model the stellar interior, clever observational techniques continue to be developed to decipher the pulsations. One of the primary goals of this thesis is to further improve upon these techniques.

1.2.2 Driving Mechanism

The fact that we see pulsations means that the star is not in hydrostatic equilibrium. This section addresses what physical mechanism might cause the DAVs to pulsate. Work must be done to create pulsations; the driving mechanism is a description of the engine that provides the energy to do this work. In a basic heat engine, energy or heat is added to the system during compression, causing the gas to expand beyond its neutral position. Then heat leaves the gas as it expands, causing it to contract again. As long as the driving force is larger than any damping mechanism a pulsation mode will grow.

Essentially two driving mechanisms have been proposed for the pulsations; both place the driving in the outer atmosphere. While one uses the opacity variations in the partial ionization zone, the other uses the outer convection zone to drive the pulsations.

κ-γ Mechanism. This mechanism is used to explain the pulsations on the well-known Cepheid stars. Interestingly, if the Cepheid instability strip is extrapolated blue-ward on an H-R diagram it reaches the ZZ Ceti instability strip (Vauclair 1971). In the κ-mechanism, driving occurs because the variation of opacity (denoted as κ) with pressure is steep. A small increase in pressure, will cause the gas to become more opaque and less radiation can leak out. The net result is that during compression, the net heat energy of the gas increases. This excess heat drives the gas to expand beyond its neutral state. During expansion, its opacity decreases and excess energy is radiated away. The γ-mechanism adds to this picture the energy variations that follow from changing the ionization of the gas. Some of the work of compression goes into further ionizing the gas instead of increasing the temperature. This causes more

heat to flow into the compressed, ionized regions to equilibrate the lower temperature. Here again, the heat energy increases during compression, enforcing the driving.

The κ-γ-mechanism was the first proposed mechanism to drive the instabilities on a DAV star (Winget et al. 1982b; Dziembowski & Koester 1981; Dolez & Vauclair 1981; McGraw 1979;Vauclair 1971). The opacity due to hydrogen is near a maximum for the DAVs. It creates a steep temperature gradient and a partial ionization zone common in pulsators driven by this mechanism.

Convective Driving. The κ-γ mechanism ignores changes to the outer convection zone of the star, another result of the steep temperature gradient. Brickhill (1983) showed that the convective turn-over time is much less than the period of the modes and concluded that this would wash-out any perturbations introduced by the κ-γ-mechanism. But, it could also be the source of driving for these stars. With a short mixing time, the entire convection zone effectively responds simultaneously to pressure perturbations from the radiative region below. Brickhill (1991) argued that due to the specific heat of this ionization zone, it takes a characteristic amount of time to heat and cool the region.[4] As a result, the pressure perturbations are out of phase with the temperature changes. As long as the time scale is similar to the pulsation period, the phase delay is enough to cause driving. Because of this delay, the temperature increase that would radiate away the non-adiabatic heating of compression does not occur concurrently with the compression. Essentially, this creates an increase in heat during compression that drives the expansion beyond equilibrium.

Goldreich & Wu (1999a) and Wu & Goldreich (1999) analytically confirmed his results and developed a non-adiabatic model. In the series of papers describing this driving model (Goldreich & Wu 1999a; Wu & Goldreich 1999; Goldreich & Wu 1999b; Wu & Goldreich 2001; Wu 2001), they extended Brickhill's results and were able to reproduce many of the observed qualities of the DAV pulsators. For instance, they established an upper limit on observed periods because of the condition that

[4]Brickhill (1983) defines the characteristic time for the change in luminosity (ΔL) corresponding to the change in temperature (ΔT) as $D = (\frac{1}{\Delta L}) \int_M^{M_\star} (C_p \Delta T) dM$, where C_p is the specific heat at constant pressure. Goldreich & Wu (1999a) define the value τ_c for their thermal time constant.

modes can only be driven if their periods are less than a characteristic thermal time constant of the convection zone ($\omega\tau_c > 1$). They reproduced the range of periods and amplitudes observed on DAVs. By including resonant coupling with other modes, energy is transfered from the parent modes and the growth of the pulsations is limited. This produces the trend that cooler DAVs show larger, more unstable modes.

According to the convective driving mechanism, as the convection zone drives the pulsations, it distorts, diminishes and delays the flux perturbations. Because of the heat capacity of the convection zone, the flux variations take time to appear in the convection zone. According to the theory, the phase is delayed by the amount $90^\circ - \arctan(\omega\tau_c)$ between the base of the convection zone and the surface of the star. As some of the heat energy drives the modes, the amplitude is reduced by a factor of $(1 + (\omega\tau_c)^2)^{-0.5}$. Notice that the flux attenuation and phase delay depend on the frequency of the mode. The time it takes to heat-up and cool-down the convection zone is a more significant portion of the shorter period modes. This theory describes both the motion of the gas during the pulsation and the corresponding flux variations. According to the convective driving theory, the motion of the gas is not affected by the convection zone, allowing the periodic velocities to indicate the size and phase of a pulsation at the base of the convection zone.

The pulsation distortions created by the convection zone appear as combinations modes (Wu 2001; Brickhill 1992a). The outer convection zone is heated and cooled by the pulsations causing it to change depth. How much the convection zone diminishes and delays each pulsation relies, in part, on the depth of the convection zone. During the hot part of a pulsation, the convection zone becomes thin and allows heat to flow through more quickly. During the cool part of the pulsation, the convection zone is thicker and holds on to the heat for longer. In the end, a pulsation is no longer a sine wave. It has sharp peaks and broad troughs (see G 29-38 in Figure 1.1) that produce combinations and harmonics in the Fourier transform of the light curve. Though this phenomenon is only predicted for the observed flux variations, we will report in this thesis evidence of similar non-linear effects in the movement of the gas.

This theory of the combination modes also provides a description of the amplitudes and the spatial appearance of combination modes on the surface of the star. The pre-

diction is that a combination will appear as the product of its parent mode's spherical harmonics. This description is essential as we attempt to understand an extremely large amplitude harmonic mode on one ZZ Ceti.

Observationally it is not so simple to test the driving mechanism; but the convective driving theory does make some distinct predictions regarding the characteristics of the variations of the flux and gas motions due to stellar pulsation. We place our observations in the context of this theory both to test its predictions and describe the stellar pulsations. Regardless of what drives the stellar pulsations, these stars do display brightness variations and how they vary in time and throughout the star (k,ℓ,m) are related to the physical structure of the star.

1.2.3 Asteroseismology

Just like the bassoon cannot sound like the cello, the white dwarf with a thick hydrogen layer cannot pulsate like one with the thin hydrogen layer. Though we do not see the interior of a star, the pulsations interact with the layers beneath the star and provide constraints on the structure and composition that lie below. The most successful asteroseismology has been done on the Sun. Measurements of the brightness and radial velocity oscillations across its surface have provided precise constraints on the solar model (Christensen-Dalsgaard 2002). However, because of the inability to resolve stellar surfaces, asteroseismology of other stars faces formidable challenges to achieve even a portion of the same success. Modes with a large number of surface nodes fade from view because of geometrical cancellation over the surface of the star, leaving fewer modes to constrain the properties of the stellar interior. Of the remaining observed pulsations, it is difficult to distinguish between modes of different ℓ and m. This leaves ambiguity in modeling the pulsations as more than one model can fit the same set of modes.

Asteroseismology is one of the primary reasons for measuring and understanding the DAVs. Compared to most stars, white dwarfs are simple objects; meaningful information about the star can be determined with only a few pulsations. Physical parameters measured through asteroseismology include the hydrogen and helium layer masses, the H/He transition thickness, the core composition and the description of the

convection (Bradley 2001). Seismological modeling has been performed on these DA with some success and have found Hydrogen layer masses between $2\text{x}10^{-10}$ $M_\star$ and $2\text{x}10^{-4}$ $M_\star$ (Bergeron et al. 1993; Kepler et al. 1995; Pfeiffer et al. 1996; Bradley 1998; Bradley 2001).

The key to unambiguous model fitting of stellar pulsations is an accurate identification of each period with its corresponding k, ℓ, and m. While k cannot be directly measured because it describes the oscillations radially, ℓ and m are the angular features of the pulsation that appear on the surface. Various observational techniques have been introduced to find these values for the observed modes of DAVs.

1.3 Observations of Pulsators

1.3.1 Photometry

Some clues to the mode identity can be found by knowing the relationship between mode periods and their corresponding eigenvalues. Higher values of the radial order indicate a smaller displaced mass, a reduced restoring force, and consequently longer periods. In this way an indication of the radial order can be inferred from the period. A series of consecutive k with the same ℓ will show almost equal period spacings, where the spacing is smaller for larger values of ℓ.[5] In general, ℓ of observed modes should be small because otherwise the brightness variations will cancel over the surface of the star. When an axis of symmetry is introduced via rotation each mode is split into $2\ell+1$ modes with different values of m. The frequency spacing of a split mode depends on the speed of rotation (or the strength of the magnetic field). For high radial orders, the amount of frequency splitting approaches the limit $(1 - \frac{1}{\ell(\ell+1)})\Omega$, where Ω is the frequency of rotation. By looking for these uniform period spacings and frequency splittings, some mode identification is possible with time-series photometry.

DAVs, however, do not easily lend themselves to photometric mode identification. First, long sets of observations are necessary to obtain the required frequency resolution to detect the azimuthal splitting of modes. When obtained from a single site,

[5]Due to the chemically stratified layers of a white dwarf, the period spacings are not strictly uniform. This phenomena is known as mode trapping.

data gaps due to weather and setting stars create alias peaks in the Fourier transforms that can be detrimental to secure detection of modes. Second, certain characteristics of DAVs make identification of their pulsations difficult. Many hot DAVs lack enough modes to make a secure mode identification, and the pulsations on cool DAVs are too complex and variable.

Despite these difficulties, some success has been made in identifying the modes of DAVs. The introduction of the Whole Earth Telescope (WET) (Nather et al. 1990) ameliorated the aliasing problems by using a series of telescopes around the world to obtain continuous coverage of a star. Sufficiently long photometric studies of individual DAVs with WET and single telescopes have had some success in mode identification by finding frequency splittings (Handler, Romero-Colmenero, & Montgomery 2002; Bradley 2001; Pfeiffer et al. 1996; Kepler et al. 1995; Castanheira et al. 2004). Clemens (1994) studied the pulsations of the DAVs as a group and revealed that, especially for the hot pulsators, the modes cluster around certain periods that resemble a series of $\ell = 1$ modes. Kleinman et al. (1998) made advances in the study of the complex modes of the cool DAVs by examining 10 years of observations of G 29-38. He found a series of recurring modes that resemble a series of $\ell = 1$ modes. Though these are encouraging results, lingering doubts as to the identity of the individual modes remain, prompting the introduction of a mode identification technique that does not rely on the presence of other modes.

1.3.2 Time Series Spectroscopy

Measuring mode amplitudes and phases at different wavelengths is another method to distinguish between modes of different spherical degree. This same spectroscopic data also provide a method to measure another aspect of the pulsation and subsequently test the convective driving theory. We further develop this spectroscopic technique in the following chapters as we measure the pulsations of two DAVs.

Spherical Degree. To make secure, direct measurements of the spherical degree, attempts have been made to independently measure the values of ℓ with time series spectroscopy in the optical and ultraviolet (UV). This method, introduced by Robin-

son et al. (1995), uses the wavelength dependence of limb darkening along with our expectations of how a mode is distributed along the surface of the star to measure ℓ.

Limb darkening is the term used to describe why the outer edges of the visible disk of the sun appears darker than the center. The light seen from a star basically originates at a specific optical depth. When looking at the limb of a star, the optical depth does not originate as far radially into the star. Since the atmosphere of a star is cooler in the outer layers, the light emitted from the limb of the star is dimmer. As the opacity depends on wavelength, this effect becomes stronger at shorter wavelengths. Essentially, when looking in the UV, a smaller area of the stellar surface is emphasized by the star's light at the bluer wavelengths.

The UV light originates from less of the stellar surface, altering the geometrical cancellation experienced by a pulsation mode. The amount of alteration depends on how the pulsation is distributed across the surface of the star. Robinson et al. (1995) modeled the wavelength dependence of the pulsation amplitudes for different spherical degrees and compared them to UV data on G 117-B15A. The amplitudes of the dominant mode increased at shorter wavelengths as expected and were consistent with an ℓ=1 model. For an example of how the amplitudes vary with wavelength see Figure 1.2. Thus far four DAVs (PY Vul, G 226-29, G 117-B15A, and BPM 37093; Kepler et al. 2000, Kotak, van Kerkwijk, & Clemens 2004, Robinson et al. 1995, and Nitta et al. 2000) have been measured with this method and they mostly show an increase in the UV consistent with $\ell \leq 2$. However, not all modes show the same clearly rising amplitudes as expected for these low spherical degrees. We will clear up some of the ambiguity by proposing a solution to one strangely behaving mode in PY Vul.

The pulsation amplitudes across spectral lines also depend on the geometrical distribution of the mode. Both the opacity and consequently the limb darkening change across a spectral line. Again, how the amplitude varies with wavelength depends on the spherical degree of the mode. Clemens, van Kerkwijk, & Wu (2000), acquiring high signal-to-noise spectra of the DAV G 29-38, were the first to measure the wavelength dependent amplitudes across the Balmer lines ("chromatic amplitudes") of a DAV. The studies to date (Clemens, van Kerkwijk, & Wu 2000; Kotak, van Kerkwijk, & Clemens 2002; Kotak et al. 2002; Kotak, van Kerkwijk, & Clemens 2004) success-

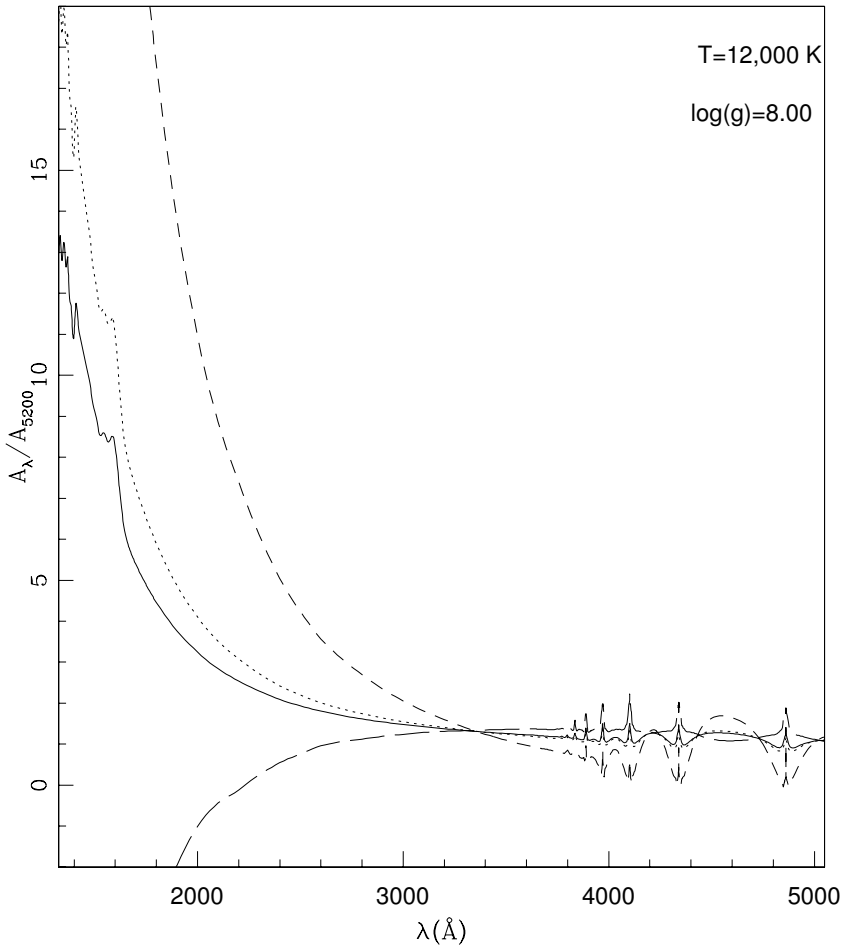

Figure 1.2 An example of how the relative amplitudes behave for different spherical degrees using a WD model atmosphere of T=12,000 K and log(g)=8.0. Solid is ℓ=1; dotted is ℓ=2; short dashed is ℓ=3; and long dashed is ℓ=4.

fully identify modes with $\ell \leq 2$. To obtain the necessary signal-to-noise at the required short exposure times on even these bright DAVs involved using the Keck 10-m telescope. This severely limits the usefulness of this mode identification technique on ZZ Cetis. We give hope to this technique by showing an innovative analysis technique that improves our ability to gain information from these spectra.

Velocity. Time-series spectroscopy can be used to measure another aspect of the stellar pulsations. As discussed earlier, the pulsations are non-radial, so stellar material moves parallel to the surface of the star. The portion that moves along our line-of-sight will produce periodic Doppler shifts of the spectral lines. As the flux and velocity do not have the same geometric cancellation for different values of ℓ, the ratio of the velocity and the flux can also indicate the spherical degree. Measurements of the velocity curve of a DAV were first performed by van Kerkwijk, Clemens, & Wu (2000). They found velocity amplitudes as high as 4 km s^{-1} for one mode on G 29-38. Thus far, the FTs of measured velocities have a relatively high noise level compared to their flux measurements, preventing accurate amplitude and phase measurements. By using a variation of this observational technique, we will show how to improve the measured velocities.

The measurements of the periodic velocity variations provide a way to test the convective driving theory described earlier. This theory predicts that the velocity is not affected by the convection zone like the flux variations. While the fluxes are delayed, diminished and distorted by the convection zone, the corresponding motion is not. In other words, the velocity is a measure of the amplitude and phase of the pulsations below the convection zone. The convective driving theory makes specific predictions about the frequency dependence of the attenuation and phase delay caused by the convection zone (see §1.2.2). Comparing the velocity and flux amplitudes and phases for different frequency modes tests this prediction of the convective driving theory. Van Kerkwijk, Clemens & Wu (2000), Kotak et al. (2002), Kotak, van Kerkwijk, & Clemens (2002) have measured velocity amplitudes and phases for 3 DAVs. Their data are insufficient to attest to the predictions of the convective driving theory, and while our velocity measurements add to the growing evidence, they also do not provide firm conclusions.

1.4 Overview

The work presented here consists of two projects that develop the use of time series spectra for studying ZZ Ceti stars. For each data set we aspire to measure the periodic velocity variations and identify the modes on each star. The general results of these efforts include improvements in the measurement of pulsation velocities, in the ability to do mode identification, and in our knowledge of ZZ Ceti pulsators.

The first project begins in the next chapter with analysis of the only high-resolution, time series spectroscopy of a DAV. As compared to its lower resolution counterpart, these data sacrifice some of the light for increased spectral resolution and ultimately better measurements of the Doppler shifts. The large amplitudes and the brightness of G 29-38 made it an ideal target for this project. We use the measurements of the velocity and flux variations to test the predictions of the convective driving theory. Also, with the improved velocity measurements, we discover a new phenomena: a combination mode in the *velocity* curve. The theories of Wu (2001) and Brickhill (1992a) that describe the combination modes in the flux curves cannot account for a velocity combination by the same mechanism. Chapter 3 discusses the observed properties of this mode and places it into the context of the current theories of pulsation.

The second project begins in Chapter 4 by showing the analysis of low-resolution, time series spectra of the star PY Vul. We find that the velocities of PY Vul are too small to measure with the LRIS data, and only present upper limits. However, these data did provide useful mode identifications for PY Vul. Though unable to obtain enough information with previous analysis strategies, a new method reveals informative chromatic amplitudes of the six dominant modes present in the star. One of these modes distinguished itself by showing distinct ℓ=4 characteristics. Having never before observed modes larger than ℓ=2 on DAVs, this result was unexpected. However, our optical chromatic amplitudes are not the only peculiar aspect to the pulsations on PY Vul and we propose the ℓ=4 mode as the solution to all its mysteries. In Chapter 5 we discuss all observations of PY Vul and find them consistent with our ℓ=4 hypothesis.

Chapter 2

High-Resolution Spectroscopy of the Pulsating White Dwarf G 29-38

Unbelievable sights
Indescribable feeling
Soaring, tumbling, free-wheeling
through an endless diamond sky.

"A Whole New World"
Lyrics by Tim Rice

We present the analysis of time-resolved, high-resolution spectra of the cool white dwarf pulsator, G 29-38.[6] From measuring the Doppler shifts of the H_α core, we detect velocity changes as large as 16.5 km s^{-1} and conclude that they are due to the horizontal motions associated with the g-mode pulsations on the star. We detect seven pulsation modes from the velocity time series and identify the same modes in the flux variations. We discuss the properties of these modes and use the advantage of having both velocity and flux measurements of the pulsations to test the convective driving theory proposed for DAVs. Our data show limited agreement with the expected relationships between the amplitudes and phases of the velocity and flux modes.

[6]This analysis of G 29-38 was originally published in the Astrophysical Journal (see Thompson et al. 2003).

2.1 Introduction

G 29-38 (ZZ Psc) is an extensively observed, V=13.05 magnitude, pulsating white dwarf that lies at the cool end of the DA instability strip. Like many cool DAVs, its oscillation properties are highly variable. In one month it may exhibit a dominant period of 615 s and amplitudes of 6% (Winget et al. 1990). In another month it may have a dominant period of 809 s and amplitudes of 4% (Kleinman et al. 1998). Occasionally it shows no measurable pulsations at all. In addition to being confusing in themselves, these amplitude changes frustrate attempts to identify eigenfrequencies that might allow seismological analysis of the internal structure of G 29-38.

Kleinman et al. (1998) accomplished a breakthrough in seismology of G 29-38 by compiling and analyzing many months of time series photometric observations. They found a consistent pattern of recurring frequencies in the data. This result is reassuring to seismologists because it suggests that the observed frequencies represent eigenfrequencies that carry information about internal structure. Kleinman et al. (1998) presented an analysis of the pattern of modes, concluding they are most likely modes of the first spherical harmonic degree (ℓ= 1). The conclusion was based on the match of the spacing between modes to theoretical expectations for ℓ= 1 modes of consecutive radial eigennumber, and upon the observation of triplet structure in some of the modes. Rotation should split ℓ= 1 modes into three components of different azimuthal quantum number (m). Seismological analysis of the mode pattern by Kleinman et al. (1998) yielded a mass estimate of 0.6 $M_{\odot}$ for an assumed Hydrogen layer mass of 10^{-4} $M_{\star}$.

Kleinman et al. (1998) had no way to verify their mode identification by direct observation, but subsequent time series spectroscopy at high signal-to-noise by Clemens, van Kerkwijk, & Wu (2000) provided verification for some modes. Because of the wavelength dependence of limb darkening, pulsation amplitudes at each color are sensitive to the degree (ℓ) of pulsation modes. Using time-resolved spectroscopy from Keck II LRIS (Oke et al. 1995), Clemens, van Kerkwijk, & Wu (2000) confirmed that most of the modes are ℓ= 1. The only exception is a mode at 777 s that Clemens, van Kerkwijk, & Wu (2000) identify as ℓ= 2.

In addition to mode identification, van Kerkwijk, Clemens, & Wu (2000) detected velocity shifts associated with pulsations of G 29-38, and thereby obtained the first direct measurements of the size of the surface motions in a pulsating white dwarf. Because surface velocities are distributed as the derivative of a spherical harmonic, their integrated contribution does not cancel in the same way as the spherical harmonically distributed flux variations. As a result, the ratio of velocity to flux amplitudes is sensitive to ℓ, and measurements of these ratios also support the conclusion that the 777 s mode is $\ell = 2$ and the remainder $\ell = 1$. Later, Kotak, van Kerkwijk, & Clemens (2002) showed that the 918 s mode observed by van Kerkwijk, Clemens, & Wu (2000) also has $\ell = 2$.

Encouraged by the success of the LRIS observations (van Kerkwijk, Clemens, & Wu 2000), we aspired to improve the velocity measurements by observing at higher resolution. Accordingly, we obtained a 5 hour time series of the H_α core of G 29-38 with the Keck I High Resolution Echelle Spectrograph (HIRES) (Vogt et al. 1994). We used a narrow slit to improve the velocity measurements of G 29-38 at the expense of some quality in the flux measurements. We have successfully detected the pulsation velocities, confirming the LRIS observations of van Kerkwijk, Clemens, & Wu (2000), and allowing us to measure the sizes and relative phases of the velocity and flux variations.

Beyond the insight our data offers into the physical size of pulsational motions, measuring both the velocity and flux variations of the modes provides a means to test theories of mode excitation. Originally, the classical $\kappa - \gamma$ mechanism was proposed as a plausible driving mechanism for the pulsations (Winget et al. 1982b; Dziembowski & Koester 1981; Dolez & Vauclair 1981). Later, Brickhill (1983) recognized that the convection zone responds immediately to the flux perturbations from the radiative interior and demonstrated that the convection zone could be the center of mode driving. His convective driving mechanism, as further developed by Goldreich & Wu (1999a), makes explicit, testable predictions concerning the relationship between the phases and amplitudes of the observed modes. Our measurements agree with the basic predictions of this model, but are not sufficient to provide rigorous tests of how mode qualities change with frequency.

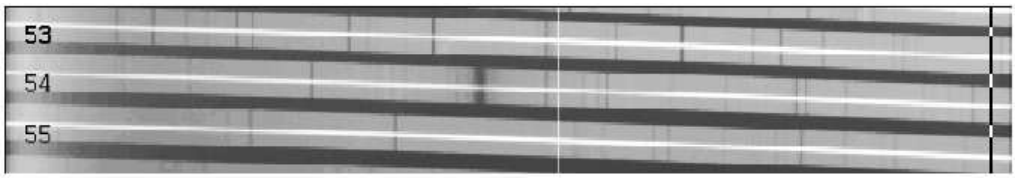

Figure 2.1 The average of the spectral images prior to reduction. The echelle orders are labeled on the left. H_α is located at the center of the 54th order.

2.2 Observations and Reduction

On September 16, 1997, we acquired a series of 236 spectra of G 29-38 using HIRES (Vogt et al. 1994) on the Keck I telescope. We used the red collimator, the KV408 order blocking filter, and the C2 decker, which yielded a slit width of 0.861". In this configuration, the 24-micron pixel Tektronix 2048EB2 CCD with 2x2 binning gave a dispersion of 0.095 Å per binned pixel, and a scale of 0.38" per binned pixel in the spatial direction. The effective spectral resolution, defined by the slit width, was 0.215 Å.

We began our sequence of exposures at 08:28:02 UT (measured by the observatory clock and recorded in the image headers). The exposure time for each spectrum was 50 seconds with an additional 28 seconds required to read and wipe the CCD, yielding a duty cycle of 64%. Since reading the entire CCD would have taken much longer and thus unacceptably reduced the duty cycle, we only read a region containing three orders (53, 54, and 55) with the middle order centered on H_α. For this small region, the readout time with two amplifiers was not significantly better than with one, so we used one amplifier to eliminate complications arising from differences in gain and linearity. The exposure levels in our 50 second integrations ranged from 35 electrons in the core of H_α to 70 in the wings. The moon was full, so the background sky was relatively high, ranging from 16 to 40 electrons with clearly visible features of the solar spectrum, and the shot noise from the sky is comparable to the read noise of 4.5 electrons. In Figure 2.1 we show a raw spectral image for the average of all 236 images. We reduced only the central order since we were interested in the H_α line and did not need the extended continuum in the other orders.

We acquired a well-exposed spectrum of the halogen lamp to use for spectral flats and of the Thorium-Argon lamp to use for wavelength calibration. We also acquired spectra of the flux standard G 126-18, but in this paper we present only relative photometry, and have made no attempt at absolute flux calibration.

The seeing during our run, as measured from spatial profiles, averaged about 1.2" fwhm, so the relatively narrow slit makes photometry problematic. Moreover, to avoid introducing potential periodic variations, we did not use the image rotator; so differential refraction slowly changed the amount of light passing through the slit. As we shall see, these losses did not prevent us from measuring periodic variations in the brightness of G 29-38.

We reduced our 236 spectral images using standard Image Reduction and Analysis Facility (IRAF) routines (Tody 1986). We removed the bias level by fitting and subtracting a plane to the prescan region of each image. We removed the blaze function and the flat field variations in one step by dividing the data by the normalized average of the halogen lamp exposures. Normalization was accomplished by dividing the average image by the mean pixel value of the image. To extract individual spectra, we first calibrated our extraction parameters using the average spectrum (see Figure 2.2) and the IRAF apall routine. This gave values for the slope, curvature, and spatial profile of the average spectrum. We assumed individual spectra would have similar values, but might be shifted along the slit, and conducted optimal extraction of the lower signal-to-noise, individual spectra with spatial position as the only free parameter. The apextract algorithms we applied are based on the work of (Horne 1986). The measured motion of G 29-38 along the slit provides an estimate of the motion across the slit; we used these to assess the slit losses and wavelength stability.

Figure 2.2 shows a typical individual spectrum after reduction and wavelength calibration. The signal-to-noise is about 8 in the wings of the line and 5 in the line core. The lower panel shows an average of all 236 spectra and was constructed by averaging the reduced spectral images and performing a single extraction. We extracted two time series from the individual spectra, one representing the changes in velocity and the other representing changes in flux.

To examine the line-of-sight velocity modes on the star, we measured the Doppler

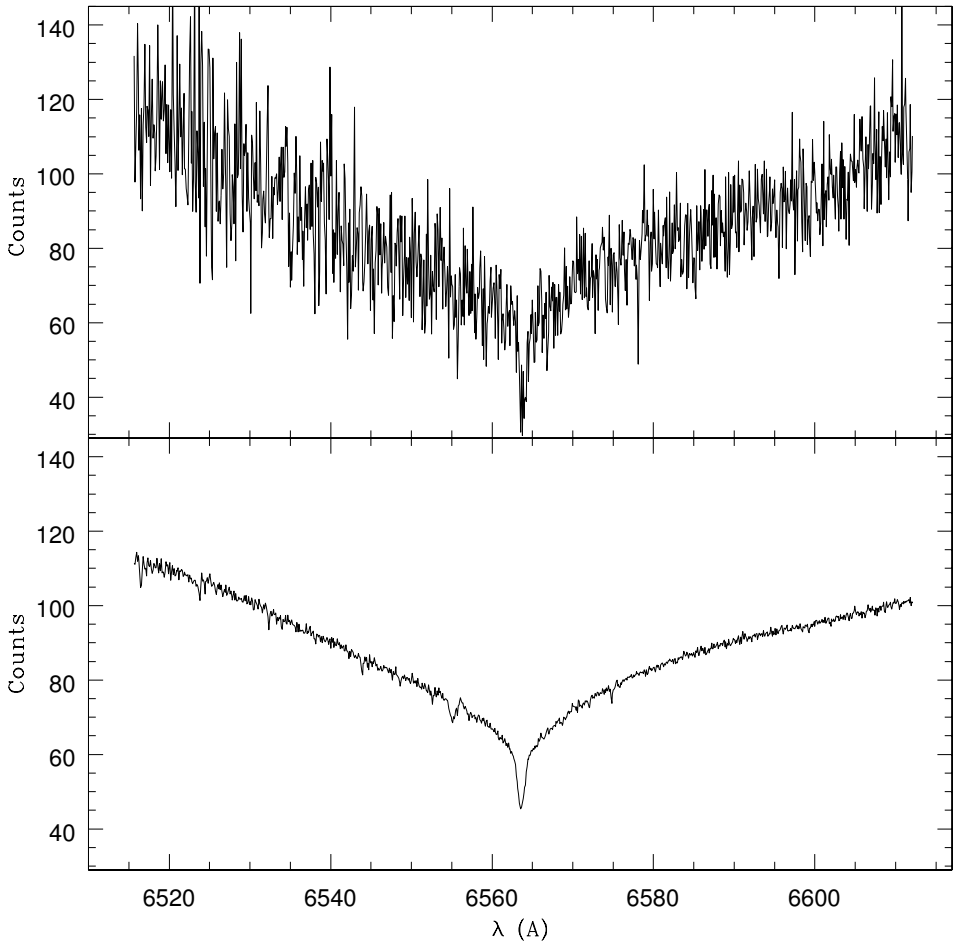

Figure 2.2 An example of an individual spectrum (top panel) and the spectrum extracted from the average of all 236 spectral images (bottom panel). The dominant feature at 6555 Å is due to scattered light. Other features are telluric water lines.

shift of the H_α line in each spectrum. Attempts at using cross-correlation against a smoothed average spectrum yielded inconsistent results; the amplitude of the shift was skewed by the amount of the spectrum included in the correlation. As an alternative, we fitted each spectral line to obtain the location of the central wavelength. A Gaussian and Lorentzian, forced to have the same central wavelength, super-imposed on a linear continuum, were fit to the average spectrum over the range 6557.5-6570.0 Å. Using this description of the line, we fit the average spectrum until no significant improvement

in chi-square was achieved; resulting in a reduced chi-square of about 0.5. We then fit each individual spectrum using the average spectrum's fit as the initial conditions; allowing only the central wavelength, the height of the continuum, the slope of the continuum, and the flux contained in both the Gaussian and Lorentzian to vary for each fit. The width of the Gaussian and the Lorentzian were fixed to the average spectrum's fitted values. A subtraction of the central wavelength, established with the average spectrum, yielded the spectral shift for each spectrum, and thus line-of-sight velocities. We observe Doppler shifts as large as 0.36 Å (3.8 binned pixels), corresponding to a velocity of 16.5 km s^{-1}. Figure 2.3 shows the velocity curve resulting from this reduction.

To obtain the relative changes in the flux of the star, we summed each spectrum from 6553 to 6573 Å and divided the resulting light curve by the mean of these values. The light curve, presented in the lower panel of Figure 2.3, is normalized by a second order polynomial fit in order to remove long period variations introduced by extinction and differential refraction and yield fractional changes in flux. We observe flux variations as large as 20% from the mean flux. Two sections of the light curve, as indicated in Figure 2.3, appear to be obstructed by clouds and thus not included in the analysis of the light curve. Increased sky levels concurrent with the decrease in star light confirms this conclusion for the latter region. The Fourier transform and least squares fits of the light curve discussed in §2.3 do not include these regions.

We measured the effect of flexure on our data by performing this same fitting technique on the spectrum of the sky background in each spectrum. The central wavelength of the sky showed little trend and only varied by at most 0.2 pixels ($\sim$ 1 km s^{-1}).

To be certain the velocities detected are not due to the star moving perpendicular to the slit, we estimated the loss of light that would also result from this motion. We fitted a Gaussian distribution to the spatial profile and assumed the same profile in the dispersion direction (correcting for the different spatial scales). For a 0.36 Å shift (16.5 km s^{-1}), the largest detected spectral shifts, we would expect to see flux variations as large as 30% correlated with the shifts. The largest measured flux variations are less than 20% and are not concurrent with the largest spectral shifts. Furthermore,

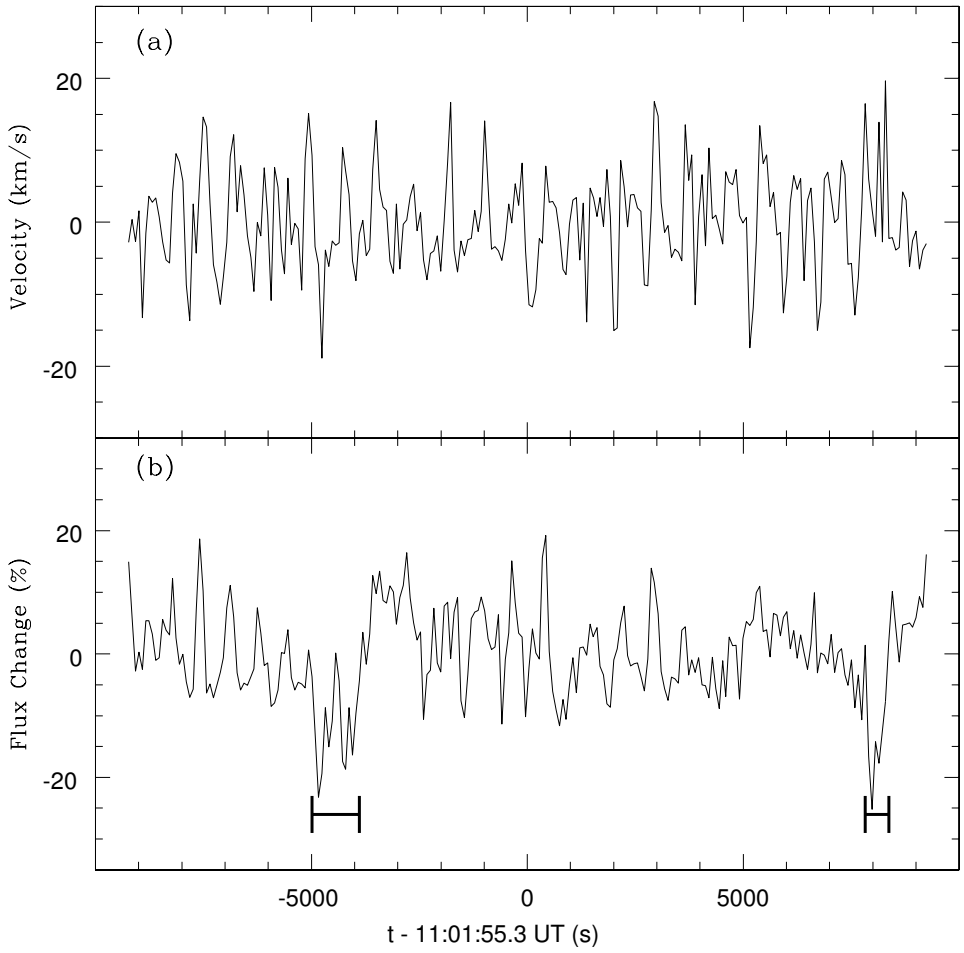

Figure 2.3 **(a)** The line-of-sight velocity curve, where a positive velocity indicates a red shift. A typical error on a velocity measurement is 3 km s^{-1}. **(b)** The change in flux normalized by a fitted parabola. The marked regions are not used in the Fourier transform or the least-square fits of the flux curve.

if stellar wander caused the observed spectral shifts, we would expect to see peaks at half the period of the velocity modes. Looking ahead to the Fourier transforms of the velocity and flux variations (Figure 2.4), we do not see peaks of this sort. Thus, we conclude that stellar motion in the slit is not the primary source of the detected wavelength shifts.

2.3 Flux and Velocity Periodicities

We began analysis of the velocity and flux time series by investigating the periodicities present in both. Figure 2.4 shows the Fourier transforms (FTs) of the velocity and flux curves introduced earlier. The three dominant modes in both curves appear at approximately the same frequencies, indicating that the velocity and flux modes are correlated. As such, our data confirm the results of van Kerkwijk, Clemens, & Wu (2000), showing significant line-of-sight velocity variations due to the g-mode pulsations on the star.

To further convince ourselves that these Doppler shifts exist in the spectra, we averaged together individual spectra with similar velocities. Figure 2.5 shows two spectra created by averaging together 30 spectra fit with large positive velocities (redshifts greater than 6.9 km s^{-1}) and 30 spectra with large negative velocities (blue-shifts greater than 6.9 km s^{-1}). A noticeable wavelength shift in the center of the line can be seen between these two averages. Hence, we conclude that these Doppler shifts are indeed apparent in the data and not just artifacts of the fits.

The noise level in our velocity curve is significantly better than that measured by van Kerkwijk, Clemens, & Wu (2000) while the noise in the flux is worse. This is expected since our technique used a narrow slit to improve velocity measurements at the expense of flux. Our lower noise velocity curve makes the detection and identification of frequencies more reliable relative to our flux measurements. Moreover, there are significant peaks in the velocity transform with no apparent counterparts in the flux transform. Consequently, we analyzed the velocities first and then fitted the flux amplitudes under the assumption that the modes identified have the frequencies measured in the velocity transform.

We began by identifying the periodicities in the velocity curve and removing them consecutively in order of decreasing amplitude. Using the FT's value for the frequencies and phases as the initial conditions, the velocity curve was fit to a function of the form $A_v \cos(2\pi f t - \Phi_v) + C$ where A_v is the amplitude, f is the frequency, Φ_v is the phase and C is a constant offset. We removed this fitted cosine wave from the data and then repeated the process by identifying the next frequency until no significant peaks could

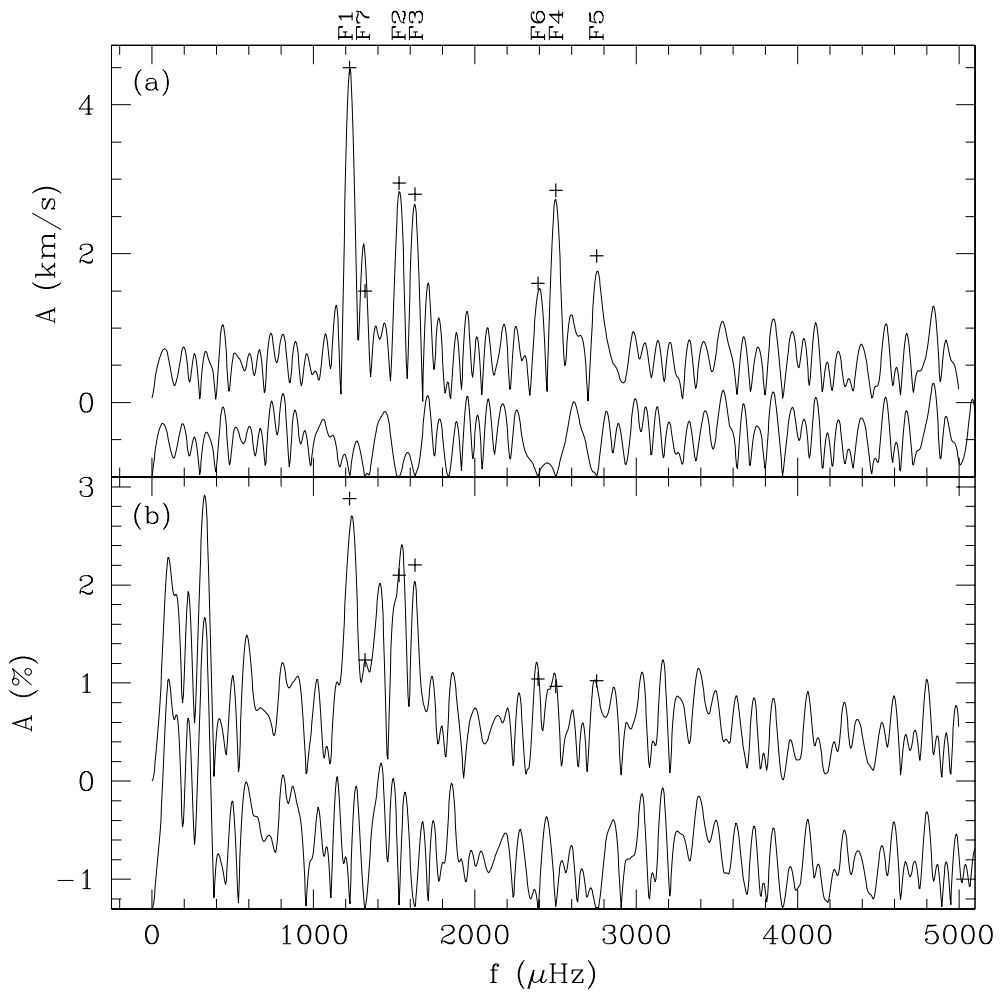

Figure 2.4 The amplitude Fourier transforms of the line-of sight velocity curve **(a)** and relative flux curve **(b)**. The seven modes are marked at the extracted values in both FTs. The amplitude FTs of the residuals are plotted below each FT. The flux residual is off-set by 1.3% while the velocity residual is off-set by 1.0 km s^{-1}. The low frequency peaks not extracted from the flux transform are probably atmospheric effects and not inherent to the star.

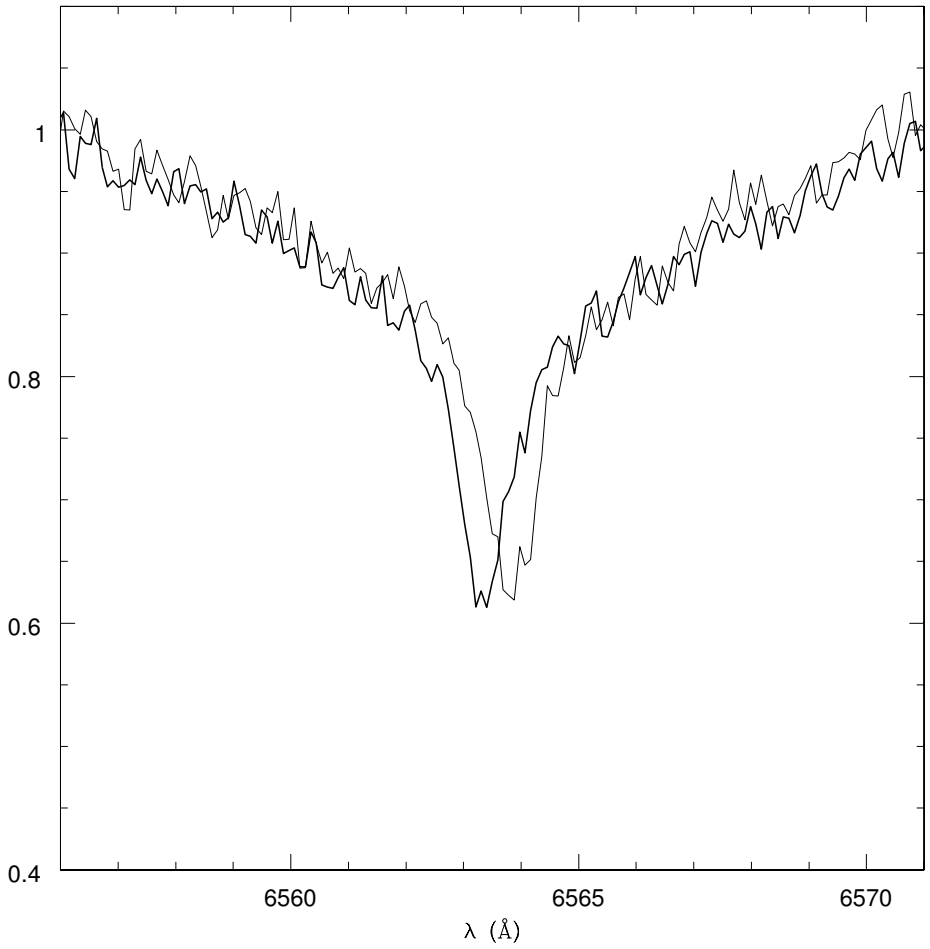

Figure 2.5 The average of 30 blue shift spectra (thick line) and 30 red shift spectra (thin line). The spectra included in each average is measured with a red or blue shift greater than 6.9 km s^{-1}.

be determined from the Fourier spectrum. A final simultaneous fit of the data to a linear combination of the cosine waves for all identified frequencies yielded the values for A_v, f and Φ_v (Table 2.1). We used the average of the time stamps on the 236 spectra (11:01:55.3 UT) as the zero point for determining the phase.

We estimated the expected noise in the velocity time series by considering two components: one from the wandering of the star's position within the slit and the other from our ability to fit the line center in the relatively noisy individual spectra.

By measuring the motions of the star along the slit, and removing a parabola to account for slow changes in position with airmass, we constructed an estimate of the rms amplitude of the motions. If we assume that motions across the slit have the same amplitude, this translates into an rms velocity error of 0.4 km s^{-1} with the largest extent being 1 km s^{-1} (0.36 pixels spatially). To assess the possible impact of periodic wandering, we calculated a Fourier transform of the motions. It shows significant peaks at various guiding frequencies, but they are all far smaller (a factor of 10 to 20 times) than the velocity amplitudes detected in G 29-38 and do not have the same frequencies. The formal error of our velocity fits to individual spectra is $\sim$ 3.8 km s^{-1}, much larger than the errors from slit motions. If we assume these are Gaussian, then they should translate into an average noise in the fourier transform[7] of 0.5 km s^{-1}. Using this noise level, our fits to the velocity curve yield a reduced chi-square of about 1.4, confirming that 0.5 km s^{-1} is a slight underestimate of the noise. We can get a separate estimate of the noise by averaging the power in the 3.5-5.0 mHz region of the velocity FT. This yields an error of $\sim$ 0.6 km s^{-1}. We believe that the slight excess may be intrinsic variations due to the low-amplitude pulsations, which are known to exist in this frequency range. The noise level of 0.6 km s^{-1} gives a reduced chi-square of about 1.0; we use this noise level to determine the errors reported in Table 2.1.

To determine the significance of the identified velocity peaks, we conservatively used the noise level determined from the background average power of the FT (0.6 km s^{-1}). As such, all 7 modes lie at or above 3σ. However, to be certain that these amplitudes could not occur by chance, we calculated the false alarm probability[8] (Horne & Baliunas 1986; Kepler 1993). The five largest velocity modes have less than 1% chance of only being due to noise. The significance of F6 and F7 are questionable since they have a false alarm probability of $\sim$ 0.5. They appear more significant in the FT because the side lobes of F1 and F4 respectively increase their apparent size.

[7]Since the FT is normalized in order to conserve the amplitudes, the noise in the data, σ_{data}, relates to a noise level of the FT, σ_{ft}, according to the relation $\sigma_{data} = \frac{1}{2}\sqrt{N}\sigma_{ft}$, where N is the number of data points.

[8]The false alarm probability is the probability that one peak of randomly distributed noise in N independently sampled frequencies would appear at or above the power of the observed mode. For $z = P_{obs}/ < P >$, FALSE is given by $1 - [1 - e^{-z}]^N$.

Table 2.1. The amplitudes, phases, R_v, and $\Delta\Phi$ for each mode observed in G 29-38.

	P (s)	f (μHz)	A_v (km s^{-1})	Φ_v (°)	A_L (%)	Φ_L (°)	R_v ($\frac{10km}{rad/\%}$)	$\Delta\Phi$ (°)
F1	816	1224.9 ± 3	4.53 ± 0.4	270 ± 6	2.88 ± 0.5	224 ± 11	20.4 ± 4	46 ± 12
F2	653	1532.1 ± 5	2.95 ± 0.4	216 ± 9	2.11 ± 0.5	165 ± 15	14.5 ± 4	52 ± 17
F3	614	1629.1 ± 5	2.79 ± 0.4	304 ± 9	2.20 ± 0.5	253 ± 14	12.4 ± 4	50 ± 17
F4	399	2503.4 ± 5	2.84 ± 0.4	177 ± 9	0.97 ± 0.5	12 ± 32	18.7 ± 11	165 ± 33
F5*	363	2754.9 ± 7	1.97 ± 0.4	31 ± 13	1.02 ± 0.5	35 ± 30	11.1 ± 6	-5 ± 33
F6	418	2391.9 ± 8	1.57 ± 0.4	280 ± 16	1.04 ± 0.5	4 ± 30	10.0 ± 6	275 ± 34
F7	757	1321.1 ± 9	1.48 ± 0.4	137 ± 17	1.23 ± 0.5	260 ± 25	14.4 ± 8	-124 ± 31

*F5 is the combination mode, its frequency is the sum of F1 and F2.

Note. — For each mode, $R_v = (A_v/\omega)/A_L$ and $\Delta\Phi = \Phi_v - \Phi_L$. The reported errors reflect a reduced chi-squared of 1 for the least-square fits to the flux and velocity curves.

After completing our fits to the velocity curve, we extracted the periodicities in the flux curve by fitting it with a combination of cosine waves, fixing the frequencies to the fitted velocity frequencies. Table 2.1 contains the amplitudes and phases for the seven modes extracted using this technique. The low frequency peaks in the flux FT are not included since they are not present in the velocity curves and likely result from atmospheric effects, and from an observational technique not optimized for flux measurements. Consequently, the flux curve is not well accounted for by the linear combination of the seven cosine waves. To obtain the errors from the fit we scaled up the error on each measurement to obtain a reduced chi-square of 1. This is reflected in the errors presented in Table 2.1.

Since we measured the flux modes by fixing the frequencies to the velocity mode frequencies, we determined their significance by calculating the odds that noise would create a peak of that amplitude at the exact frequency we expected to see one. We

estimated the noise level from the average of the flux power FT in the region from 3.5-5.0 mHz to be 0.5%. The smallest flux peaks (F4, F5, and F6) lie around 2.3σ and have a 2% probability that Gaussian distributed noise would show a peak of that power at the expected frequency.

The frequencies we have measured are all similar or identical to g-mode frequencies previously measured in flux variations of this star. The mode F4 is almost, but not exactly, two times the largest mode F1. Both of these modes are listed in the tabulated photometric modes for G 29-38 (see Kleinman et al. 1998 and Vuille 2000a). Near-resonances of this sort are common in the large amplitude ZZ Ceti stars (e.g. BPM 31595; O'Donoghue, Warner, & Cropper 1992) but not understood. They do not originate from harmonic distortion of pulse shapes, because that mechanism generates exact frequency combinations.

However, the signal at F5 is the exact sum of the two largest modes to within the measurement error, as we might expect from pulse shape distortion. We do not see any other combinations or harmonics in the spectrum. It is quite common in flux measurements to see a signal at the sum of two large modes, but not be able to detect their individual harmonics (see Handler, Romero-Colmenero, & Montgomery 2002 or McGraw & Robinson 1975). In this respect, the velocity transform of Figure 2.4 resembles a typical flux transform for G 29-38. However, the existence of a velocity combination presents a challenge for the convective driving theory, which does not predict distortion in velocity variations. We discuss a possibility for answering this challenge in Chapter 3.

Because F5 is unexpected, we have worried about possible non-linearities in our fitting procedure that might generate a false combination signal. If the spectral fitting process is non-linear in some way, or if it is biased by the flux, which is varying at the same frequencies but different phase, then harmonics or combination frequencies might be generated as artifacts during the analysis. We have experimented with different fitting routines and also applied cross correlation between the average spectrum and each individual spectrum. In every case, the time series shows a signal at F5, although its significance is sometimes lower. Furthermore, none of the techniques generates combinations or harmonics of other modes in the Fourier transform. We conclude

that F5 is a combination frequency present in the star, but emphasize the need for further observations to establish whether velocity combinations are a persistent feature of large amplitude ZZ Ceti pulsators. The first measurement of pulsational velocities by van Kerkwijk, Clemens, & Wu (2000) did not show velocity combinations, but the signal-to-noise in their velocity curve was less than one-half of ours, and they would not have been able to detect a signal the size of our F5.

2.4 Testing the Convective Driving Theory

With the amplitudes and phases of the seven detected pulsation modes, we have knowledge of the motions and the temperature changes at the surface of this ZZ Ceti. The usefulness of these measurements goes beyond calibrating the size of the velocity variations at the surface of G 29-38; it allows us to test specific predictions of the convective driving theory, concerning the relationship between the flux and velocity of the modes. In the convective driving mechanism described by Brickhill (1983) and Goldreich & Wu (1999a), driving occurs because of the convection zone's response to the flux perturbations. From this interaction, the flux variations are distorted while the velocities basically traverse the convection zone undiminished. Having both velocity and flux measurements of the pulsation modes, we are able to test the convective driving theory by comparing our data with the analytic predictions of Goldreich & Wu (1999a) and the numerical model of Wu & Goldreich (1999).

We have presented the frequency, amplitudes and phases of all seven extracted modes in Table 2.1. Of these modes, the first four have been previously observed in this star (Kleinman et al. 1998; van Kerkwijk, Clemens, & Wu 2000). To see the relationship between the two measurements of the modes, we calculated the relative amplitude, $R_v = (A_v/\omega)/A_L$ [9], and the difference between the velocity and flux phases, $\Delta\Phi = \Phi_v - \Phi_L$, in accordance with the conventions used by van Kerkwijk, Clemens, & Wu (2000). The relative amplitude is a ratio of the velocity amplitude (A_v), scaled by the radian frequency ($\omega = 2\pi f$), and the flux amplitude (A_L); by including the frequency, R_v depends only on ℓ, and not on frequency, for adiabatic pulsations (see

[9] The units of R_v are reported as $10 km/rad/\% = 1000 km/rad = Mm/rad$.

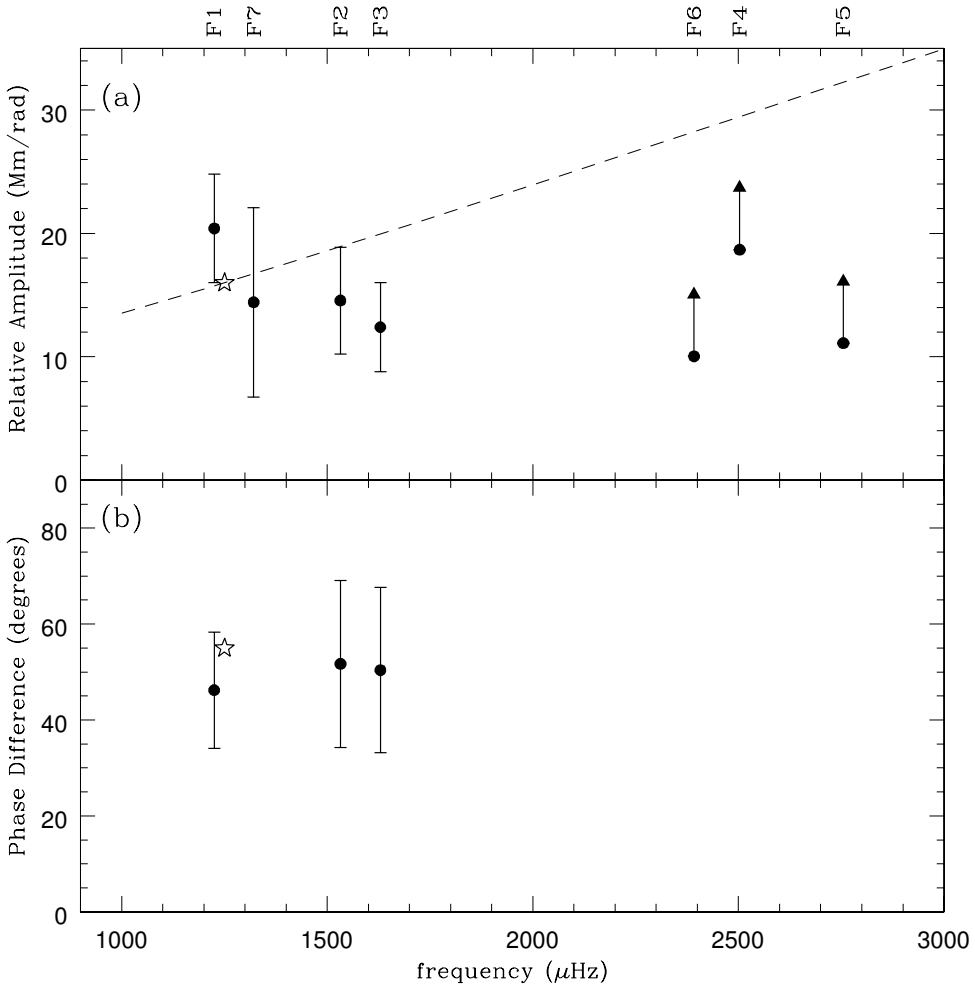

Figure 2.6 A plot of the relative amplitude R_v **(a)**, and the phase difference $\Delta\Phi$ **(b)** versus frequency for each mode. The star in each plot represents the prediction made by Wu & Goldreich (1999) with their nonadiabatic calculations of g-modes. The dashed line represents the increase in R_v expected from the predictions of Goldreich & Wu (1999) (for $\tau_c = 250$ s).

Dziembowski 1977; Clemens, van Kerkwijk, & Wu 2000). Only $\Delta\Phi$ of the first three modes were confidently measured and have values around 50°. The other modes have such low flux amplitudes that the fitted phases could have been easily swayed by noise. Both the relative amplitudes and the phase differences have values similar to the previous measurements of this star (van Kerkwijk, Clemens, & Wu 2000). The

R_v range from 10 to 20 Mm/rad; none is as high as the mode identified as $\ell = 2$ by van Kerkwijk, Clemens, & Wu (2000) and Clemens, van Kerkwijk, & Wu (2000) ($R_v = 27 \pm 11$ Mm/rad for the 777 s mode). Hence, these modes likely have a spherical degree of one, as expected from the conclusions of Kleinman et al. (1998), and measured directly for F1, F2 and F3 by Clemens, van Kerkwijk, & Wu (2000).

We can interpret some of these measurements in the context of the analytical theory of the convective driving mechanism (Goldreich & Wu 1999a). During an adiabatic pulsation, the maximum velocity occurs a quarter cycle after the flux maximum. However, the large heat capacity of the convection zone alters this basic picture by bottling up heat, thereby reducing the amplitude and delaying the phase of the flux perturbations. This will decrease the difference between the phases of the velocity and flux and increase the ratio between the velocity and flux amplitudes.

Our measurements agree with these basic predictions of the model; we observe the values of $\Delta\Phi$ to be less than 90° and R_v is larger than expected for an adiabatic mode (van Kerkwijk, Clemens, & Wu 2000). We can also specifically compare our data to the model since Wu & Goldreich (1999) calculated their model for a star similar to G 29-38. For a 800 s mode on a 12,160 K star with $\omega\tau_{th} = 0.8$, their model shows a phase difference of 55° and relative amplitude of 16 Mm/rad. The 818 s mode measured by van Kerkwijk, Clemens, & Wu (2000) confirmed this prediction ($\Delta\Phi = 44° \pm 19°$; $R_v = 11 \pm 4$ Mm/rad). Our measurements of F1 at 817 s mode also agree within the errors to the model calculations. For a graphical comparison, Figure 2.6 plots our data along with the results of this model.

Another result of the convective driving mechanism (Goldreich & Wu 1999a) is the frequency dependence of the interaction between the convection zone and the temperature variations. For larger values of the product of the thermal adjustment time, τ_c, and the radian frequency, ω, the convection zone has a larger effect on the flux variations. In fact, convective driving can only cause overstability of a mode when the inequality $\omega\tau_c \geq 1$ is satisfied. As such, we are able to determine a low estimate of the thermal adjustment time from the longest period mode ($\tau_c \geq 130$ s).

From this $\omega\tau_c$ dependence, we expect frequency trends in the relative amplitude and phase difference. With increasing frequency, more flux is absorbed, reducing

the measured flux amplitude (A_L) with respect to the distance the material travels on the star (A_v/ω). Thus, the relative amplitude should increase. Also, with smaller periods, the flux variations experience more phase delay and the difference between the velocity and flux phases become smaller and farther from 90°. Goldreich & Wu (1999a) quantifies these trends with expressions for the attenuation and phase delay of the flux variations. The observed flux amplitude is attenuated by the factor $(1 + (\omega\tau_c)^2)^{-0.5}$ and the flux phase is delayed by $\arctan(\omega\tau_c)$. Thus, due to the presence of $\omega\tau_c$ in these expressions, larger frequencies in the same star should have larger values of R_v and smaller values of $\Delta\Phi$.

Figure 2.6 shows our measurements of R_v and $\Delta\Phi$ as a function of frequency for the purpose of looking for these trends. Neither plot appears to behave as expected, basically showing no obvious variations with frequency. Unfortunately, the comparison to the model is drastically limited by the size of our errors. This is especially notable for modes F4, F5 and F6. Their flux amplitudes are likely inflated by noise and thus, the values for R_v are underestimated. For this reason, we indicate lower limits for these modes in Figure 2.6. To compare the measurements with the model we have plotted the trend in R_v expected by theory in Figure 2.6. The predicted trend is not apparent in our data. However, due to our large error bars we cannot rule it out. We are not the first to fail to detect the trend; time-resolved spectra of HS 0507+0434B (Kotak, van Kerkwijk, & Clemens 2002) failed to show the predicted trend for R_v and showed the opposite trend for $\Delta\Phi$.

2.5 The Spectral Profile of G 29-38

The time-resolved, high-resolution spectroscopy of G 29-38 enables us to explore a mystery concerning the observed line profile of the H_α core of ZZ Cetis. Our data are similar to the observations made by Koester et al. (1998) to measure the rotation rate of DA white dwarf stars except that we have a time series of 50 second exposures instead of one, hour long exposure. Thus, the average of our spectra can confirm their rotationally broadened fit to G 29-38, while the short exposure times allow us to test the possibility that the line shape is altered by the pulsational shifts.

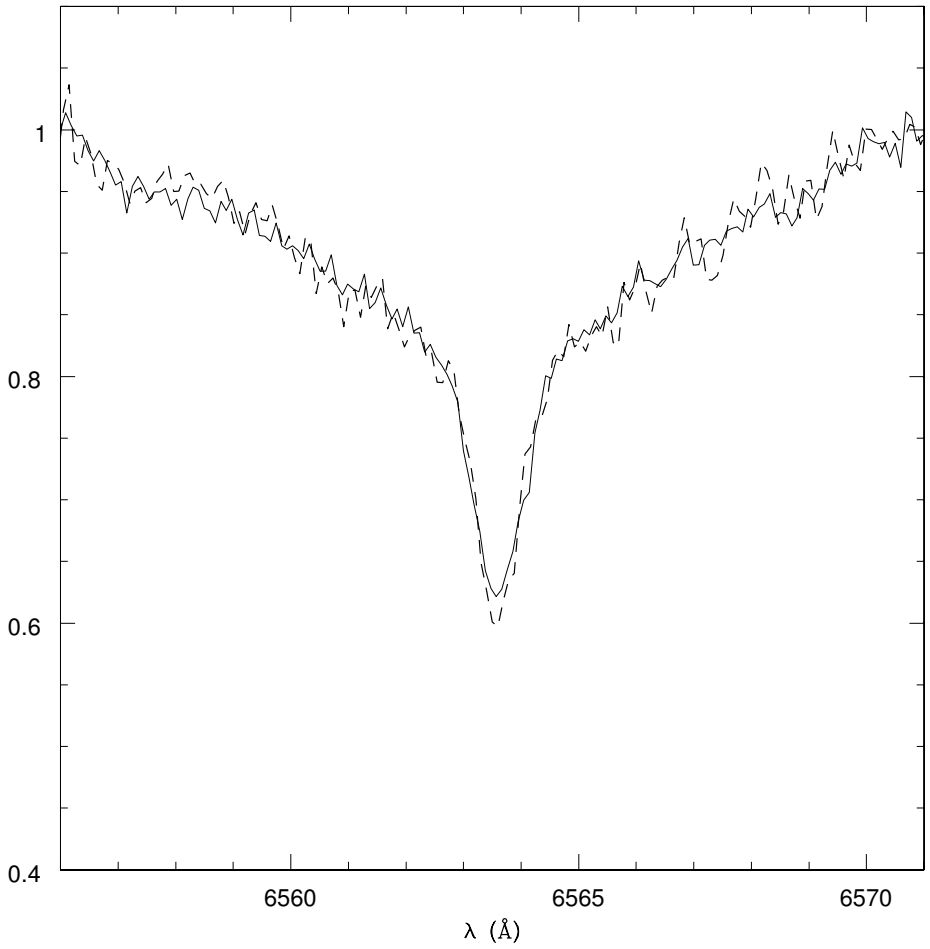

Figure 2.7 The average of the spectra with small measured velocities (dashed line) overplotted on the average spectrum (solid line).

Koester et al. (1998) modeled the H_α line to determine the rotation rates of 28 DA white dwarfs. They found that the majority of the stars have small rotation rates with an upper limit of 15 km s^{-1}. However, the $v \sin i$ for each of the three ZZ Ceti stars, including G 29-38, is between 30 and 45 km s^{-1}. This fitted velocity drastically exceeds what is expected from rotational splitting (Kleinman et al. 1998), and it seems unlikely that white dwarf stars spin-up as they cool into the instability strip. On close inspection of the data obtained by Koester et al. (1998), the shape of H_α core resembles the zero rotation model except for the depth of the line; the model is

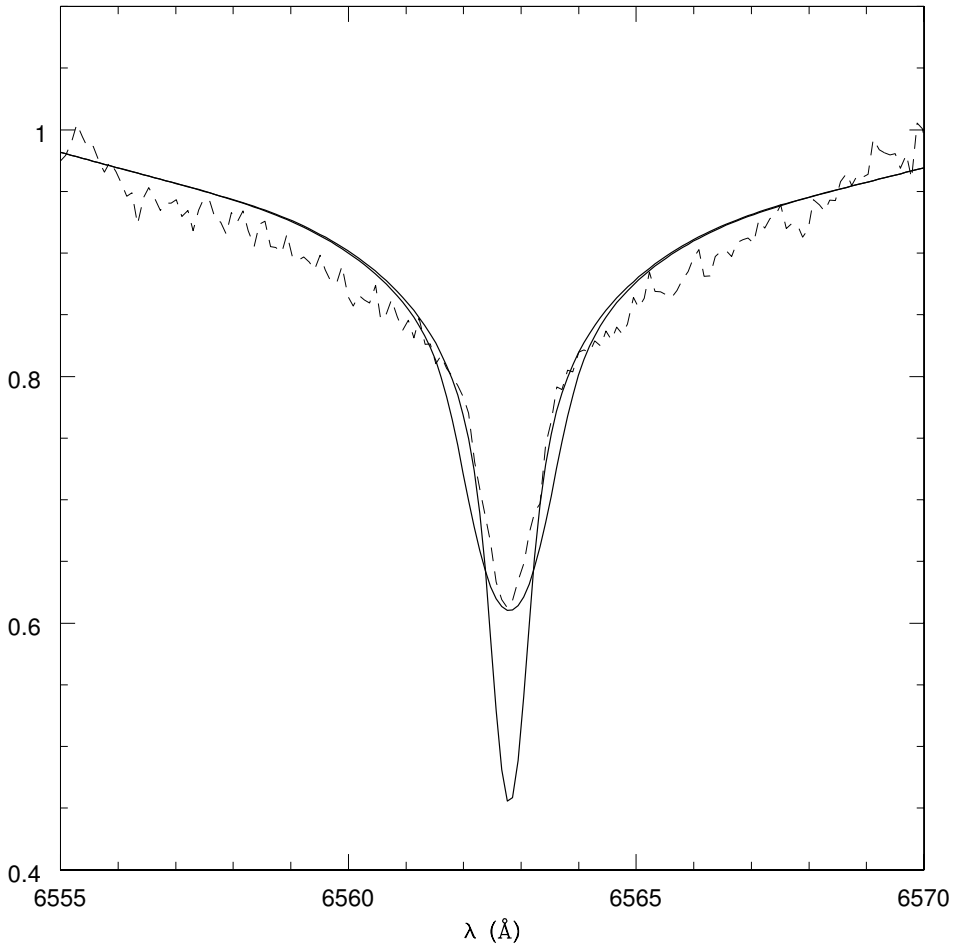

Figure 2.8 Fits to the average spectrum. The deep core is the model with zero rotational velocity and the shallow core is the rotational broadened model corresponding to a velocity of 42.2± 3 km s^{-1}.

almost 20% deeper than the spectrum. A large rotation model successfully fits the depth of the line, but appears to be too broad.

Reassuringly, our average spectrum is identical in shape and depth to the 1-hour exposure of Koester et al. (1998). We fit the same rotationally broadened model used in Koester et al. (1998) to our average spectrum and present the results in Figure 2.8. Again, the best fit, with $v \sin i$ of 42.2 ± 3 km s^{-1}, is able to emulate the depth of the line, but does not fit the width as well as the zero rotation model. With the increased

signal-to-noise of our average spectrum, we can confidently confirm the statement made by Koester et al. (1998) that the large rotation fit is forced by the shallow cores and is too wide for the observations. To quantify the discrepancy between the model and the observations we calculate a reduced chi-square of 3 for the fit using an error of 1.6% (estimated from the observational scatter outside the line core) for the average spectrum in Figure 2.7. The model is too wide to properly simulate the data.

Because rotation fails to account for the line shape, we tested the hypothesis that the altered shape of the spectral line is due to pulsation. As shown above, the g-mode pulsations create small Doppler shifts of the line. Since the exposure time used by Koester et al. (1998) is much longer than the period of the modes, the spectrum could be smeared-out by these velocity shifts. If true, each of our spectra will have a line shape with a deeper core.

Because the signal-to-noise of each individual spectrum is not sufficient to examine a change in the line shape, we reduced the noise by averaging spectra with similar measured velocities. The high and low velocity averages, presented earlier to show the spectral shifts (Figure 2.5), have approximately the same shape as the average spectrum. We also averaged together 30 spectra with velocities between 1.1 and -1.1 km s^{-1} to see the line shape unaffected by the spectral shifts. Figure 2.7, a plot of the small velocity and total averages, demonstrates how little change occurs in the line shape when the spectra with large velocities are excluded.

The small velocity average shows a slightly deeper core; however, this 2% drop is not nearly large enough to reproduce the zero velocity spectral line in Figure 2.7. By convolving the low velocity average spectrum with a gaussian whose fwhm is equal to the root-mean-square of the velocity curve (6.8 km s^{-1} or 0.15 Å), we see that this 2% drop is exactly what is expected for the size of the pulsation velocities. In fact, we would need to convolve the zero-rotation spectrum with a velocity four times larger than measured to achieve the average spectrum line depth; this convolved spectrum is also too wide to emulate the observed spectral line. Though the pulsation motions do present themselves as Doppler shifts, these shifts do not have a significant effect on the shape of the time-averaged H_α spectrum.

Our high signal-to-noise spectra have now eliminated two possible explanations for the line shape of the H_α core of ZZ Cetis: rotation and pulsation. Our average spectrum convincingly demonstrates that the rotationally broadened line does not fit the line profile. An average spectrum created by binning spectra with similar velocities did not result in a significantly different line profile, eradicating the possibility that the pulsations truncate an intrinsically deeper line. The only remaining explanation is that some aspect of the stellar atmosphere must be missing in the model spectrum. The shallow core suggests that the outer atmosphere is hotter than expected. We do not know a good physical reason for this, and therefore, must leave the question concerning the ZZ Ceti line shapes unanswered.

2.6 Conclusions

We have introduced high-resolution, time-resolved spectroscopy to the study of cool white dwarf pulsators with observations of the DAV G 29-38. This technique enabled us to measure the line-of-sight velocities and the flux variations associated with the g-mode pulsations. Despite the low signal-to-noise for each individual spectrum, the fits to the H_α core successfully reveal the Doppler shift of each spectrum, revealing seven velocity modes with corresponding flux modes. The obvious spectral shifts and the frequency correlation between velocity and flux modes confirm the previous velocity detections in G 29-38 by van Kerkwijk, Clemens, & Wu (2000) with low-resolution spectra.

As with the low-resolution data, we compared the amplitudes and phases of the velocity and flux measurements of each mode. To that end, we calculated the relative amplitude R_v and phase difference $\Delta\Phi$ of each mode. Overall, these values agree with the previous measurements of G 29-38 (van Kerkwijk, Clemens, & Wu 2000). The value of $\Delta\Phi$ for the three largest modes shows that the velocity maximum leads the flux maximum by less than a quarter cycle, as expected. The values of R_v are in the same range as the previous measurements. None of the values are as high as the mode identified to be $\ell = 2$ (Clemens, van Kerkwijk, & Wu 2000), indicating that all the modes measured here have a spherical degree of one.

We also compared the relative amplitude and phase difference with the predictions made by the models of Goldreich & Wu (1999a) and Wu & Goldreich (1999) which describe the pulsations on ZZ Ceti stars in the context of a convective driving theory. The values of R_v and $\Delta\Phi$ agree with the model; however, they do not show the trend with frequency predicted from the convection zone's interaction with the flux variations. Considering the size of our errors, this lack of agreement has questionable value. However, since other observations (Kotak, van Kerkwijk, & Clemens 2002; van Kerkwijk, Clemens, & Wu 2000) also did not see the predicted trends, our data add to growing evidence of a problem with the convective driving model.

Finally, we investigated the effects of pulsation velocities on the shape of the H_α line core. The Doppler shifts could potentially broaden the line when observed with a long exposure. Our short exposure times enabled us to examine the line shape of the NLTE core of H_α without this effect. We discovered that removing the spectra with large Doppler shifts from the average line did not significantly alter the shape of the line, indicating that the pulsations are not causing the broadened profile. Rotation, another notorious line broadener, also appears unlikely because the best rotation model failed to fit the width of the line while yielding an unbelievably large velocity (Koester et al. 1998). With both pulsation and rotation eliminated as potential answers, the cause for the truncated shape of the H_α core remains a mystery.

Chapter 3

Detection of a Combination Frequency in the *Velocity* Curve of G29-38

It went "Zip" when it moved
And "Bop" when it stopped
And "Whirr" when it stood still.
I never knew just what it was,
and I guess I never will.

"The Marvelous Toy"
Lyrics by Tom Paxton

Unexpectedly, our *velocity* curve shows evidence for harmonic distortion, in the form of a peak in the Fourier transform whose frequency is the exact sum of the two largest frequencies. Combination frequencies are a characteristic feature of the Fourier transforms of light curves of G 29-38, but before now have not been detected in the velocities, nor does published theory predict that they should exist. We compare our velocity combination frequency to combination frequencies found in the analysis of light curves of G 29-38, and discuss what might account for the existence of velocity combinations with the properties we observe.

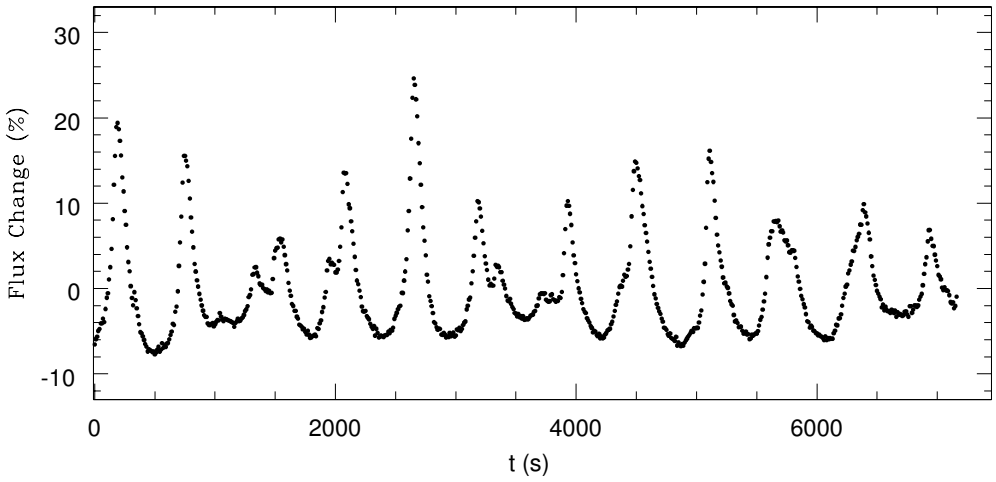

Figure 3.1 A typical light curve of G 29-38 showing the non-sinusoidal character of the pulsations, courtesy the Whole Earth Telescope data archives. These data were obtained by M. Wood using the 82" Struve telescope at McDonald Observatory and a Nather two-star photometer with 10 s sampling times.

3.1 Introduction

The shapes of the light curves of pulsating DA white dwarf (ZZ Ceti) stars have been a puzzle since Warner & Nather (1970) published the first time-series photometry of HL Tau 76. Small-amplitude ZZ Ceti pulsators, now identified as the hotter members of the class, have nearly sine-like photometric variations, but cooler, large-amplitude pulsators show distinctive non-sinusoidal shapes, with broad, flat minima and sharp maxima (see Figure 3.1). Corresponding to these shapes are the appearance of sum and difference frequencies in the Fourier spectrum

Theoretical calculations, first by Brickhill (1983,1992b), and later by Wu (2001) and Ising & Koester (2001), explain this phenomenom within the context of the convective driving theory. Brickhill built a numerical model of a ZZ Ceti surface convection zone and showed that sinusoidal flux variations at its base are attenuated and delayed

in phase before reaching the surface. Moreover, because the thickness of the model convection zone decreases between flux minimum and flux maximum, the amount of attenuation and delay changes within a cycle. This non-linearity distorts the sinusoidal input variation into a surface flux variation whose shape in the model is similar to that we observe. Wu (2001) has found the same result analytically, while Ising & Koester (2001) have confirmed and extended the numerical results of Brickhill (1983). In all of these models, the pulsations are driven by the absorption of heat by the model convection zone during compression rather than by the κ-γ mechanism proposed by Winget et al. (1982b) (see also Dziembowski & Koester 1981 and Dolez & Vauclair 1981).

Other theories for the origin of the pulse shapes invoke the non-linear relationship between flux and surface temperature ($F \propto T^4$; Brassard, Fontaine, & Wesemael 1995), or the excitation of independent pulsation modes by resonant mode coupling. In a recent series of papers, Vuille and collaborators show that the former theory cannot account for the large sizes of the combination frequencies in the large amplitude pulsator G 29-38 (Vuille & Brassard 2000) and the latter cannot naturally explain the phasing of modes with their combinations (Vuille 2000b). They conclude that the majority of combination frequencies in G 29-38 and, by inference, the other large amplitude pulsators arise from harmonic distortion like that described in the models of Brickhill (1983,1992b), Wu (2001), and Ising & Koester (2001).

Our HIRES data complicate matters further by revealing the first combination frequency in the Fourier transform of the *velocity* curve of a ZZ Ceti star. This detection is a surprise, because Brickhill (1983) and Wu (2001) both maintain that surface velocities should not be distorted by the convection zone in their models. Van Kerkwijk, Clemens, & Wu (2000) first detected the surface pulsational motions of G 29-38 through shifts in the positions of the Balmer absorption lines. Their detection required high signal-to-noise spectrophotometry with the Keck LRIS spectrograph (Oke et al. 1995) operated with a very large slit to preserve photometric quality. The results we present in Chapter 2 rely on data from the Keck HIRES echelle spectrograph (Vogt et al. 1994) operated with a narrow slit to preserve velocity precision at the expense of photometric quality.

We will speculate about what might account for our observations, using the relative phase of the velocity combination we have measured as our only clue. Because we have detected only a single combination peak, we will require more observations to establish whether or not its properties are typical of large amplitude ZZ Ceti pulsations.

3.2 The Combination Frequency in the Velocity Curve

The analytic theory presented by Goldreich & Wu (1999a) makes specific predictions about the existence and behavior of combination frequencies in the Fourier transforms of ZZ Ceti light curves. In their simplest models, which do not incorporate the effects of changing convection zone thickness during pulsation cycles, the flux variations at the photosphere are a diminished and delayed version of the variations that occur at the base of the convection zone. The size of the diminution and delay for a given mode is dependent on the thermal adjustment time of the convection zone and the mode frequency. As long as neither of these change, the effects are linear and do not generate combination frequencies (assuming the variations at the convection base are sinusoidal). However, as first Brickhill (1983) and later Wu (2001) point out, this is unrealistic. The modes in ZZ Cetis are large enough to substantially increase the surface temperature of the star. Equilibrium models of hotter ZZ Ceti stars have thinner surface convection zones, suggesting that pulsating stars will have thinner convection zones at pulsation maxima than at minima. The detailed calculations of Brickhill (1992b) and Ising & Koester (2001) confirm this suggestion. The effect of this change in convection zone thickness is that the flux is less diminished at maximum than at minimum, i.e. the maxima rise higher above the mean flux than the minima descend below it. This property of the models corresponds qualitatively, and often quantitatively, to the behavior of the light curves we see.

In the Fourier transforms, this behavior of the models predicts combination frequencies and harmonics that are nearly in phase with the modes that generate them, a condition written by Vuille (2000b) as $\phi_r = \phi_{1,2} - (\phi_1 + \phi_2) \approx 0$, where $\phi_{1,2}$ is the phase of the combination and ϕ_1 and ϕ_2 are the phases of its parent modes. The analysis of modes in G 29-38 by Vuille (2000b) shows that the combination frequencies

show ϕ_r near an average value of 22°, consistent with their harmonic distortions being generated by the changing convection zone depth, just as the models describe.

The prediction of the models with respect to velocity combinations is harder to discern. Brickhill (1990) and Wu (2001) assume that turbulent viscosity in the convection zone enforces uniform velocity with depth. Thus their model convection zone does not introduce any delay or diminishment of velocities between its base and the surface, so the mechanism responsible for the distorted light curves does not operate on the velocites. Furthermore, Brickhill (1992b) argues that second order perturbations to the horizontal motions should be smaller than the linear perturbations by a factor of 10 or more. Based on this argument, Brickhill *imposes* sinusoidal pressure variations and displacements in his model. Because his model does not allow feedback that could alter the imposed variations, it can never exhibit non-sinusoidal horizontal motions. The models of Ising & Koester (2001) and the analytic treatment of Wu (2001) also assume sinusoidal pressure variations and have no feedback. Consequently, none of the published models have any ability to predict the shape of velocity curves: they only reap what they have sown.

Fortunately, the phase of our velocity combination offers a clue to its origin. If we define the relative phase in the same way as for the flux combinations, then we find from Table 2.1 that $\phi_{r,velocity} = \phi_{F5} - (\phi_{F1} + \phi_{F2}) = -95°$. A phase difference of $-95°$ suggests a simple possibility. If the horizontal *displacements* are distorted in the same way as the flux curves we observe, then they would generate combination frequencies with $\phi_{r,displacement} \approx 0$. The velocities we measure are the time derivatives of the displacements, and the derivative introduces a 90° phase shift in both of the parent frequencies and in the combination, so we expect $\phi_{r,velocity} \approx 270° = -90°$. That is, the relative phase of the velocity combination frequency we have measured is close to the value we expect if the horizontal displacements vary in a manner similar to the flux variations. See Figure 3.2 for an example of the displacements and the corresponding velocities for one mode and its harmonics. Though both curves have the same set of harmonics (see the FTs), phase of *maximum* displacement is aligned for the displacement harmonics, while the phase of *zero* velocity is aligned for the velocity harmonics.

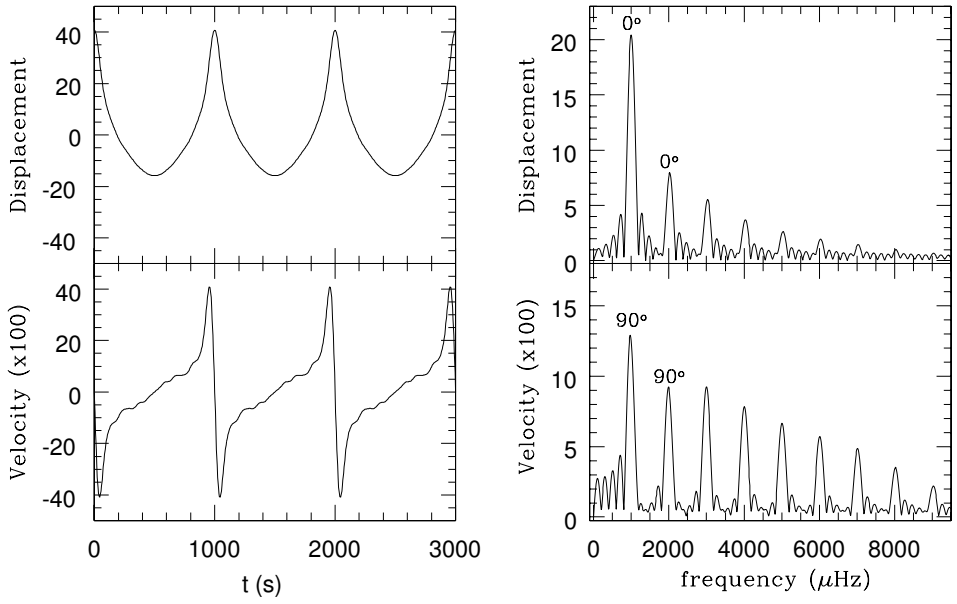

Figure 3.2 An example of displacement and velocity variations with their FTs (phase of the parent and first harmonic are labeled). The top plot was created by combining 12 cosine waves, a parent mode and 11 harmonics of decreasing amplitudes. As the displacement harmonics are in phase with the parent mode, this combination of modes produces a curve similar to the shape of the flux variations. The bottom plot shows the corresponding horizontal velocity variations, created by taking the time derivative of the displacements in the top plot. The FT shows that the derivative introduces a 90 degree phase shift and an increase in the relative amplitudes of the modes.

This does not answer the question of why the measured displacements should show this behavior. The observations require that in the half cycle where horizontal displacements are directed toward a surface anti-node, material travels farther from its equilibrium position than it does in the half cycle where displacements are directed toward a node. Perhaps this is an overlooked consequence of the strongly non-sinusoidal temperature variations at the pulsation anti-nodes. Alternatively, it is possible that the uniform (with depth) horizontal velocities enforced by the convection zone introduce a non-sinusoidal component into the velocities as the thickness of the convection

zone changes during a pulsation cycle. In the models, the convection zone "averages" the horizontal velocites to a value somewhere between the values that would be present at its base and surface if turbulent viscosity did not enforce uniform horizontal motion (see Figure 5 of Wu & Goldreich 1999). As the convection zone changes depth, and perhaps even entirely evaporates at the anti-nodes, the effect on the surface motions might change during a cycle, yielding a non-sinusoidal component. However, it is not clear that the relative phase of this component would match the relative phase of the combination peak we have measured.

We can speculate further, but we are far from understanding the origin of the velocity combination F5. First, we cannot make any statistical arguments on the basis of one mode, so we cannot rule out the possibility that F1, F2, and F5 represent an example of resonant mode coupling as described by Wu & Goldreich (2001) and Dziembowski (1982), in which case the phase relationship measured is accidental. Second, without actual calculations extending the works of Brickhill (1983), Brickhill (1992b), Wu (2001) and Ising & Koester (2001), we do not know what detailed models will predict for the phase of velocity combination modes. Nonetheless, we think the speculation we have presented represents the most fruitful immediate direction for observational and theoretical investigations.

3.3 Conclusions

We have acquired the first low-noise velocity curve of a ZZ Ceti star using time resolved spectroscopy at high-resolution. Not surprisingly, the new technique has uncovered a new phenomenon—a velocity combination frequency. Although it is dangerous to generalize from a single detection, it appears that the surface velocity variations for large amplitude ZZ Cetis can experience harmonic distortion just as the flux variations do. We have discussed this as the product of an underlying distortion in the horizontal displacements that has properties similar to the distortions in the flux variations. Unfortunately, none of the existing models are capable of predicting, or even reproducing, this behavior. We believe that some effort in this direction could resolve many mysteries surrounding G 29-38 and the entire class of ZZ Ceti pulsators.

Chapter 4

The Peculiar Pulsations of PY Vul

Soon you'll zoom all around the room,
All it takes is faith and trust;
But the thing that's a positive must
is a little bit of Pixie Dust.
The dust is a positive must.

"You Can Fly!"
Lyrics by Sammy Cahn

The pulsating white dwarf star PY Vul exhibits pulsation modes with peculiar properties that set it apart from other variable stars in the ZZ Ceti class. These peculiarities include a low total pulsation amplitude, a mode with bizarre amplitudes in the ultraviolet, and a mode harmonic that exceeds the amplitude of its fundamental. Here, we present optical, time series spectroscopy of PY Vul acquired with the Keck II LRIS spectrograph. Our analysis has revealed that the mode with unusual UV amplitudes also has distinguishing characteristics in the optical. Comparison of its line profile variations to models suggests that this mode has a spherical degree of four.[10]

[10]This analysis of PY Vul has been accepted for publication in the August edition of the Astrophysical Journal.

4.1 Introduction

While each member of the variable DA white dwarfs (DAVs) shows its own unique set of pulsations, this group of pulsators share many similar characteristics. They all have a pure hydrogen atmosphere and reside in a narrow temperature strip near 11,500 K, making them the coolest known class of white dwarf pulsators. The multi-periodic brightness variations of these stars are due to non-radial, g-mode pulsations (Robinson, Kepler, & Nather 1982) with periods between 100 s and 1000 s and amplitudes less than a few percent. Those pulsators near the blue end of the instability strip tend to show fewer modes with shorter periods and smaller amplitudes than the pulsators near the red edge (Winget & Fontaine 1982).

Understanding the characteristics of the pulsations of individual DAVs provides the opportunity to model their interiors. The ability to model the pulsations is limited by our ability to identify the modes. Pulsations are described by the spherical degree (ℓ), azimuthal order (m), and radial order (k). Unfortunately, the paucity of observed modes in DAVs creates an obstacle to using period spacings for mode identification. Yet, some successful mode identification has been performed on DAVs. Long data sets from a single site, or using the Whole Earth Telescope (Nather et al. 1990) has resolved azimuthal splittings, yielding the identification of ℓ and m for a few DAVs. Time-resolved spectroscopy in both the UV and optical wavelengths, has been applied to the brighter DAVs (see Robinson et al. 1995; van Kerkwijk, Clemens, & Wu 2000; Kepler et al. 2000; Kotak et al. 2002; Kotak, van Kerkwijk, & Clemens 2002; Thompson et al. 2003; Kotak, van Kerkwijk, & Clemens 2004). This method identifies the spherical degree by measuring how the amplitude of the mode changes with wavelength. Here, we apply the technique of optical, time-resolved spectroscopy to the bright DAV, PY Vul and attempt to decipher its prominent pulsation modes.

About PY Vul One of the brightest known DAVs (V= 12.97 mag) with some of the smallest amplitude pulsations ($< 0.3\%$) is PY Vul (G 185-32, WD 1935+276). Since its discovery as a pulsator (McGraw et al. 1981), it was noted as having a curious pulsation spectrum. Atypical of small amplitude pulsators, PY Vul displays a wide range of periods, including prominent modes near 370 s, 300 s, 215 s, 142 s, 72 s and

71 s (McGraw et al. 1981; Kepler et al. 2000; Castanheira et al. 2004). Given the star's shorter periods, low amplitudes, relatively stable modes, and temperature, this star is grouped with the pulsators near the blue edge of the instability strip.

The pulsation amplitudes on PY Vul are much lower than expected for DAVs of similar periods. DAVs follow a distinct trend: those with larger amplitude modes have larger mean periods (Clemens 1994). The trend created by these stars (see Figure 5.4) reflects their similarities and follows the expectations of mode driving mechanisms (Wu & Goldreich 1999; Brickhill 1992b; Winget 1982). PY Vul remains the exception to this trend. Both its average mode amplitude and the amplitude of its largest mode are approximately a factor of ten smaller than the other DAVs. Suggested explanations for the low amplitudes have included nonlinear pulsation modes with a relatively large number of surface nodes (McGraw et al. 1981), a large magnetic field limiting the growth of its modes (Clemens 1994), and a large inclination causing cancellation of the modes (Thompson & Clemens 2003).

The mode at 71 s, the harmonic of the 142 s mode, is a curious feature of PY Vul. First, the presence of large harmonic modes is normally reserved for the large amplitude pulsators. Second, the amplitude of this harmonic has an amplitude similar to the 142 s mode and has been observed to occasionally exceed the parent mode (see McGraw et al. 1981); all other DAVs show harmonics consistently smaller than the parent mode. The non-linear effects in the outer layers of DAVs, believed to be responsible for the presence of harmonics, should be small for low amplitude pulsations (Brickhill 1992b; Wu 2001; Ising & Koester 2001). Some possible explanations for why a low amplitude pulsator might display harmonics were discussed in general by Ising & Koester (2001) in their study of nonlinear effects on pulsations. Nonlinear effects could appear with small amplitude pulsations if the star has an unusual surface convection zone, the star has a large inclination, or the mode has a large spherical degree.

The most recent addition to the mysteries of the pulsations of PY Vul came from time-resolved UV spectroscopy from the Hubble Space Telescope (HST) (Kepler et al. 2000). They observed that each of the modes' relative amplitudes increased in the UV as an $\ell = 1$ or 2 mode except for the 142 s mode. It shows no appreciable increase

in amplitude while its harmonic at 71 s still resembles a mode of $\ell \leq 2$. Kepler et al. (2000) suggest that the 142 s mode is a result of nonlinear mixing while the other modes, including the 71 s mode, are real pulsations.

Here, we add our analysis of optical time-resolved spectroscopy which offers an appealing explanation for all the mysterious observations of PY Vul's modes. Our analysis of variations in the H_β and H_γ lines show that the 142 s mode behaves like ℓ=4. We therefore propose that this mode is the dominant mode in the star and that it has a spherical degree of four. We discuss the implication of this hypothesis on the other observations of PY Vul in the following chapter.

4.2 Time-Series Spectroscopy

By analyzing the light curves at different wavelengths, we can learn about the distribution of a pulsation mode across the surface of a star. Robinson et al. (1995) introduced this type of analysis for DAVs by using broad-band observations in the UV to measure the wavelength dependent amplitudes, thereby identifying ℓ of individual pulsation modes in G 117-B15A. This method uses the wavelength dependence of limb darkening and different cancellation effects to distinguish between different spherical degrees. Figure 4.1 shows model relative amplitude variations across the optical and ultraviolet wavelengths for the first four spherical degrees.

Van Kerkwijk, Clemens, & Wu (2000) extended this technique to optical, time-resolved spectroscopy of the bright large amplitude DAV, G 29-38 and measured periodic shifts in the location of the spectral lines associated with the motion of the stellar material during the g-mode pulsations. Clemens, van Kerkwijk, & Wu (2000) measured the wavelength dependence of the pulsation amplitudes of each mode (hereafter "chromatic amplitudes") and showed that with the presence of velocities an asymmetry occurs in the shape of the chromatic amplitudes. Since then, optical time-resolved spectroscopy has been applied to HS 0507+0434B, HL Tau 76, and G 117-B15A (Kotak, van Kerkwijk, & Clemens 2002; Kotak et al. 2002; Kotak, van Kerkwijk, & Clemens 2004). By comparing these results to model chromatic amplitudes similar to

the one presented in Figure 4.1, these studies were able to distingish some ℓ=2 modes from ℓ=1 modes.

The brightness of PY Vul suggested to us that similar observations of this star would be productive. In the following section, we discuss observations acquired with the Keck II LRIS spectrograph. The analysis of our low-resolution, time-resolved spectra shows that the signal-to-noise of the spectra is too low to see line profile variations in the chromatic amplitudes. However, we will introduce a new analysis technique that enables us to extract information about the spherical degree from the series of spectra.

4.3 Observations

We observed PY Vul for two nights with the Low-Resolution Imaging Spectrometer (LRIS; Oke et al. 1995) at the Keck II Observatory. On August 12, 1997 we took 410 spectral images between 06:33:15.35 and 10:12:08.17 U.T.; on August 13, 1997 we took 396 images between 06:00:52.95 and 09:32:41.40 U.T.; times are as recorded by the image headers. The times in these headers are known to have substantial errors but the timing intervals accurate enough for our analysis. The images collected during this 7.4 hours of data had an exposure time of 18 s with a read-out time of approximately 14 s, achieved by reading the images through two amplifiers, binning the chip by two in the spatial direction, and reading only 50 rows of the CCD. We used the 600 line mm^{-1} grating and the 8.7" wide long slit such that the seeing on the first night of 0.9" resulted in a resolution of 4.9 Å. On the second night our seeing was 0.7" yielding a resolution of 3.9 Å. On each night, the series of exposures included images of the Hg-Mg-Ar lamp for wavelength calibration and of the flux standard Feige 110.

We reduced the spectral images by removing the bias, measured from the over-scan regions of both amplifiers and adjusting for the difference in gain of the two amplifiers. We did not apply flat fields because we did not obtain enough images to sufficiently reduce the stochastic noise in the average flat; application of the flat only increased the noise of the spectra. Using the apall routine of IRAF (Imaging Reduction and Analysis Facility; Tody 1986) we traced and extracted the spectra from these images

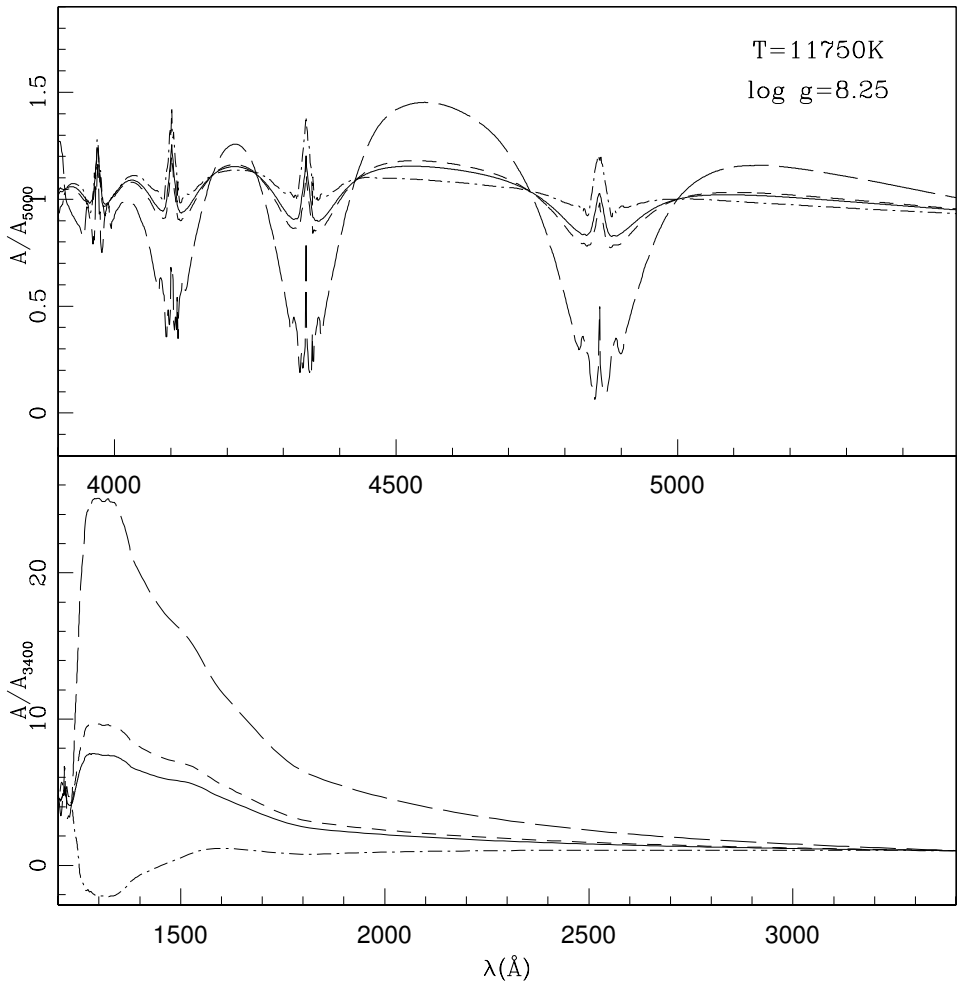

Figure 4.1 Models of relative amplitudes for ℓ=1,2,3,4 (solid, short dash, long dash and dot-dash) created using models for a star at T=11,750 and log(g)=8.25. Top panel covers the optical wavelengths and has been normalized at 5000 Å. The bottom panel covers the UV and are normalized at 3400 Å.

removing the sky background and rejecting cosmic rays. We applied the wavelength calibration and the flux calibration images to each spectrum. The extracted spectra cover a wavelength range from 3800 to 5700 Å with a dispersion of 1.23 Å pixel^{-1}. Measured at the continuum near 5000 Å, the signal-to-noise of an individual spectrum is $\sim$ 180 per pixel while the average spectrum has a signal-to-noise of $\sim$ 2200 (See Figure 4.2). The signal-to-noise of the average is less than expected from poisson statistics; possibly because of sensitivity variation between pixels normally reduced by flat fielding.

4.4 Light and Velocity Curves

Time-resolved spectroscopy provides the opportunity to measure two aspects of a non-radial mode's pulsation, the brightness and the line profile variations. The variations in the shape of the line are seen as both wavelength shifts and changes in the depth of the line (see Clemens, van Kerkwijk, & Wu 2000). In the following section, we set out to extract this information from the spectra of PY Vul.

To create a light curve from the 7.4 hours of data, we averaged the flux contained in the continuum between 5080 and 5420 Å. We divided by a 4th order polynomial, and transformed the light curve to fractional variations (1 mma=0.1%). Figure 4.3 and 4.4 show the light curve and its Fourier transform (FT). The six largest periodicities in these data, the ones we will concern ourselves with here, have all previously been observed on this star, most recently during a 76 hour run with the Whole Earth Telescope (Castanheira et al. 2004). Several other modes are present in Castanheira et al. (2004), including possible frequency splittings of our F2 and F3. The mode labeled F2 is the perplexing 142 s mode noted in the introduction for its unusual behavior in the ultraviolet; F5 is its harmonic.

The noise level of this FT, as determined from the square-root of the average power in the frequency range 8000 – 12000 μHz, is 0.1 mma (Horne & Baliunas 1986). Each of the six modes listed in Table 4.1 are significantly above this noise level. The appearance of the light curves reveal that the nights were not perfectly photometric; as such, we do not attempt to discuss any peaks in the FT not detected

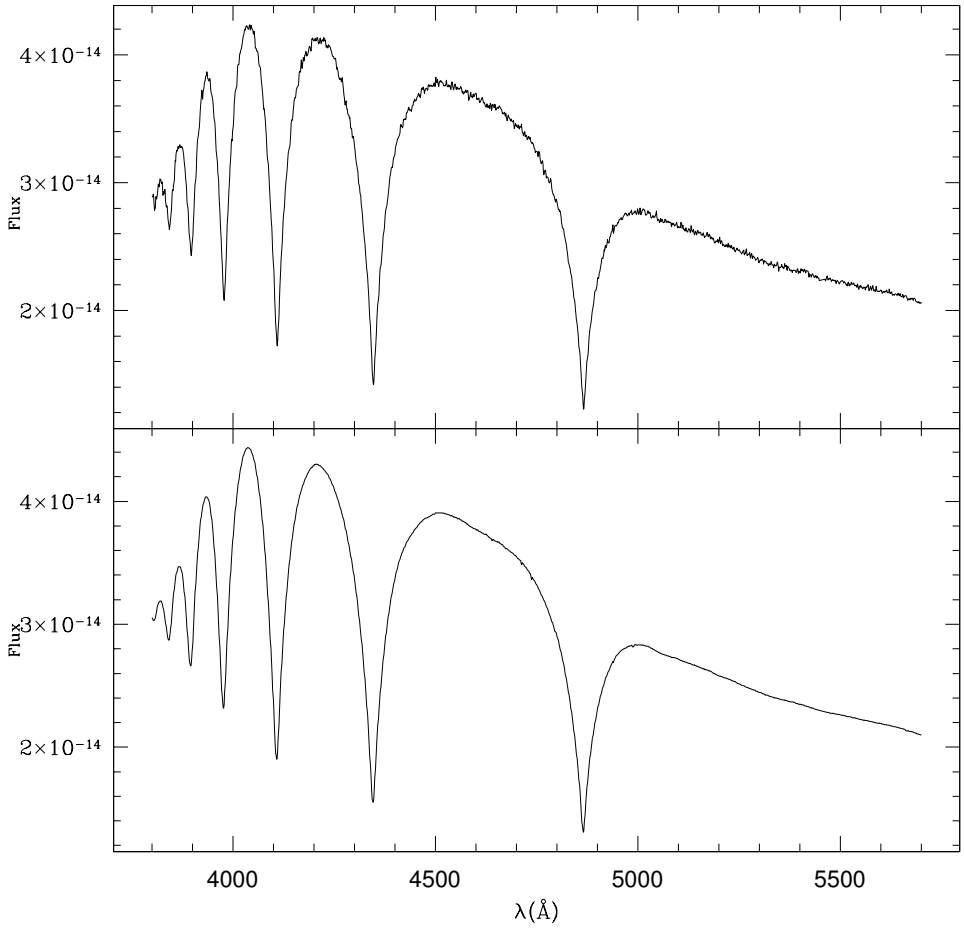

Figure 4.2 An individual (top panel) and the average (bottom panel) reduced spectra of PY Vul taken on August 13, 1997.

in previous observations. For our purposes, we are content with focusing on the six largest, previously observed modes.

Since we intended to measure the pulsation velocity variations, we gauged how much the star moved in the slit during the observations by measuring the location of the star in the spatial direction at the 500th column of each image. A quick look at each curve, after a low order trend was removed, revealed that on the first night

the motion of the star along the slit was a factor of ten larger than the second night. The standard deviation of the motion of the star, translated into a velocity for the same motion in the dispersive direction, on the first night is 32 km s^{-1} while it is 2.5 km s^{-1} on the second. Measuring the velocity on each night by fitting the spectral lines further confirmed this excessive motion on the first night. On the first night we used a B filter for the the guide star, in a misguided attempt to remove the effects of differential refraction. This made the guide star too dim for the auto-guider to consistently maintain a lock on the star and resulted in more random motion in the slit. No filter was used on the guide star on the second night and the result was much improved auto-guiding. Our analysis only includes the velocity measurements from the second night.

To measure the wavelength shifts in each spectrum, we measured the central wavelength of the spectral lines relative to the average spectrum. We individually fitted the 5 Hydrogen lines (H_β-H_8) with a Lorentzian and Gaussian function imposed on a sloped continuum with the specfit routine of the STSDAS[11] package in IRAF. We required the Lorentzian and Gaussian to have the same central wavelength. The slope and flux of the continuum, the flux in the Lorentzian and Gaussian, and the central wavelength varied to fit each spectrum. A fit to the average spectrum determined the initial conditions of each fit. We averaged together the velocities measured from each line, weighting each by the formal error of the fit. We removed a low order trend due to the differential refraction and flexure. Figure 4.3 shows our velocity curve.

In contrast to the data on G 29-38 presented by van Kerkwijk, Clemens, & Wu (2000), no obvious pulsations are present in the FT of our velocity measurements (see Figure 4.4). The few periodicities present just above the noise level (σ=0.4 km s^{-1}) are not present in the light curve's FT and are most likely due to motions of the star in the slit. The analysis of this data can at most reveal an upper limit for the velocity associated with the flux variations ($\sim$ 1.2 km s^{-1}). Comparing our velocity FT to the similar LRIS data of G 29-38 presented in van Kerkwijk, Clemens, & Wu (2000), our velocity noise level is smaller than what they achieved. If the velocity amplitudes of

[11]STSDAS is a product of the Space Telescope Science Institute, which is operated by AURA for NASA

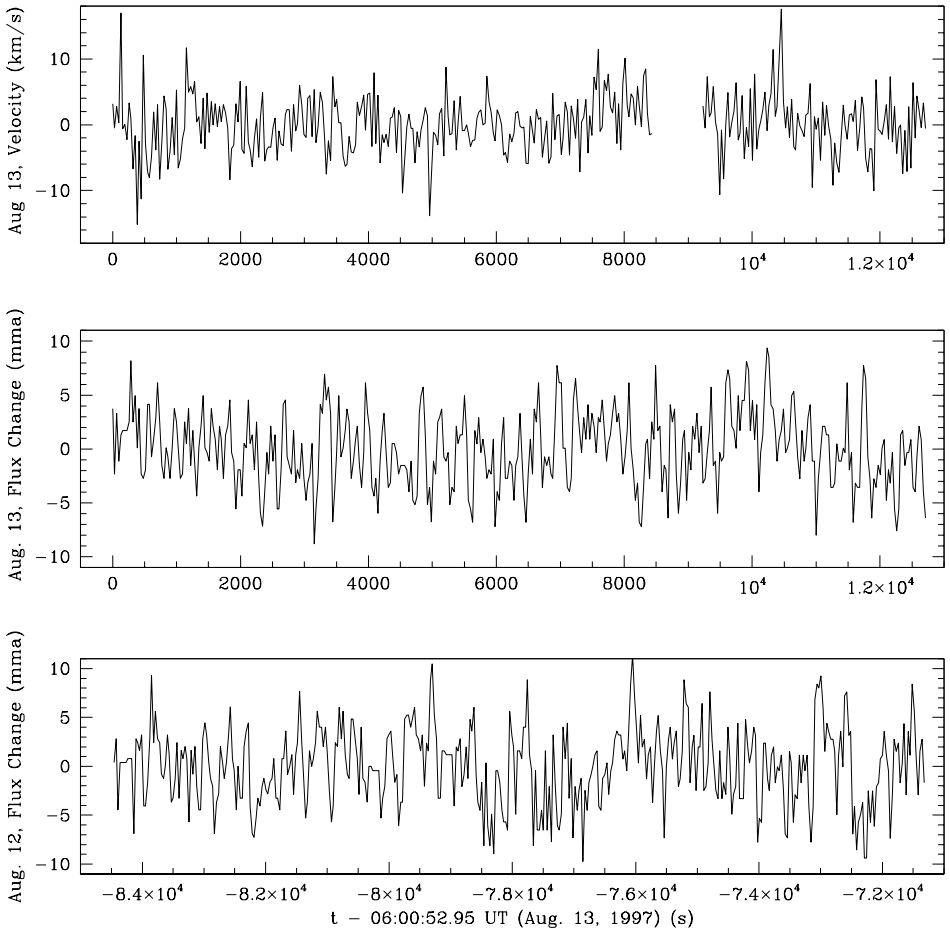

Figure 4.3 The light curve for both nights and the velocities measured on the second night. The portion of the velocity curve near 9000 s was removed because it was obviously dominated by the motion of the star in the slit.

PY Vul were as large as the velocities on G 29-38, we would have been able to detect them in our data.

We performed a non-linear least squares fit to the six largest modes found in the flux curve and, for completeness, fitted the velocity curve of the second night at those same frequencies. Table 4.1 shows the frequencies, amplitudes and phases of the six modes. All phases are reported with time zero as August 13, 1997 at 6:00:52.95 UT.

4.5 Chromatic Amplitudes

In hopes of determining the spherical degree of each of the observed modes, we created a light curve at each wavelength and measured the amplitude from the FT for the six modes in Table 4.1. The plot of amplitude versus wavelength, named chromatic amplitudes by van Kerkwijk, Clemens, & Wu (2000), were normalized by the ampli-

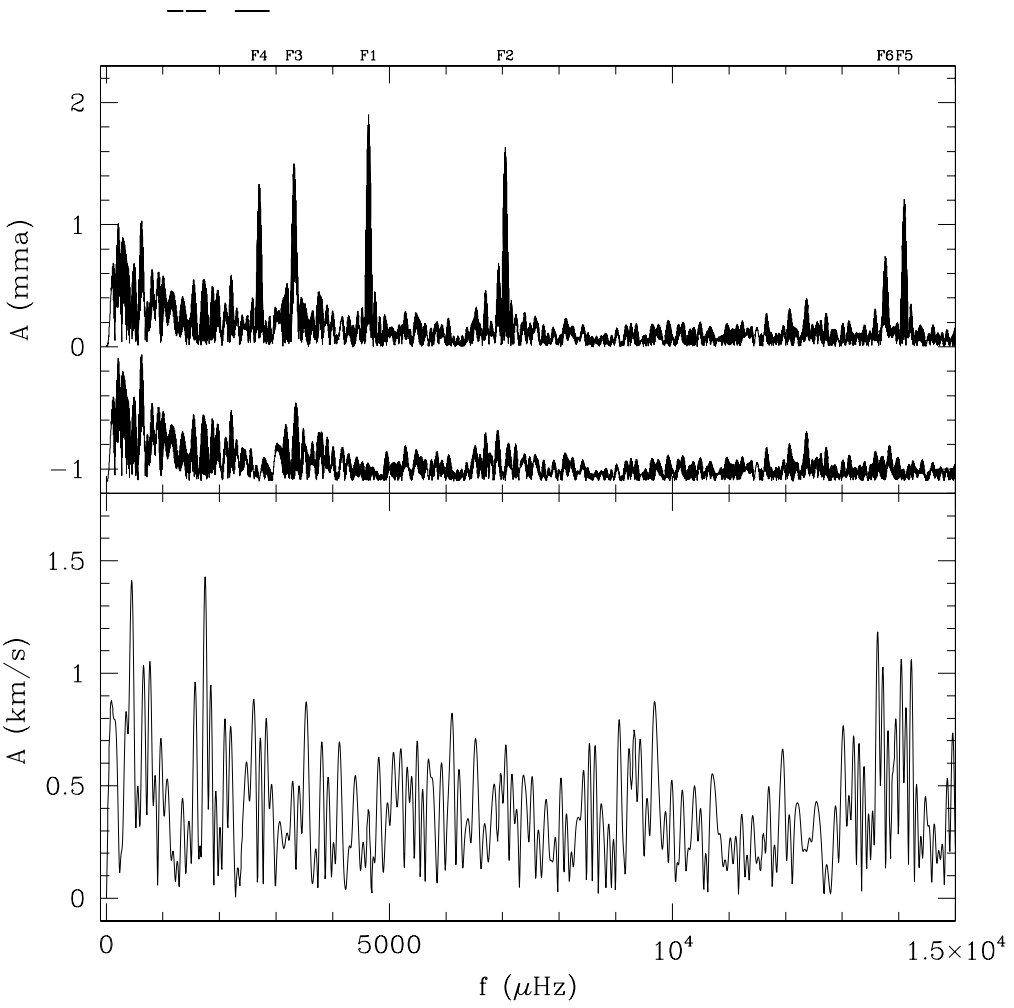

Figure 4.4 The Fourier transforms of the combined light curve of both nights and the velocity curve from the second night. The modes listed in Table 4.1 are listed at the top of the light curve FT. An FT of the residuals after the six largest modes are removed is shown below the light curve FT.

Table 4.1. The fitted modes of the light and velocity curves of PY Vul.

mode	P(s)	$f(\mu\text{Hz})$	A_f(mma)	Φ_f(deg)	A_v(km/s)
F1	215.7	4634.9±.3	1.9±.1	77±5	0.37±.3
F2	141.9	7048.5±.3	1.5±.1	268±7	0.64±.3
F3	301.6	3315.8±.3	1.5±.1	281±7	0.45±.3
F4	370.2	2701.1±.4	1.3±.1	202±8	0.52±.3
F5*	70.9	14097.1±.4	1.2±.1	217±8	0.55±.3
F6	72.6	13772.7±.7	0.7±.1	268±15	0.17±.3

*$F5 = 2 * F2$

Note. — The errors reflect the formal errors of the fit. The reported velocity amplitudes are not significant detections.

tudes measured from the continuum light curve. Figure 4.5 shows the disappointing chromatic amplitudes determined directly from the data. Except for the amplitude peak that occurs at the center of some spectral lines, this analysis revealed nothing useful.

The reason for the poor chromatic amplitudes is the low signal-to-noise ratio in any pixel ($\sim$ 1.23 Å). To circumvent this problem we attempted to smooth the data, effectively increasing the wavelength coverage of each element. The application of a boxcar smooth to our spectra did decrease the noise in each element. However, when we sufficiently reduced the noise by averaging together a larger number of pixels, the wavelength coverage of any one bin became so large that the spectral lines were washed out. In spite of these discouraging results, we endeavored to find another method to measure the chromatic amplitudes. We discovered that when we imposed information about the shape of the spectral line derived from the high signal-to-noise average spectrum, we were able to improve the appearance of the amplitude variations. Essentially, we fitted the average spectrum to establish an expected shape of the

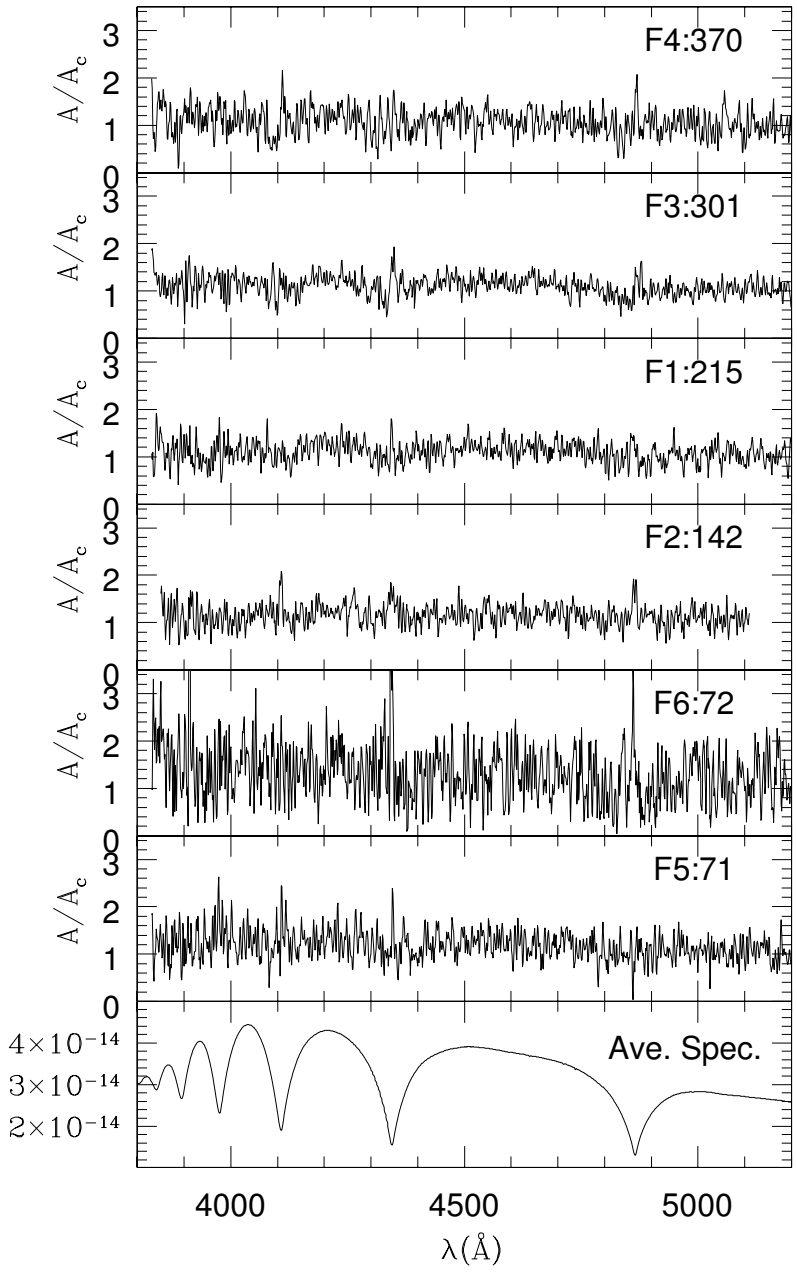

Figure 4.5 Chromatic amplitudes for each of the modes in Table 4.1 determined directly from the data. Each plots the fractional flux change as a function of wavelength normalized by the continuum amplitudes in Table 4.1.

spectra and then fitted each individual spectrum, allowing variations only in a few free parameters. We then used these fits to measure the chromatic amplitudes instead of the original data. Constraining the variations of the line shape in this way has greatly reduced noise while still maintaining information about the actual line profile variations. Since this is a new method for analyzing this type of data, we continue by providing more details.

We applied the same technique to both the H_β and H_γ lines. First, we measured the spectral shifts of the line itself by fitting the line as described in §4.4. We then removed those spectral shifts because the velocities due to the motion of the star were too small to observe and the spectral shifts would not add useful information to the results. Additionally, removing the velocities ultimately makes comparison with the models simpler. Next, we created an average spectrum from the deshifted spectra and used its fit as the initial conditions for the fit to the individual spectra. The same parameters were used here as for measuring the velocities, a Gaussian and Lorentzian applied to a flat continuum. As we fitted each spectrum, we only allowed four parameters to vary: the continuum flux, the continuum slope, and the flux in the Gaussian and Lorentzian. Since we removed the spectral shifts, the central wavelength of the fit is fixed to that of the average spectrum. We show a typical example of a fit to an individual spectrum and the residual in Figure 4.6. We fitted across the region 4220-4470 Å for H_γ and the region 4760-4960 Å for H_β.

We then created chromatic amplitudes from the fits to each spectrum instead of directly from the data. For each wavelength we created a light curve of fractional changes in flux and took a Fourier transform at each wavelength. We determined the amplitude of the FT at each of the six modes listed in Table 4.1 and normalized the curves by the amplitudes measured at 5000 Å. Figure 4.7 has the plot of these chromatic amplitudes for the H_β and H_γ lines on each day for the five largest modes. The noise level of the FT at each individual wavelength is approximately 0.2 mma. As a result, the low amplitude mode, F6, is not significantly above the noise and shows sporadic results.

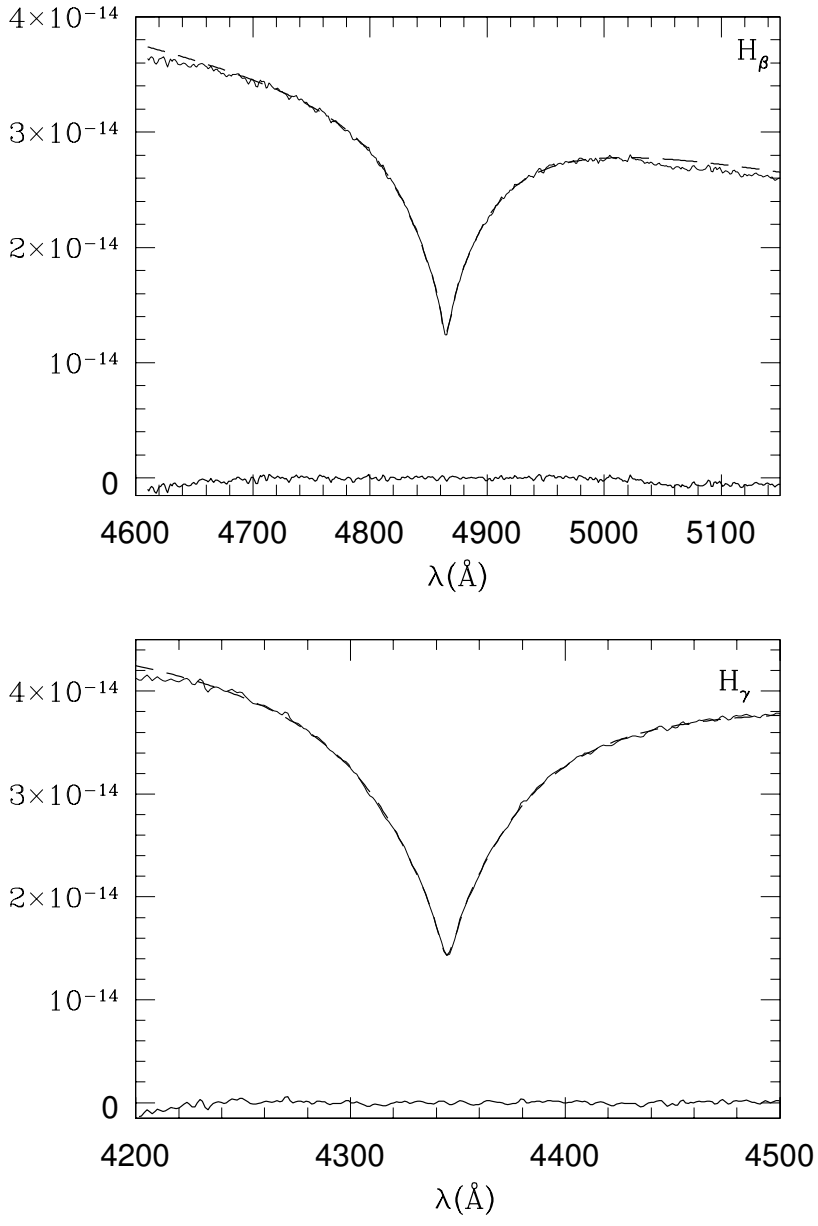

Figure 4.6 The solid curve shows an individual spectrum while the dashed line is the fit to that spectrum. Top panel is H_β and the bottom panel is H_γ. The residuals are plotted at the bottom of each panel.

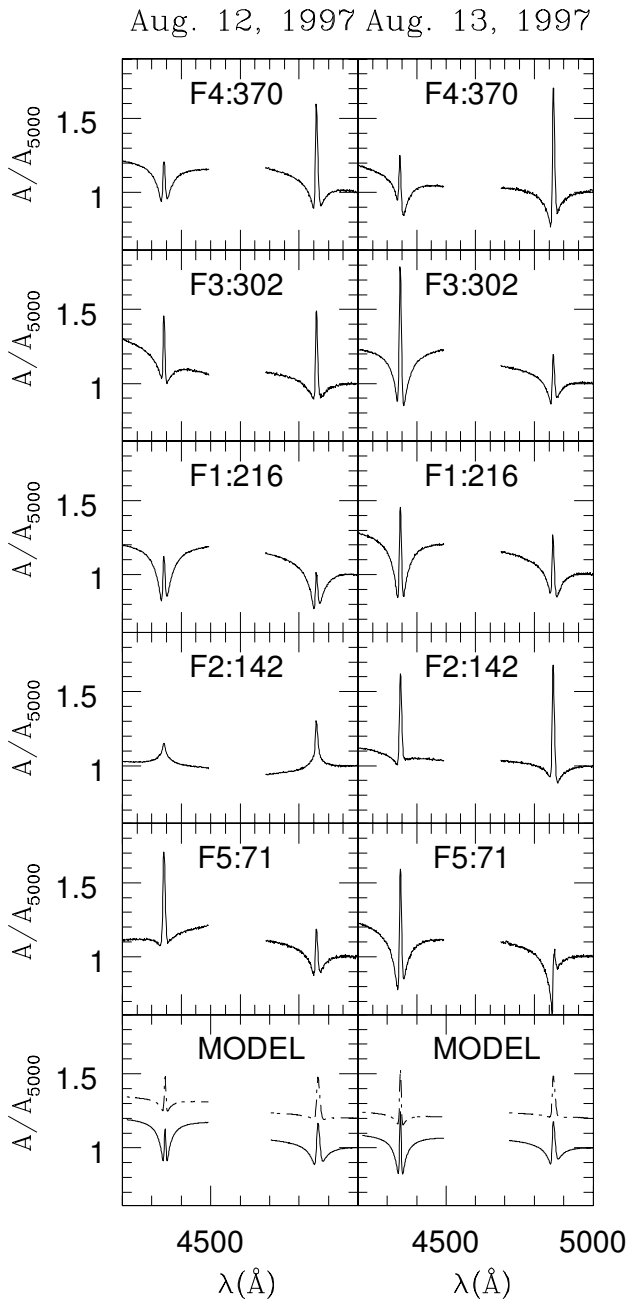

Figure 4.7 Chromatic amplitudes of the H_β and H_γ lines created from the fits to the spectral lines for both nights of data. Each plot has been normalized at 5000 Å and labeled with the mode number and period. The bottom plot contains model chromatic amplitudes of ℓ=1 (solid) and ℓ=4 (dash) created with simulated spectra gaussian smoothed according to the resolution of each night. For clarity, the normalized amplitude of the ℓ=4 model has been offset by 0.2.

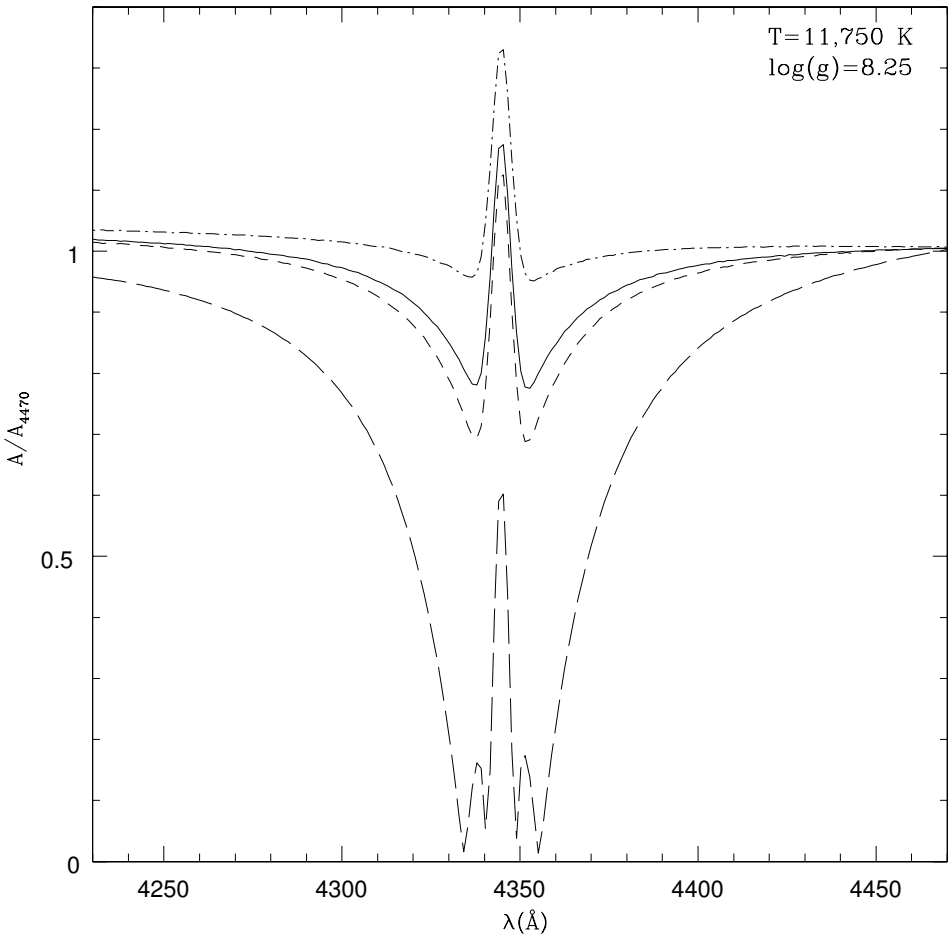

Figure 4.8 Chromatic Amplitudes of H_γ created from the fitted model spectra. Each spectrum was created by adjusting the model spectrum according to the expected model chromatic amplitudes in Figure 1 and using a fit to re-create the chromatic amplitudes. Each have been normalized to 4470 Å and shifted in wavelength to align with our spectra. The first four spherical degrees are shown as solid, short-dashed, long-dashed, and dot-dashed in order of increasing ℓ.

4.6 Spectral Fit Chromatic Amplitudes

The chromatic amplitudes are a way of examining how the shape of the spectral line changes during a pulsation cycle. This depends on how the flux variations are distributed across the surface of the star, which change with ℓ. In Figure 4.1 we showed model calculations for how the chromatic amplitudes differ for values of ℓ=1 to 4.

We are encouraged that the chromatic amplitudes in Figure 4.7 have the same basic features as the model chromatic amplitudes. Since we did not fit the continuum to create the chromatic amplitudes, we do not expect the region outside of the fitted wavelengths to closely follow the models. Hence, we do not see the arches between the spectral lines apparent in the models. Also, the seeing on the first night was worse than the second, possibly washing out more of the information concerning the changing line shape. This may account for the differences between the chromatic amplitudes on different nights.

The drastic improvement in the appearance of chromatic amplitudes seen in Figure 4.7 is very encouraging. However, the danger in using spectral fits instead of the original spectra is a possible introduction of systematic effects that could alter the final results. We are making an assumption about the appearance of the spectral line that might not be entirely accurate.

To test how our technique alters the appearance of the chromatic amplitudes, we created a time series of 410 simulated spectra. We introduced the line profile variations to the spectra by adding a product of the spectrum, the model chromatic amplitude, and $\cos(\omega t + \phi)$. We introduced a strong signal for modes from ℓ=1 to ℓ=4, convolved each spectrum with a gaussian to emulate the resolution of our data (3.9 Å), and then produced chromatic amplitudes in the same way described above by fitting each spectrum with a Lorentzian plus a Gaussian. The chromatic amplitudes created by this experiment (Figure 4.7 and 4.8) show a few differences from the original model chromatic amplitudes in Figure 4.1. The new model chromatic amplitudes show a narrower peak and shallower dips on either side, making their appearance similar to our chromatic amplitudes in Figure 4.7.

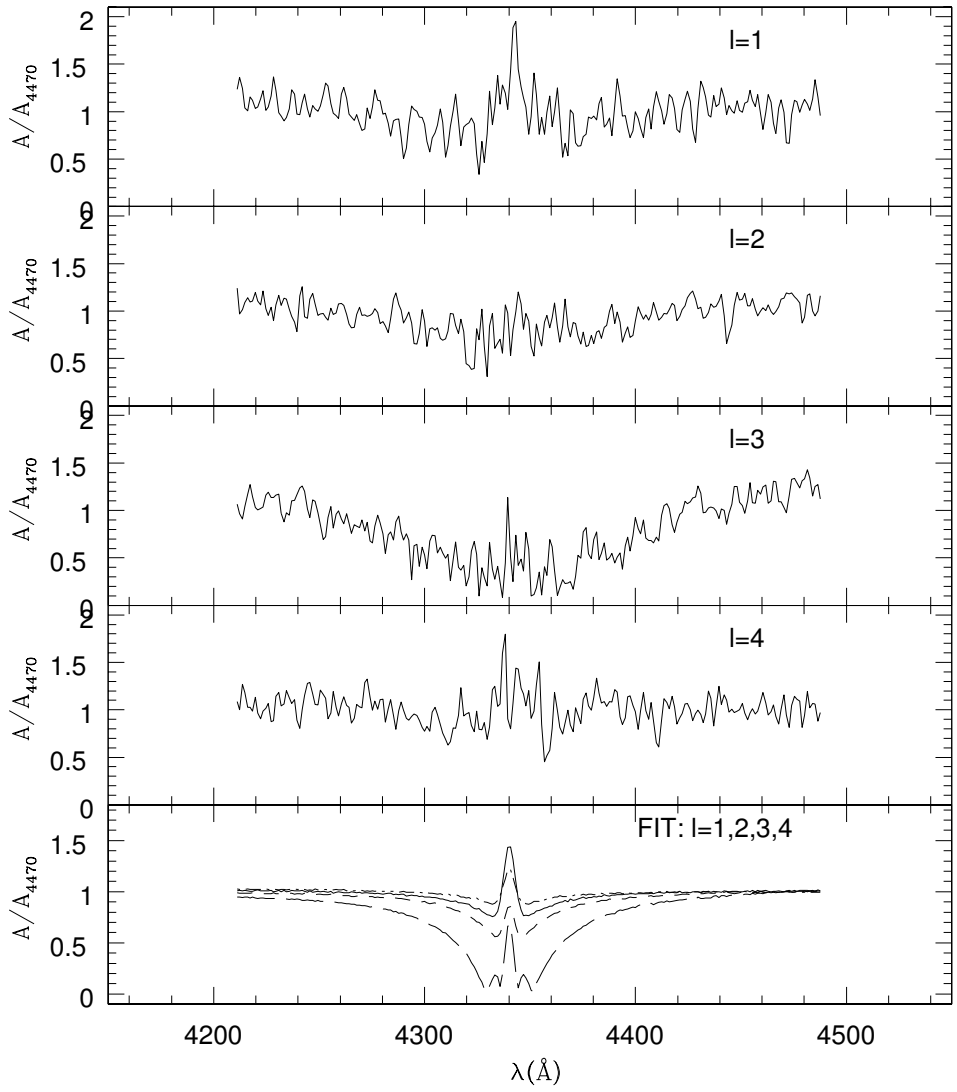

Figure 4.9 Chromatic amplitudes created from noisy simulated spectra. The first four show the chromatic amplitudes as measured directly from the fake spectra. The bottom panel shows four chromatic amplitudes created from fits to those spectra. The lines are solid, short-dashed, long-dashed, and dot-dashed in order of increasing ℓ.

To further test the validity of this technique we added random noise to the same series of fake spectra, giving them the signal-to-noise of our spectra. We used the model chromatic amplitudes to introduce pulsations of different spherical degrees with amplitudes near 2 mma at 4470 Å. We then measured the amplitudes at each wavelength both directly from the noisy fake spectra and the fits to the spectra. The results of this experiment can be found in Figure 4.9. The raw chromatic amplitudes resemble those from our data in Figure 4.5. In spite of their poor appearence, application of the spectral fitting technique to the noisy fake spectra successfully recovered the shape of the model chromatic amplitudes. From this experiment we have shown that the addition of information about the shape of the spectrum can overcome a series of spectra with a signal-to-noise too poor to create meaningful chromatic amplitudes directly from the data.

We performed the same experiment for different periods and different amounts of noise in order to see how they could affect the appearance of the chromatic amplitudes. Even with moderately noisier spectra, the basic distinctions between the different spherical degrees remain. The largest variation from the models occurs at the central peak; noise can both increase and decrease the height of this peak. The line center is described by the Gaussian portion of the fit and is dominated by only a few points, so we might expect noise to have a greater effect on the central region of the line.

In the fits shown in Figure 4.7, the chromatic amplitudes of F1, F3, and F4 all appear to have the familiar 'w' shape of the ℓ=1 or 2 modes. They mostly show no significant asymmetries, expected since we removed the velocities prior to the fits. The chromatic amplitudes of F2, the 142 s mode, measured for H_β and H_γ on both nights shows a distinctly different shape. This mode has almost no drop on either side of the central peak. When compared to the model chromatic amplitudes in Figures 4.1 and 4.8, it most resembles the characteristics of the ℓ=4 model. All modes identified on DAVs thus far have had $\ell \leq 2$, expected since higher spherical degrees suffer from increased geometric cancellation.

For direct comparison we show the chromatic amplitudes for the second night of H_γ of the four largest modes along with the model chromatic amplitudes created by fitting the simulated spectra (Figure 4.10). In order to make an accurate comparison,

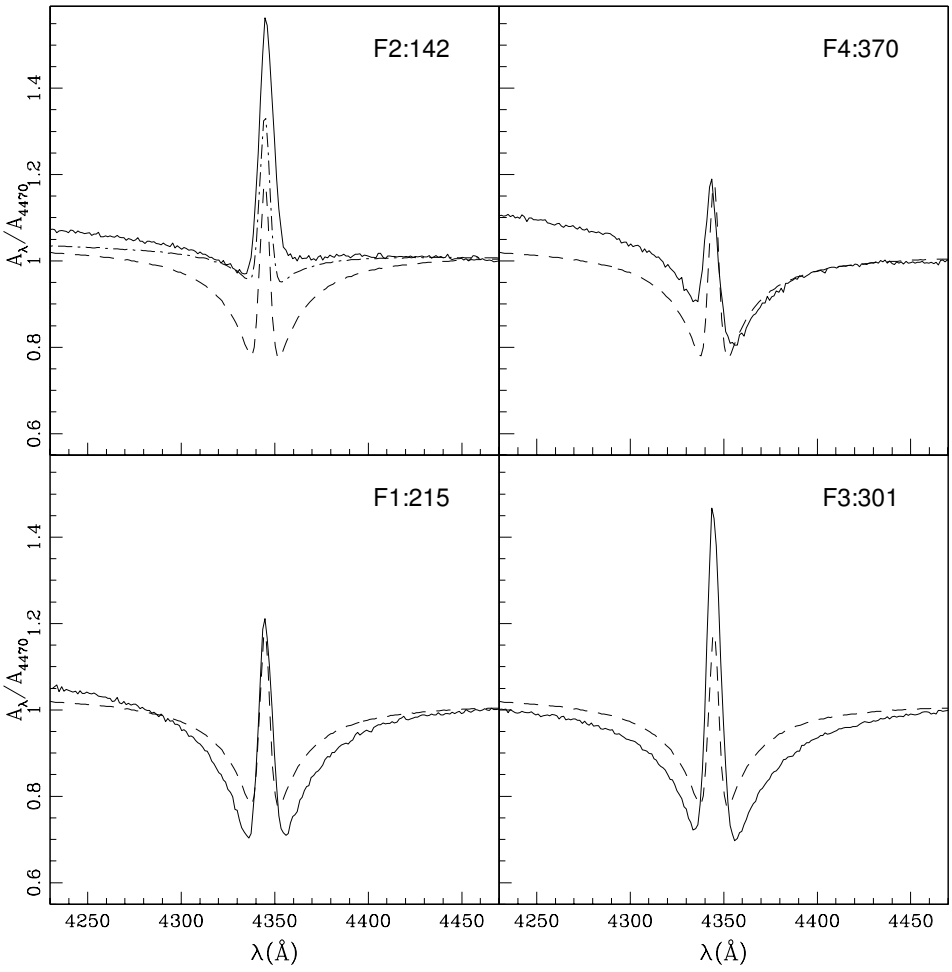

Figure 4.10 Comparison of the fitted model chromatic amplitudes to the fitted observed chromatic amplitudes. The solid line is the observed chromatic amplitude from the gamma line on the second night and the dashed line is the ℓ=1 model. For the 142 s mode the dot-dash line is ℓ=4. Models were calculated using a mean temperature of 11,750 K and log(g)=8.25. Each curve has been normalized at 4470 Å.

the simulated spectra were shifted in wavelength to agree with the central wavelength of our average spectrum. F1, F3 and F4 all show similarities with an ℓ=1 mode while F2 resembles an ℓ=4. The discrepancy between the model and our chromatic amplitudes lies mostly in the central peak. The bottom of the spectral line has a smaller signal-to-noise and as we discussed earlier, noise appears to mostly affect the size of that central peak. Regardless, the differences between the ℓ=1 and ℓ=4 remain and can clearly be seen in the plot of F2 in Figure 4.10.

4.7 Conclusions

We have developed a new analysis technique for low-resolution time series spectroscopy that can reveal mode identifications from relatively poor signal-to-noise data. By using fits to the spectral lines, we have discovered a method to discern the spherical degree of pulsation modes on DAVs. For PY Vul, applicaton of this technique has led us to the conclusion that its dominant pulsation mode has a spherical degree of four.

As we shall see, the idea of an ℓ=4 is not as outlandish as it first seems. An ℓ=4 mode, as suggested by the chromatic amplitudes, can also explain the unusual behavior in the UV, the large harmonic mode, and the low amplitudes of PY Vul. In the next chapter, we will discuss the previously published observations in light of this new hypothesis.

Chapter 5

The ℓ=4 Hypothesis for PY Vul

I'm looking over a four-leaf clover
That I overlooked before.

Lyrics by Mort Dixon

The addition of optical time-resolved spectroscopy has led us to present a hypothesis that potentially explains all the mysterious observations of PY Vul. The frequency spectra of simple, blue-edge DAVs are commonly dominated by one mode. In this chapter, we consider our F2, the 142 s mode, to be the dominant pulsation mode of this star and to have a spherical degree of four. The remaining modes are either weakly driven ℓ=1,2 modes or combination modes. We will now consider to what extent this hypothesis can account for previous observations of PY Vul. We then discuss other proposed scenarios to explain the pulsation characteristics and show why they are inferior to the ℓ=4 hypothesis.

5.1 Previous Observations

While the chromatic amplitudes of PY Vul are consistent with an ℓ=4 pulsation, here we consider the other peculiar observations of this star. We find that the unusual UV properties, the large harmonic, and the small amplitudes of PY Vul are also consistent with the ℓ=4 hypothesis.

5.1.1 UV observations with HST

In the UV observations presented by Kepler et al. (2000), the relative amplitudes of the modes on PY Vul significantly increase at shorter wavelengths except for the 142 s mode. The amplitude rise is a result of both the increased effect of temperature on flux and the increased limb darkening at these shorter wavelengths. The 142 s mode is perplexing because it does not match the other modes or the models of $\ell \leq 2$. Considering modes of higher ℓ, we note that in Figure 4.1 the ℓ=4 mode does not increase in amplitude like the lower order spherical degrees. The negative amplitudes shown in the model would be measured with a positive amplitude and a 180 degree phase shift. We examined the UV data presented in Kepler et al. (2000) to judge the agreement of the phases and amplitudes of the 142 s mode with the ℓ=4 model.

To obtain the amplitudes and phases at each wavelength of the HST data we fit the zero-order light curve ($\sim$3400 Å) with the seven dominant modes to find the frequencies, amplitudes and phases. We then fixed the frequencies, fit each wavelength bin with all seven modes and normalized the amplitudes and phases by the zeroth order fit. The relative amplitudes are presented in Figure 5.1 along with the ℓ=1 and ℓ=4 models. As mentioned before, the measured amplitudes do not rise as quickly as the ℓ=1 model and are more consistent with the ℓ=4 model.

Figure 5.2 shows the phase at each wavelength for the 142 s mode and its harmonic (71 s). While the harmonic shows no phase reversal, at wavelengths less than 1500 Å, our proposed ℓ=4 mode shows three points with a phase change greater than 100°. Though the change in phase of those points is less than 180°, they occur where the ℓ=4 model shows a phase change. We conclude that while these measured phases do not prove the ℓ=4 hypothesis, they also do not exclude it.

The minor inconsistencies between the data and the ℓ=4 model could be in part due to third order combinations with the same frequency as F2 (i.e. F2=2F2-F2). Though small in amplitude, they would have low ℓ components, increasing in amplitude and having no phase change at UV wavelengths. The added amplitude and different phase of this mode could interfere with F2 and create the small discrepancies with the ℓ=4 model.

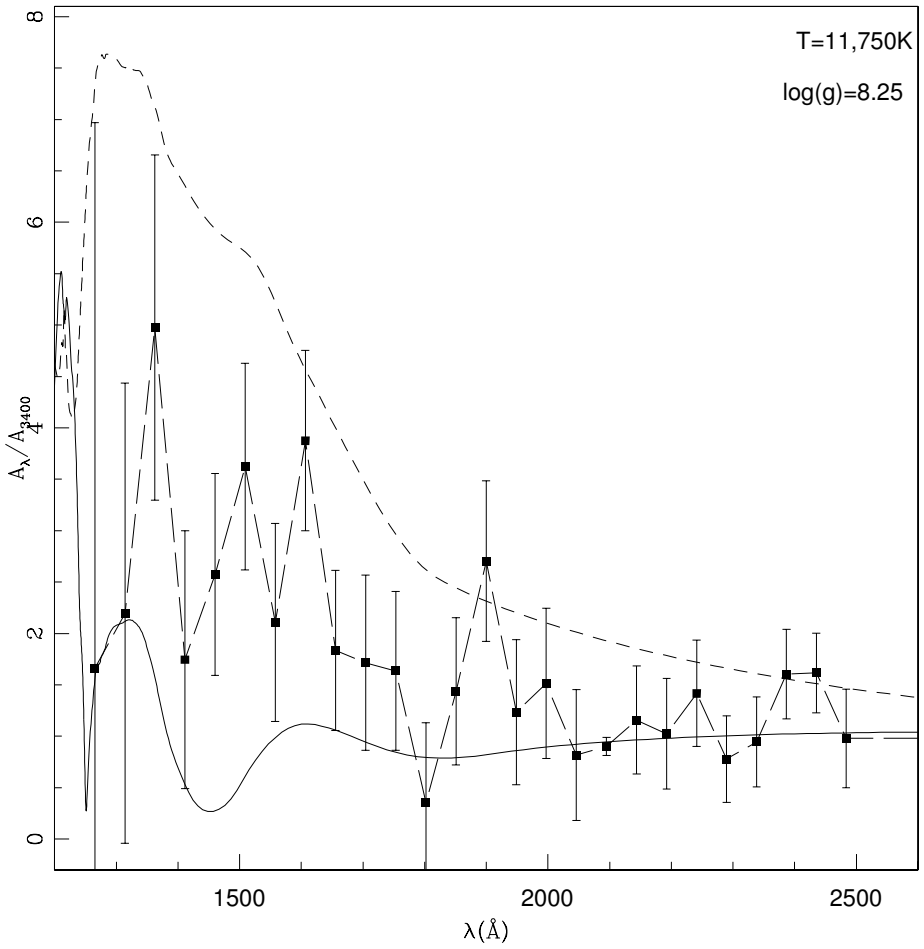

Figure 5.1 Amplitude variations in the UV. Absolute value of the ℓ=1 (short dashed) and ℓ=4 (solid) model plotted with the measured amplitudes of the 142 s (F2) (squares). The observed UV amplitudes are from the HST data (Kepler et al. 2000).

We note that the 142 s mode is not the only mode that shows a curious UV behavior. Observations of the DAV, G 117-B15A (Kotak, van Kerkwijk, & Clemens 2004), reveals a mode that does not increase in the UV, but no other evidence suggests that this mode should be an ℓ=4. Also, unlike our observations, the same mode on G 117-B15A shows an unusual trend at the blue end of the optical wavelengths. Apparently, this failure to rise in the UV is not an exclusive signature of a higher degree mode.

Some of the inconsistencies could result because it might not be entirely appropriate to use the linear models for comparison with the measured wavelength dependence of the amplitudes and phase. Ising & Koester (2001) performed non-linear simulations and showed that the size of the amplitude and inclination can play a role in how the relative amplitudes and phases vary with wavelength in both the UV and optical wavelengths. Their study concurs that a failure to rise in the UV is consistent with ℓ>2.

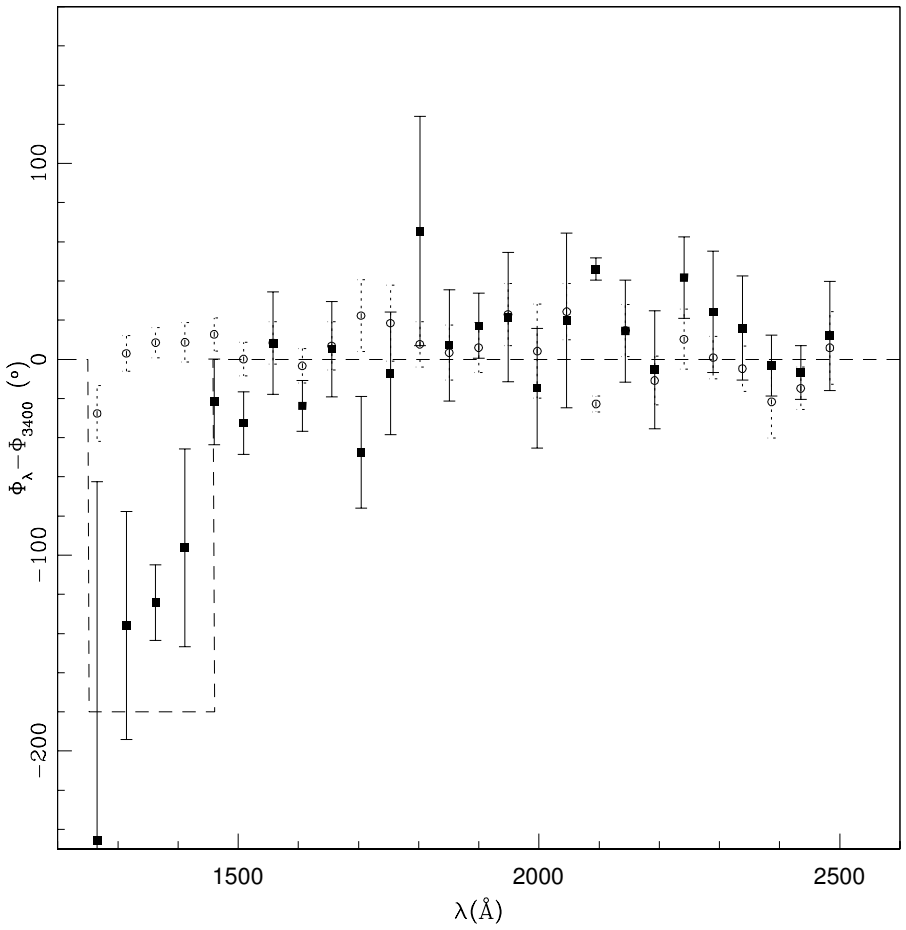

Figure 5.2 The phases for the 142 s (F2) (squares) and the 71 s (F5) (circles) modes relative to the phase measured at 3400 Å. The error bars reflect a reduced chi-square of one for each wavelength bin. The dashed line represents the phases expected for an ℓ=4 model. The ℓ=1,2,3 models would show no phase change.

We conclude that though the UV data is not a perfect match to the ℓ=4 hypothesis, it is a better fit to the observations than any other available choice.

5.1.2 The Harmonic Mode

We consider the implications of the ℓ=4 hypothesis on the harmonic of the 142 s mode. The 71 s (F5) mode, is exactly twice the frequency of the proposed ℓ=4 mode. Castanheira et al. (2004) found combinations between the 142 s (F2) mode, the 72 s (F6) mode, and a mode at 148 s. In our hypothesis F5 (and either F6 or 148 s) is not a real mode; it is the result of nonlinear effects most likely caused by the surface convection zone (Wu 2001; Ising & Koester 2001). Large combination modes are uncommon on blue-edge DAVs like PY Vul, and unexpected for low amplitude pulsations. If F2 is indeed an ℓ=4 mode, its actual amplitude is much larger than observed, removing this inconsistency with the theories.

Wu (2001) has provided an analytic description of how a harmonic mode is distributed on the surface of the DAV, and concluded that a harmonic mode appears as the square of the parent mode's distribution. From this theory, only two scenarios can create a harmonic similar in size to its parent. First, a large inclination of the star, as proposed by Thompson & Clemens (2003), could provide large cancellation of the parent mode but leaves the harmonic unaffected. However, as we shall discuss in §5.2, this theory is unable to explain the UV characteristics of PY Vul. Second, if the parent mode has a larger spherical degree, it will suffer from cancellation over the surface of the star while the harmonic mode, appearing as the square of the parent, does not. Though the total power of the harmonic mode is less than the power of its parent, the severe cancellation of the parent mode can make the harmonic mode appear larger in the observed light curve. Having the 142 s mode be an ℓ=4 mode is consistent with this picture; the 142 s mode is innately canceled while its harmonic at 71 s is not.

If the chromatic amplitudes are modeled in the same way as Figures 4.1 and 4.10 for the surface distribution of a harmonic, we notice a resemblance to an ℓ=2 mode. This similarity is not surprising; the square of an ℓ=4 spherical harmonic has most of its flux changes at the pole and suffers from no cancellation over the surface of

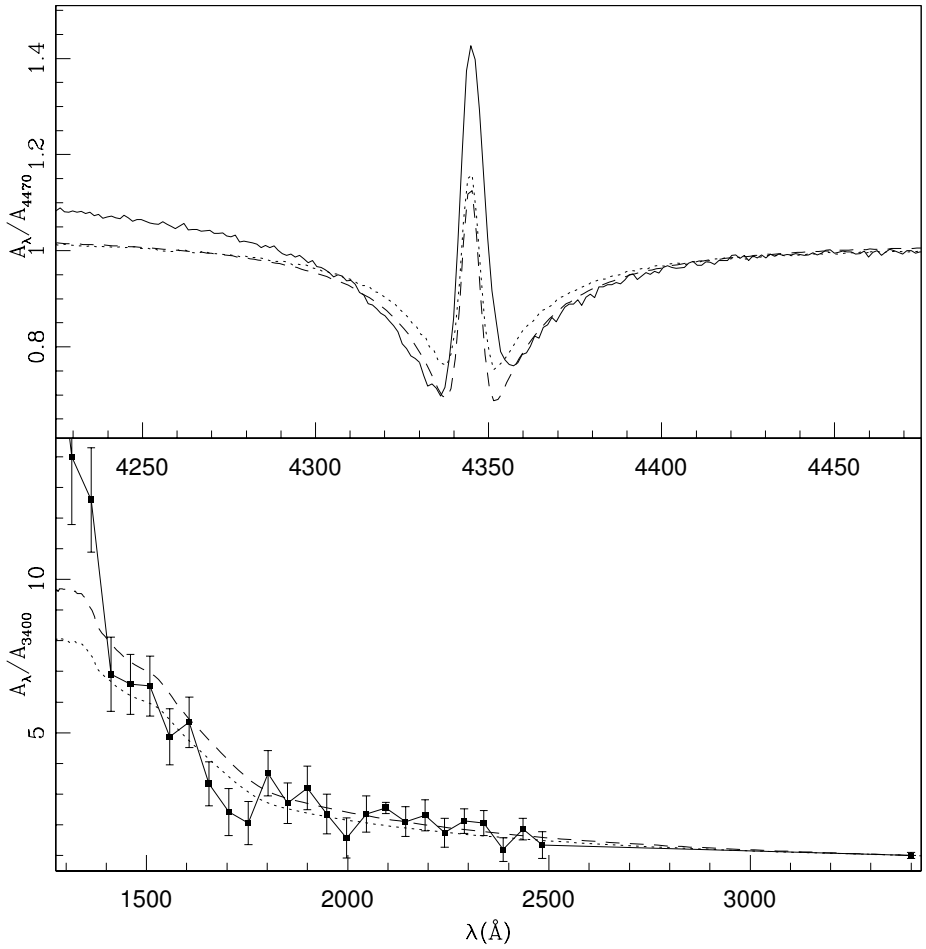

Figure 5.3 Comparison of models (Dotted is ℓ=2 and dashed is (ℓ=4, $m = 0$)^2) to the optical chromatic amplitudes (solid line) and UV data (solid squares) (Kepler et al. 2000) for F5, the 71 s mode. The optical model chromatic amplitudes are created from simulated spectra and treated in the same way as the data. For both figures we used the model corresponding to T=11,750 and log(g)=8.25.

the star just like a lower ℓ mode. Figure 5.3 compares the expected variations of amplitude with wavelength for an (ℓ=4, m=0)^2 distribution to both the HST data and our H_γ chromatic amplitude of the 71 s mode from the second night. Both curves show agreement with the models.

The ℓ=4 scenario implies that the parent mode has a low value of m. A harmonic created by an ℓ=4, $m\geq$2 mode will resemble an $\ell\geq$4 mode. Only combinations created by ℓ=4, $|m|\leq$1 modes will have a large amplitude, increase in the UV, and have chromatic amplitudes similar to $\ell\leq$2. Similarly, any azimuthally split modes, as the possible one observed by Castanheira et al. (2004), would have harmonics with large ℓ characters and small amplitudes.

5.1.3 Optical Amplitudes

If the 142 s is the dominant ℓ=4 mode, then this might explain the low amplitudes of this star's pulsations. The measured amplitude of an ℓ=4 mode would be limited by cancellation as the observed flux variations result from a sum across the visible surface of the star. To test this, we calculated how much brighter an ℓ=4, m=0 mode would look if it appeared as an ℓ=1, m=0 mode. To determine this factor we integrated both modes over the visible surface of a star seen at its pole using limb darkened models (T=11,750, log(g)=8.25) and summing the flux change over the visible wavelengths (4000-5500 Å). We concluded that an ℓ=4 mode would be observed approximately 13 times smaller than an ℓ=1. So, if PY Vul is dominated by an ℓ=4 mode, its amplitude has been reduced by a factor of thirteen, meaning that our F2 would be $\sim$ 19.5 mma if it were an ℓ=1 mode. Hot DAV stars have been observed with amplitudes as high as 23 mma (see Kepler et al. 1991 and Clemens 1994).

Assuming that the other DAVs are generally dominated by ℓ=1 modes, as deduced by Clemens (1994), we compared PY Vul to the class of DAVs after applying this scaling factor. To illustrate the results, we reproduced the plot of weighted mean period verses power from Clemens (1994) and added the location of an ℓ=1 dominated PY Vul (Figure 5.4). While the observed location of PY Vul has a low amplitude, placing it below the trend of the other DAVs, a PY Vul that does not suffer the geometric cancellation of an ℓ=4 mode would be located at the plus sign in Figure 5.4.

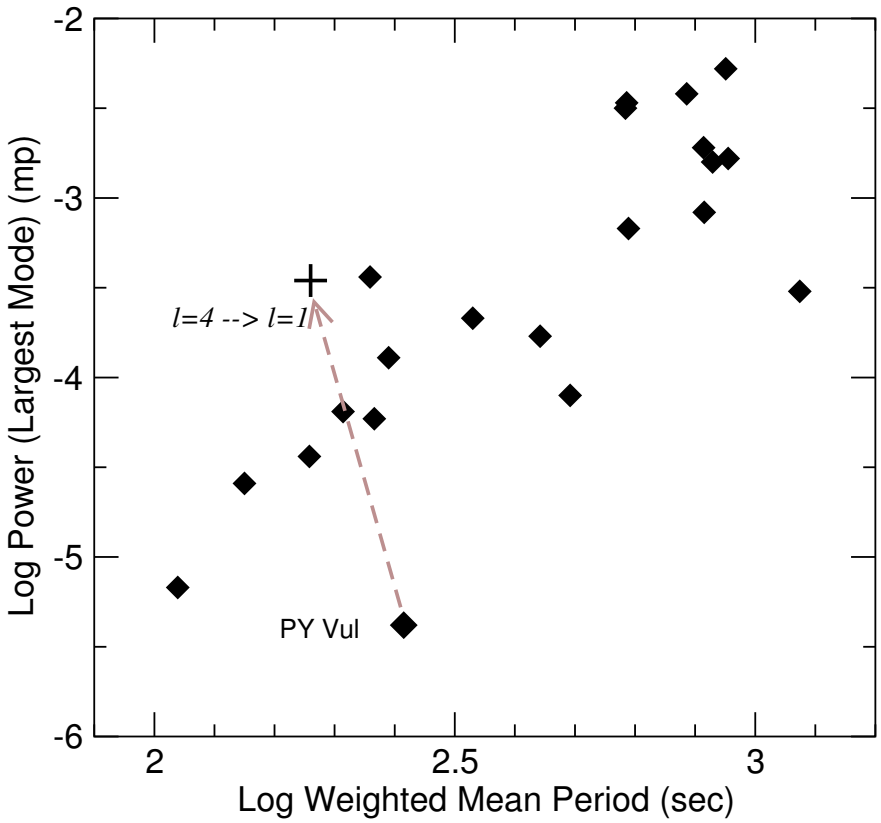

Figure 5.4 The power of the largest mode plotted against the weighted mean period of 21 known DAVs. The diamonds are 21 DAVs studied by Clemens (1994). PY Vul is the diamond labeled at the bottom of the plot. The location of PY Vul after scaling by the factor discussed in §5.1.3 and adjusting for a new weighted mean period is represented by the plus sign. This plot demonstrates that by assuming an ℓ=4 mode we can account for the low amplitudes of PY Vul. When adjusting for the increased cancellation, PY Vul agrees with the trend created by the other DAVs.

The ℓ=4 hypothesis satisfyingly explains all the above characteristics of the pulsation spectrum of PY Vul. Our only hesitation is the failure to see 8 azimuthally split modes associated with the ℓ=4 mode. However, we also do not see triplets for the other modes. Either the star does not excite higher m modes, or is rotating so slowly that we have failed to resolve them.

5.2 Other Proposed Scenarios

Other suggestions have been made to explain the character of the pulsations of PY Vul. After a preliminary analysis of the same data presented here, Thompson & Clemens (2003) proposed that a large inclination could account for the low mode amplitudes. In this scenario, the 142 s mode is the first harmonic of a mostly cancelled mode found near 285 s, while the 71 s mode is the third harmonic. This hypothesis did explain the failure of the 142 s mode to rise in the UV. However, it failed to explain the behaviour of the 71 s in the UV. Furthermore, the 285 s parent mode required by this scenario was only marginally detected on the first night of the LRIS observations, and the extensive coverage of the WET run on PY Vul (Castanheira et al. 2004) failed to find any significant signal near 285 s. This requirement of almost total cancellation imposed by the WET data requires an extreme inclination.[12] To achieve the ratio between the amplitudes of the proposed 285 s and 142 s modes, the star would have to be viewed within approximately 1° of its equator. Because of this need for fine tuning and the inability to explain the UV amplitudes, this model is inferior to the ℓ=4 hypothesis we have presented.

Castanheira et al. (2004) and Kepler et al. (2000) maintain that since the 142 s mode shows the atypical behavior in the UV, it must be due to some nonlinear effect and both the 71 s and 72 s modes are real modes. As they point out, a real mode with such short periods forces asteroseismological models to use masses near the Chandrasekhar limit in order to create an ℓ=1, k=1 mode with such a low period (Bradley 2001). As the mass of this star is near 0.6 $M_\odot$ (Castanheira et al. 2004), they

[12]The star must be inclined within 1 degree of the equator to achieve this cancellation. The probability of a star having this inclination is 0.02.

conclude these modes must be ℓ=2. They agree with Thompson & Clemens (2003) that the star must have an unfavorable inclination to create the low amplitudes and possibly the character of the 142 s mode in the UV. The largest problem with this scenario comes from the nature of the 142 s mode. Combination and harmonic modes are believed to be a result of nonlinear effects in the atmosphere of the star. However, the theories concerning the nonlinear interaction between the outer atmosphere and the pulsation modes predict the existence of harmonic modes but not sub-harmonics (Brickhill 1992b; Wu 2001). The 142 s mode, as a subharmonic, would have to be created by some new type of mechanism that operates over every other cycle of the real, parent mode. Unlike this scenario, our ℓ=4 hypothesis does not require the addition of any new physics. The nonlinear effects discussed by Brickhill (1992b) and Wu (2001) act on the 142 s mode to create a harmonic near 71 s.

5.3 Conclusions

The DAV star PY Vul has a perplexing pulsation spectrum that has challenged attempts to understand the star. We have analyzed line profile variations that suggest the 142 s pulsation mode in PY Vul has a spherical degree of four. If this mode is the star's dominant pulsation mode, then we can explain the star's overall low pulsation amplitude by geometric cancellation without the need to invoke improbable inclinations. Furthermore, because the pulse shape harmonic of an ℓ=4 mode has lower ℓ characteristics, it cancels less effectively, explaining the unusually large amplitude of the mode's harmonic. Finally, an ℓ=4 character of the 142 s mode and the consequent ℓ=0 and 2 character of its harmonic are the very values most consistent with the UV amplitudes measured by the Hubble Space Telescope, although problems with pulsation phases remain. Together, these results yield a satisfying and unified picture of the star's pulsations, and the only one consistent with all the data.

If our assignment of ℓ=4 to the 142 s mode is correct, then it is a surprise since we have never before seen even ℓ=3 and only seldom ℓ=2. Interestingly, the assignment of ℓ=1 to most of the modes in hot DAVs by Clemens (1994) does not apply to the 142 s region of PY Vul, which was one of two stars thought to have ℓ>1. Based on period

spacings alone, Clemens (1994) recognized that the 142 s or its nearby 148 s mode must be higher ℓ but had suspected ℓ=2, not 4. If we are forced to consider higher ℓ during mode identification, then it will make that process difficult because the high ℓ modes are closely space in period. Fortunately, it appears that high ℓ modes advertise that fact by having large harmonics which may assist in their identification.

Chapter 6

Finale

This is the song that never ends.
It just goes on and on my friend.

Anonymous

Though this is the final chapter, it may appear to act more as a beginning than an end. Everything presented here has either shown a new method to apply to further DAVs, or created questions for further exploration. Our new strategies for time series spectroscopy increase the ability to measure mode identifications and pulsation velocities. Their application on two ZZ Cetis has already discovered new phenomena, showing the potential of pursuing this direction of research.

6.1 Velocities with High-Resolution Spectra

Previously, velocity measurements of DAV pulsations were made using spectra whose resolution was set by the seeing. The advantage of the wide slit is that more light is collected, creating better signal-to-noise in the spectra and improving the measured light curve. However, the motion of the star in the slit creates more noise in the velocity curve, and the low resolution limits the ability to measure the small Doppler shifts. Because of the poor noise-level of the velocity FTs, many detected velocity periodicities are only deemed significant because of a corresponding mode in the flux FT. The velocity curve of PY Vul presented in Chapter 4 exemplifies the

limitations of low-resolution spectroscopy. The low amplitudes of PY Vul were easily detected in the flux curve, but could not be seen in the velocity curve. Plus, because essentially no slit was used, those potentially significant peaks in the velocity FT are most likely due to movement of the star in the slit and are not intrinsic to the star. While low-resolution spectroscopy has detected periodic velocity variations (Kotak, van Kerkwijk, & Clemens 2004; Kotak et al. 2002; Kotak, van Kerkwijk, & Clemens 2002; van Kerkwijk, Clemens, & Wu 2000), they must be associated with periodicities in the flux curve to be considered real.

The application of high-resolution spectroscopy on G 29-38 proved to be a successful variation on the optical time series spectral method introduced by van Kerkwijk, Clemens, & Wu (2000). Using a higher resolution spectrograph and a slit, our velocity curve had a relatively lower noise level than the flux curve. The HIRES data afforded a 1 km s^{-1} detection limit, an improvement over the 2 km s^{-1} limit of the LRIS data (van Kerkwijk, Clemens, & Wu 2000) on the same star. Unfortunately, even using a 10-m telescope and observing one of the brightest DAVs, each individual spectrum only had a signal-to-noise of $\sim$8. As such, this technique is currently limited to only a few DAVs until larger telescopes or more efficient spectrographs are built to gather the light.

Even if high-resolution spectroscopy is out of reach for the majority of DAVs, it has already proved beneficial with the data on G 29-38. Despite the fact that current theories suggest non-linear effects are only present in the flux variations, we found a contrary example in our *velocity* curve of G 29-38. Though we only have the one example, and confirmation is necessary, the combination velocity mode challenges the current theories regarding the physics of DAV pulsations. By seeking low-noise velocity curves of these more complex pulsators, we have the potential to find further examples of combinations and harmonics in the velocity variations. More data on G 29-38, or a similar star, would make it possible to confirm our combination velocity mode and begin to understand the nature of this new phenomena.

With the advantages of both low and high-resolution time series spectroscopy at our disposal, we can obtain the velocity measurements crucial to test the predictions of the convective driving theory (Goldreich & Wu 1999a; Brickhill 1991). Both our high-

resolution and previous low-resolution velocity measurements (Kotak, van Kerkwijk, & Clemens 2004; Kotak et al. 2002; van Kerkwijk, Clemens, & Wu 2000) agree with the relative velocity and phases predicted by the analytical convective driving models (Wu & Goldreich 1999). The data, though inconclusive, do not show the trends with frequency. The best way to gain further measurements of the amplitude and phase variations with frequency would be to have velocity and flux detections for a range of frequencies on a single star. Generally, the cooler variety of DAVs, like G 29-38, show a greater range of frequencies and larger amplitude modes. Plus, once new instruments become available, they will enable us to measure lower amplitude modes, and we will have a larger collection of modes to find any frequency trends.

6.2 Mode Identification by Improved Signal Extraction

Providing the correct values of k, ℓ and m for each pulsation mode is a fundamental prerequisite to doing asteroseismology on the ZZ Cetis. Ultimately, this information will provide the structural information necessary to answer questions regarding the development, evolution, and age of white dwarf stars. We now have a large collection of tools that can help us pursue the eigenvalues of all ZZ Ceti pulsations.

The original attempts at mode identification for DAVs were done photometrically using period spacings and multiplet splittings. However, this is near impossible with the dearth of modes on the hot DAVs, and the mode variability of the cool DAVs. Time series spectroscopy provides a method that does not rely on the presence of other modes to determine the spherical degree. Even this method has faults as the data collected from some of the best telescopes provide questionable and ambiguous results on even the brightest DAVs. Though we have only measured two DAVs and only securely measured the spherical degree of one mode, the future of mode identification looks much better. The discovery of an ℓ=4 mode on PY Vul showed how to determine secure results from the optical data, removed some of the confusion from the UV data, and demonstrated how higher spherical degrees would appear.

We found that applying some information about the shape of the spectral line can improve the chromatic amplitudes and determine mode identities. When applied to

the data of PY Vul we were led to discover the ℓ=4 mode. Despite the amplitudes of PY Vul being too small to directly measure with these data, the new technique was able to extract the necessary information. If applied to larger amplitude modes of similar quality data, we may even distinguish between the very similar ℓ=1 and ℓ=2 modes. For this reason, re-analyzing the already existing time series data is necessary. It will help in determining the abilities and limitations of this technique, while securing the mode identifications. In principle, we can now collect useful data on dimmer ZZ Cetis with current telescopes and spectrographs.[13]

Looking to the future, several telescopes with larger mirrors, and more efficient spectrographs are in development. These will provide the tools to apply time series spectroscopy to more DA pulsators. It will also create the possibility of taking high-resolution spectra while still obtaining enough flux information to create chromatic amplitudes. The signal-to-noise for an individual pixel (wavelength bin), needs to be higher to measure the chromatic amplitudes than the velocities. This is the reason we failed to measure chromatic amplitudes on G 29-38 while still measuring the velocities. As the ratio of the velocity and flux amplitudes depend on ℓ, it can provide a check to the measured spherical degree (van Kerkwijk, Clemens, & Wu 2000). Though already accomplished for low-resolution data, the high-resolution in addition to a decent measure of flux will improve these measurements.

By confidently identifying a higher degree mode in PY Vul, we have cleared up some of the questionable results in the UV amplitudes. Now we know that a failure for amplitudes to rise in the UV is consistent with this higher degree. While the UV amplitudes remain inconclusive for spherical degrees less than or equal to two, they help identify higher degree modes. Also, the discovery of an ℓ=4 has shown us that higher degree modes are present in the DAVs and can be observed if strongly driven. They should be considered as a possibility when identifying modes. Fortunately, it appears that higher spherical degrees will clearly reveal their existence by displaying low amplitudes and relatively large harmonics. By obtaining quality light curves

[13] Additionally, we may also get better signal-to-noise by using LRIS-B, the spectrograph at the Keck Observatory with improved blue sensitivity.

and measuring the relative amplitudes of observed combinations, an indication of the spherical degree may be determined.

To prevent misidentification, it is prudent to use a combination of the above techniques for measuring spherical degree. Relatively large harmonic modes, for instance, can be produced by large stellar inclinations (Thompson & Clemens 2003). Kotak, van Kerkwijk, & Clemens (2004) show evidence that other effects may prevent increasing amplitudes in the UV. The star G 117-B15A has no other evidence of having a large ℓ mode, yet shows the same type of UV amplitudes as PY Vul. As the discovery of a ZZ Ceti comes from obtaining a light curve, and since these are simpler to obtain, it is probably best to start any mode identification efforts there. These observations provide an accurate representation of the all modes present on especially the hotter DAVs. The presence of smaller modes, large combinations, or wide multiplet splittings may indicate spherical degrees higher than one. For the brighter ZZ Cetis, the suspected modes can be specifically identified with time series spectroscopy in the optical or UV.

The biggest problem remains in distinguishing ℓ=1 from ℓ=2. Many techniques, in theory, differentiate between these modes, including multiplet splittings, closely spaced periods, a larger R_v, slightly larger combination amplitudes, a steeper increase in UV amplitudes, and a different 'w' shape in the optical. However, because of the limitations and ambiguity of each method, without more than one piece of evidence, any detection remains questionable.

6.3 Loose Ends

Though we have developed strategies to better measure the DAV stars, the data here have left behind several loose ends. First, the new techniques will only fully yield their worth when applied to a larger sample of pulsators. Second, the scientific discoveries they yielded on G 29-38 and PY Vul have, in some ways, created more questions than they have answered.

The pulsation velocities measured on G 29-38 did not solve any mysteries and ended up creating another one. Having eliminated rotation and pulsation, the unusual H_α

line cores of ZZ Cetis remains inexplicable. The lack of significant flux amplitudes for short period modes, prevented conclusive trends to test the convective driving theory. And, the velocity curve produced an inexplicable combination mode. Each question needs to be pursued with either further observations or refinement of the theoretical models.

The remaining question on PY Vul, is why a star would be driven to excite an ℓ=4 mode. These higher degree modes are believed to be small in part because of geometrical cancellation, but they also take more energy to drive. The large number of opposing pulsation zones for the higher ℓ modes implies more energy leakage between the zones, decreasing their amplitude. Or, it may not be unusual for DAV stars to have higher degree pulsations; most DAVs are not bright enough for current data sets to detect the low amplitude pulsations of higher degrees.

These questions, along with the abundance of ZZ Cetis, leave a plethora of work, but we have managed to provide some answers regarding ZZ Ceti pulsations. Our new techniques have solved the mysteries behind the unusual pulsations of PY Vul, and have provided clear confirmation of the pulsation velocities on G 29-38. These results give hope that further research in this direction will create a better understanding of the ZZ Ceti pulsators.

Appendix A

More on Chromatic Amplitudes

A.1 G 226-29

To further test the spectral fitting technique and show its versatility for other data, we analyzed time-series spectra of the pulsating white dwarf G 226-29. The data for this star were collected at the Keck Observatory with the LRIS spectrograph (Oke et al. 1995) in a manner similar to the data on PY Vul (see Chapter 4). The 195 spectra analyzed here were taken on September 6, 1998 with an exposure time of 20 s and a readout time of 13.9 s.[14] The signal-to-noise per pixel of the continuum of an individual spectrum is about 250 while the average spectrum is near 1000.

G 226-29 is a hot DAV pulsator with only one pulsation mode (109 s) that is azimuthally split into a triplet. Photometric and UV observations identify the triplet as ℓ=1, but the possibility of ℓ=2 is not entirely forbidden (Kepler et al. 2000; Kepler et al. 1995; Fontaine et al. 1992). Since the spherical degree of the 109 s mode is known, We use it as a further test of the new technique introduced in Chapter 4 to measure the chromatic amplitudes of PY Vul. The 1.8 hours of data on this star reveal its pulsation mode at 109.27 s with an amplitude of 3.3 mma; the data set is too short to resolve the triplet.

The H_γ region of each spectrum was fit with the combination of a Lorentzian and Gaussian function; these fits were then used to create the chromatic amplitudes. In Figure A.1, we show the original chromatic amplitudes and the chromatic amplitudes created from the fits to the spectral lines. The average noise level of the FT of an individual wavelength bin from the fitted spectra is 1.4 mma. Notice the basic shape

[14] C. M. Yeates performed the bias subtraction, wavelength calibration, and optimal extraction of each spectral image in the series with standard routines in IRAF.

from the original is reproduced by the chromatic amplitudes from the fits. Both curves show evidence of the 'w' shape, and an unexpected asymmetry, despite removing the velocity variations. When the chromatic amplitude from the fits is compared to the model, it most closely resembles an ℓ=1. Figure A.2 shows the chromatic amplitudes created from introducing oscillations of different spherical degrees to a model atmosphere of T=12,250 K and log(g)=8.25. This is approximately the temperature and gravity of G 226-29 (Bergeron et al. 1995). The fitted chromatic amplitudes and the ℓ=1 model are in agreement as expected from our understanding of the pulsations of G 226-29.

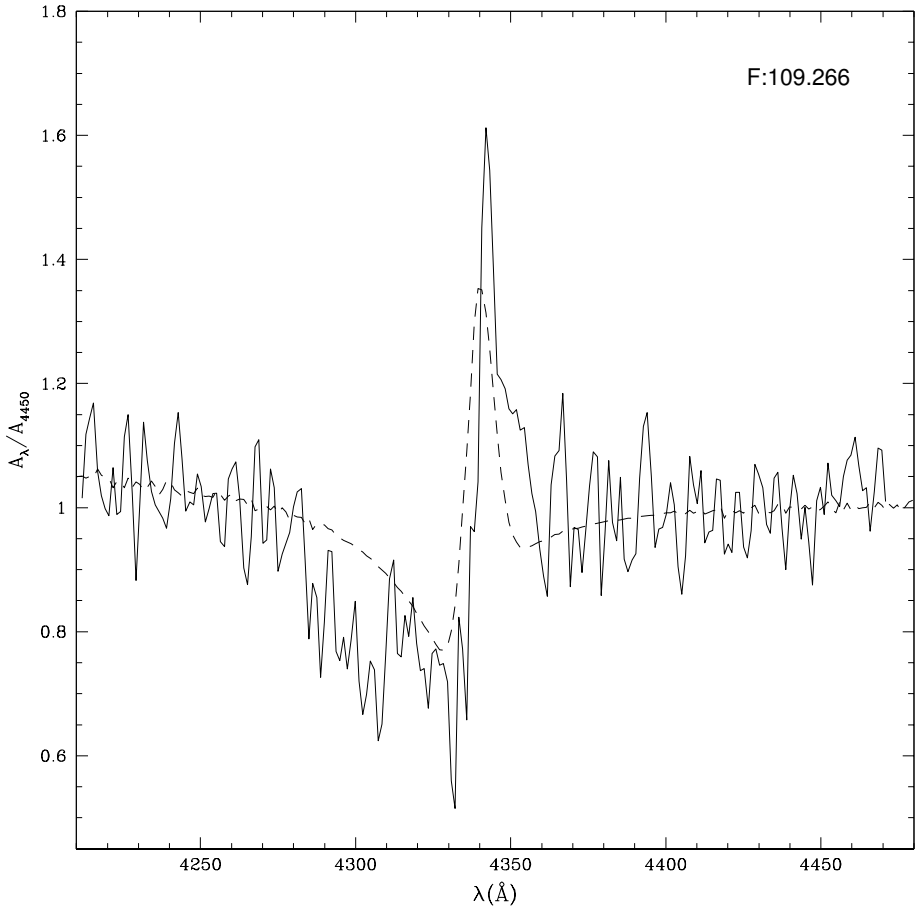

Figure A.1 Chromatic amplitudes of G 226-29 created directly from the data (solid line) and from the spectral fits (dashed line).

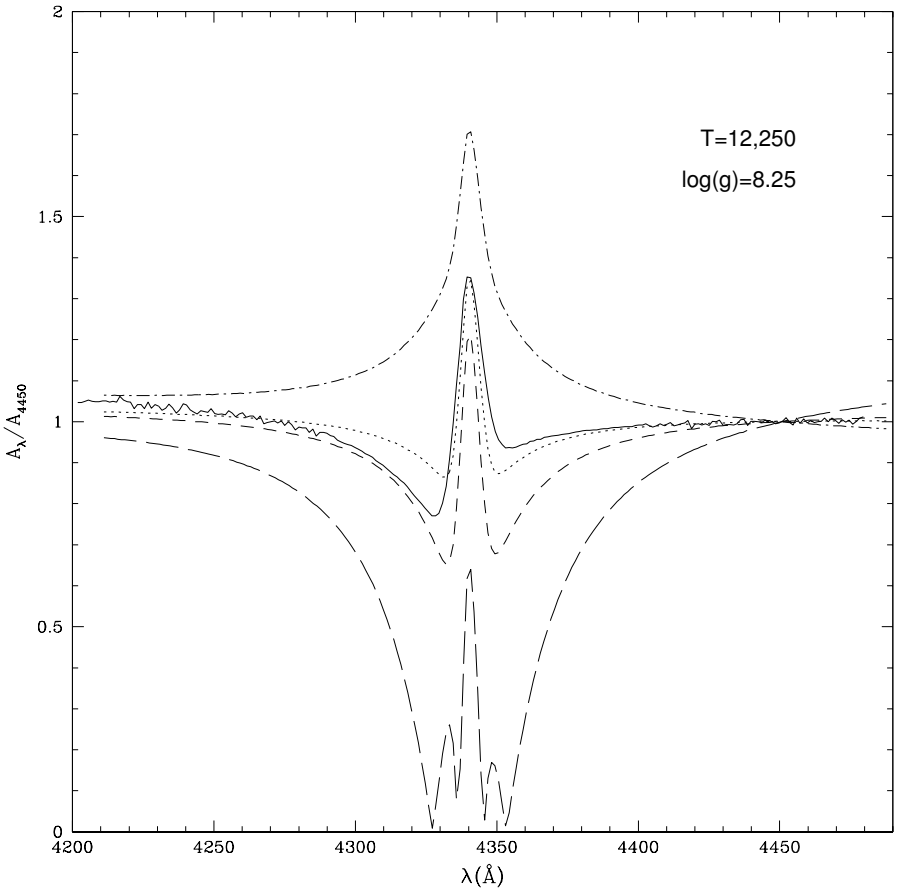

Figure A.2 Chromatic amplitude of G 226-29 created from the spectral fits (solid line) and model chromatic amplitudes (dotted is ℓ=1, dashed is ℓ=2, long dashed is ℓ=3, dot-dashed is ℓ=4).

A.2 Vary Lorentzian Width

When performing the spectral fitting to create chromatic amplitudes for PY Vul we only allowed four parameters to change. We found that this yielded the closest representation to the original model chromatic amplitudes. To further emphasize this point, we graphically demonstrate the results of allowing the width of the Lorentzian to change. As shown in Figure A.3, when the width is allowed to vary, some of the

features become washed-out. The plots show model chromatic amplitudes created from fitting model atmospheres. The plot on the left does not allow the Lorentzian width to vary while the plot on the right does. By allowing the Lorentzian width to vary, the chi-square of each fit improves slightly, but the error on the parameter containing the Lorentzian flux increases by a factor of ten. Apparently, it is more important to accurately represent the Lorentzian flux than to obtain a slightly better overall fit.

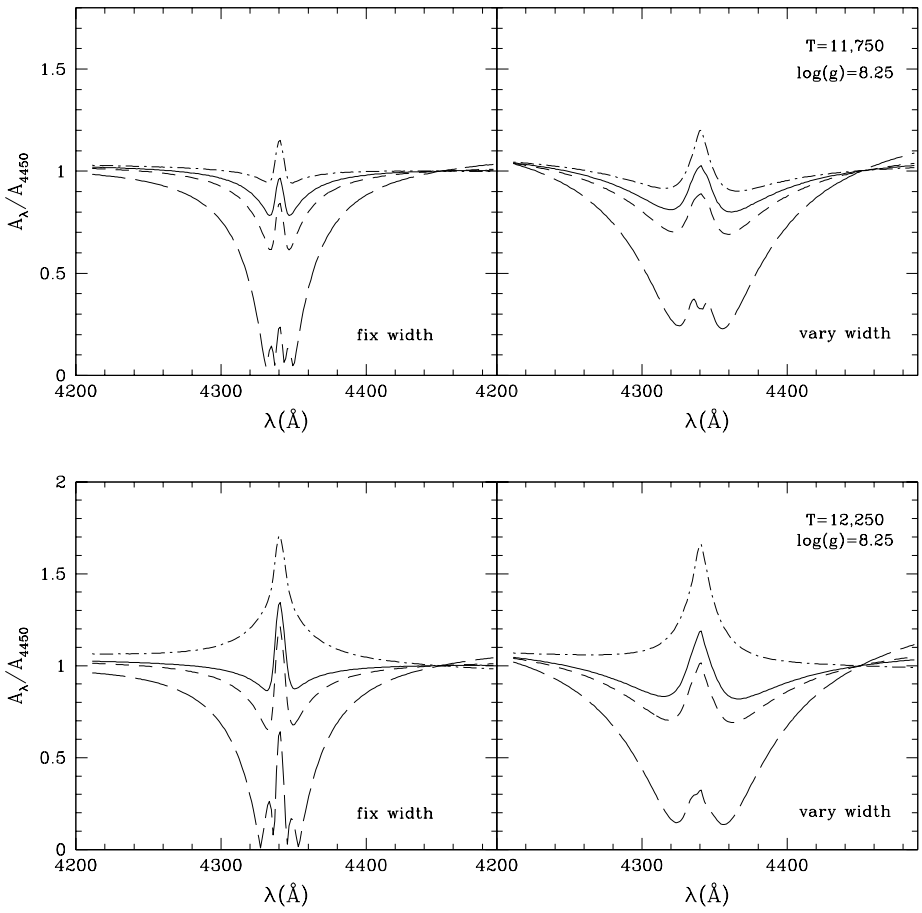

Figure A.3 Model chromatic amplitudes for T=11,750 K and log(g)=8.25 model (top) and T=12,250 K and log(g)=8.25 model (bottom) (solid is ℓ=1, dashed is ℓ=2, short dashed is ℓ=3, dot-dashed is ℓ=4). When fitting the model spectra, the width of the Lorentzian function was fixed while fitting the spectra to create the curves on the left.

REFERENCES

Adams, W. S. 1915, PASP, 27, 236

Bergeron, P., Fontaine, G., Billères, M., Boudreault, S., & Green, E. M. 2004, ApJ, 600, 404

Bergeron, P., et al. 1993, AJ, 106, 1987

Bergeron, P., Saffer, R. A., & Liebert, J. 1992, ApJ, 394, 228

Bergeron, P., Wesemael, F., Lamontagne, R., Fontaine, G., Saffer, R. A., & Allard, N. F. 1995, ApJ, 449, 258

Bessel, F. W. 1844, MNRAS, 6, 136

Bradley, P. A. 1998, ApJS, 116, 307

Bradley, P. A. 2001, ApJ, 552, 326

Brassard, P., Fontaine, G., & Wesemael, F. 1995, ApJS, 96, 545

Brickhill, A. J. 1983, MNRAS, 204, 537

Brickhill, A. J. 1990, MNRAS, 246, 510

Brickhill, A. J. 1991, MNRAS, 251, 673

Brickhill, A. J. 1992a, MNRAS, 259, 529

Brickhill, A. J. 1992b, MNRAS, 259, 519

Castanheira, B. G., et al. 2004, A&A, 413, 623

Chandrasekhar, S. 1934, The Observatory, 57, 93

Christensen-Dalsgaard, J. 2002, Reviews of Modern Physics, 74, 1073

Clemens, J. C. 1994, Ph.D. Thesis U. Texas

Clemens, J. C., van Kerkwijk, M. H., & Wu, Y. 2000, MNRAS, 314, 220

Cox, J. P. 1980, Theory of Stellar Pulsation (Princeton Univ. Press: Princeton)

Dolez, N., & Vauclair, G. 1981, A&A, 102, 375

Dziembowski, W. 1977, Acta Astron., 27, 203

Dziembowski, W. 1982, Acta Astron., 32, 147

Dziembowski, W., & Koester, D. 1981, A&A, 32, 16

Fontaine, G., Bergeron, P., Lacombe, P., Lamontagne, R., & Talon, A. 1985, AJ, 90, 1094

Fontaine, G., Brassard, P., Bergeron, P., & Wesemael, F. 1992, ApJ, 399, L91

Fontaine, G., Brassard, P., & Charpinet, S. 2003, in Asteroseismology Across the HR diagram, Astrophy. Space Sci. 284 (Kluwer Academic Publishers), 257

Fontaine, G., & Wesemael, F. 1987, in IAU Colloq. 95: Second Conference on Faint Blue Stars, 319

Goldreich, P., & Wu, Y. 1999a, ApJ, 511, 904

Goldreich, P., & Wu, Y. 1999b, ApJ, 523, 805

Handler, G., Romero-Colmenero, E., & Montgomery, M. H. 2002, MNRAS, 335, 399

Hansen, B. M. S., & Liebert, J. 2003, ARA&A, 41, 465

Hansen, C. J., & Kawaler, S. D. 1994, Stellar Interiors: Physical Principles, Structure, and Evolution (Springer-Verlag:New York)

Horne, J. H., & Baliunas, S. L. 1986, ApJ, 302, 757

Horne, K. 1986, PASP, 98, 609

Iben, I. J., & Laughlin, G. 1989, ApJ, 341, 312

Ising, J., & Koester, D. 2001, A&A, 374, 116

Kepler, S. O. 1993, Baltic Astronomy, 2, 515

Kepler, S. O., & Bradley, P. A. 1995, Baltic Astronomy, 4, 166

Kepler, S. O., et al. 1995, ApJ, 447, 874

Kepler, S. O., Robinson, E. L., Koester, D., Clemens, J. C., Nather, R. E., & Jiang, X. J. 2000, ApJ, 539, 379

Kepler, S. O., et al. 1991, ApJ, 378, L45

Kleinman, S. J., et al. 1998, ApJ, 495, 424

Koester, D. 1976, A&A, 52, 415

Koester, D. 2002, A&AR, 11, 33

Koester, D., & Chanmugam, G. 1990, Reports of Progress in Physics, 53, 837

Koester, D., Dreizler, S., Weidemann, V., & Allard, N. F. 1998, A&A, 388, 219

Koester, D., Vauclair, G., Dolez, N., Oke, J. B., Greenstein, J. L., & Weidemann, V. 1985, A&A, 149, 423

Koester, D., Weidemann, V., & Schulz, H. 1979, A&A, 76, 262

Kotak, R., van Kerkwijk, M. H., & Clemens, J. C. 2002, A&A, 388, 219

Kotak, R., van Kerkwijk, M. H., & Clemens, J. C. 2004, A&A, 413, 301

Kotak, R., van Kerkwijk, M. H., Clemens, J. C., & Bida, T. A. 2002, A&A, 391, 1005

Landolt, A. U. 1968, ApJ, 153, 151

Lasker, B. M., & Hesser, J. E. 1971, ApJL, 163, L89

Liebert, J., Dahn, C. C., & Monet, D. G. 1988, ApJ, 332, 891

Liebert, J., Wesemael, F., Hansen, C. J., Fontaine, G., Shipman, H. L., Sion, E. M., Winget, D. E., & Green, R. F. 1986, ApJ, 309, 241

McGraw, J. T. 1979, ApJ, 229, 203

McGraw, J. T., Fontaine, G., Lacombe, P., Dearborn, D. S. P., Gustafson, J., & Starrfield, S. G. 1981, ApJ, 250, 349

McGraw, J. T., & Robinson, E. L. 1975, ApJ, 200, L89

McGraw, J. T., & Robinson, E. L. 1976, ApJ, 205, L155

Mestel, L. 1952, MNRAS, 112, 583

Mukadam, A. S., et al. 2004, accepted to ApJ

Nather, R. E., & Mukadam, A. S. 2003, preprint(astro-ph/0306022)

Nather, R. E., Winget, D. E., Clemens, J. C., Hansen, C. J., & Hine, B. P. 1990, ApJ, 361, 309

Nitta, A. 2004, in 14th European Conference on White Dwarfs, in prep.

Nitta, A., Kanaan, A., Kepler, S. O., Koester, D., Montomery, M. H., & Winget, D. E. 2000, Baltic Astr., 9, 97

O'Brien, M. S. 2003, in Asteroseismology Across the HR diagram, Astrophy. Space Sci. 284 (Kluwer Academic Publishers), 45

O'Donoghue, D., Warner, B., & Cropper, M. 1992, MNRAS, 258, 415

Oke, J. B., et al. 1995, PASP, 107, 375

Pfeiffer, B., et al. 1996, A&A, 314, 182

Robinson, E. L., Kepler, S. O., & Nather, R. E. 1982, ApJ, 259, 219

Robinson, E. L., et al. 1995, ApJ, 438, 908

Thompson, S. E., & Clemens, J. C. 2003, in Asteroseismology Across the HR diagram, Astrophy. Space Sci. 284 (Kluwer Academic Publishers), P573

Thompson, S. E., Clemens, J. C., van Kerkwijk, M. H., & Koester, D. 2003, ApJ, 589, 921

Tody, D. 1986, Proc. SPIE, 627, 733

Unno, W., Osaki, Y., Ando, H., Saio, H., & Shibahashi, H. 1989, Nonradial oscillations of stars, 2nd ed. (Tokyo: University of Tokyo Press)

van Kerkwijk, M. H., Clemens, J. C., & Wu, Y. 2000, MNRAS, 314, 209

Vauclair, G. 1971, in IAU Symp. 42: White Dwarfs, 145

Vogt, S. S., et al. 1994, in Proc. SPIE Instrumentation in Astronomy VIII, David L.

Crawford; Eric R. Craine; Eds., Volume 2198, 362

Vuille, F. 2000a, MNRAS, 313, 170

Vuille, F. 2000b, MNRAS, 313, 179

Vuille, F., & Brassard, P. 2000, MNRAS, 313, 185

Warner, B., & Nather, R. E. 1970, MNRAS, 147, 21

Winget, D. E. 1982, Ph.D. Thesis, Rochester

Winget, D. E., & Fontaine, G. 1982, in Pulsations in Classical and Cataclysmic Variable Stars, 46

Winget, D. E., Hansen, C. J., Liebert, J., van Horn, H. M., Fontaine, G., Nather, R. E., Kepler, S. O., & Lamb, D. Q. 1987, ApJ, 315, L77

Winget, D. E., et al. 1990, ApJ, 357, 630

Winget, D. E., Robinson, E. L., Nather, R. D., & Fontaine, G. 1982a, ApJ, 262, L11

Winget, D. E., Van Horn, H. M., Tassoul, M., Hansen, C. J., Fontaine, G., & Carroll, B. W. 1982b, ApJ, 252, L65

Wood, M. A. 1992, ApJ, 386, 539

Wu, Y. 2001, MNRAS, 323, 248

Wu, Y., & Goldreich, P. 1999, ApJ, 519, 783

Wu, Y., & Goldreich, P. 2001, ApJ, 546, 469